Acknowledgments

Praise be to ALLAH, Lord of the whole creation and peace be upon his messenger Mohammad.

Then, I would like to express my deep appreciation to my supervisor, Dr. Ahmad K. Ahmad for suggesting the project, advices, helpful comments and stimulating discussions at all stages of the work.

I acknowledge the helpful comments assistance given to me at various stage of this work by Prof. Dr. Sabah M. Juma .

I wish to express my thanks to the staff of the Physics Department in College of science for the facilities offered during this work.

I thank the staff of the central library of University of Baghdad.

I wish I have a word better thanks to express my felling to my Father, Mother, Sisters and Aunt.

I also thank my friends Allaa A. Asal, Ammer Al-Ani, Ph.D. student Bashar Al-Ani.

Chapter Three

3- Results And Discussion Of Magnetic Deflector

3-1 Introduction

In this part of present work the synthesis approach has been used to find the optimum design of magnetic deflector. The saddle yoke coil whose magnetic field is given by equation (2-10) is used as the source of magnetic field in our present work. The MOL concept (which is shown in section 2-6) is used to find the deflection field of the magnetic deflector, i.e. by using the MOL one can find the design of magnetic deflector by knowing the design of magnetic lens or the axial magnetic field distribution of the lens, depending on equation (2-11).

Spherical and chromatic aberrations are minimized by using synthesis approach in two steps. Firstly, one can use different shapes of axial magnetic field distribution; a well known field distribution as Glaser model, Grivet-Lenz model, variable aperture projection (VAP) arrangement, and new suggested field. Secondly, in each case the geometrical shape of deflection coil is changed, where the length and the angle are varied. Then, the pole piece designs that give rise to these field distributions are found by using the reconstruction method.

3-2 The Design By Using Glaser's Model

According to Glaser's model the axial flux density distribution is given by Szilagyi [1988]:

$$B(z)=\frac{B_m}{1+(\frac{z}{a})^2} \qquad (3-1)$$

where B_m is the maximum value of magnetic field and it is calculated by using equation (2-10), and a is the field width at half maximum $B_m/2$. The axial flux density distribution of the deflector *D(z)* is computed by using equation (2-11) where *B'* is computed with the aid of equation (3-1). The shapes of the axial flux density distribution *B(z)* and the axial deflection flux density distribution *D(z)* are shown in figures (3-1) and (3-2), respectively.

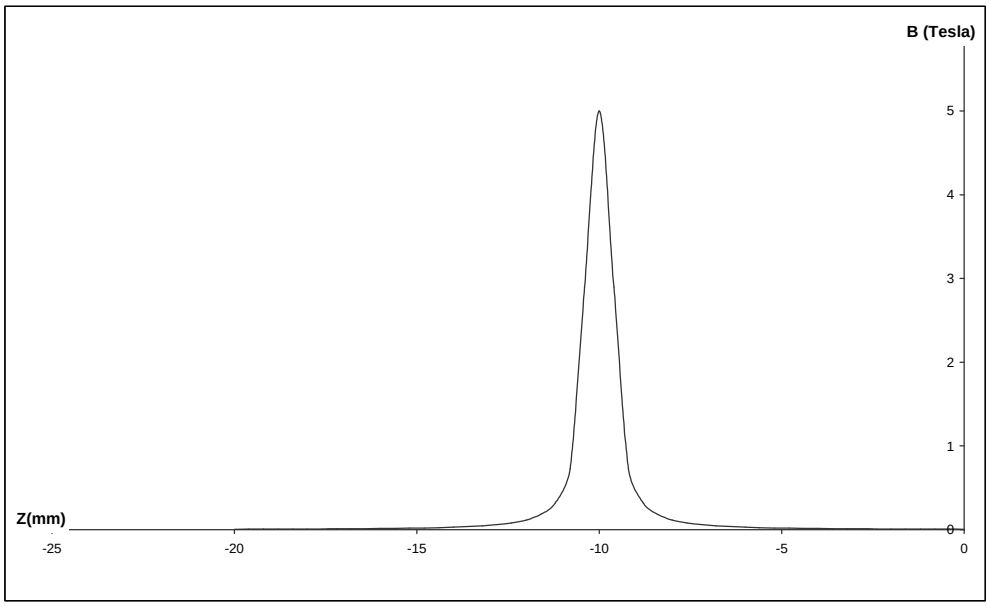

Figure (3-1): The axial flux density distribution *B(z)* of Glaser's model.

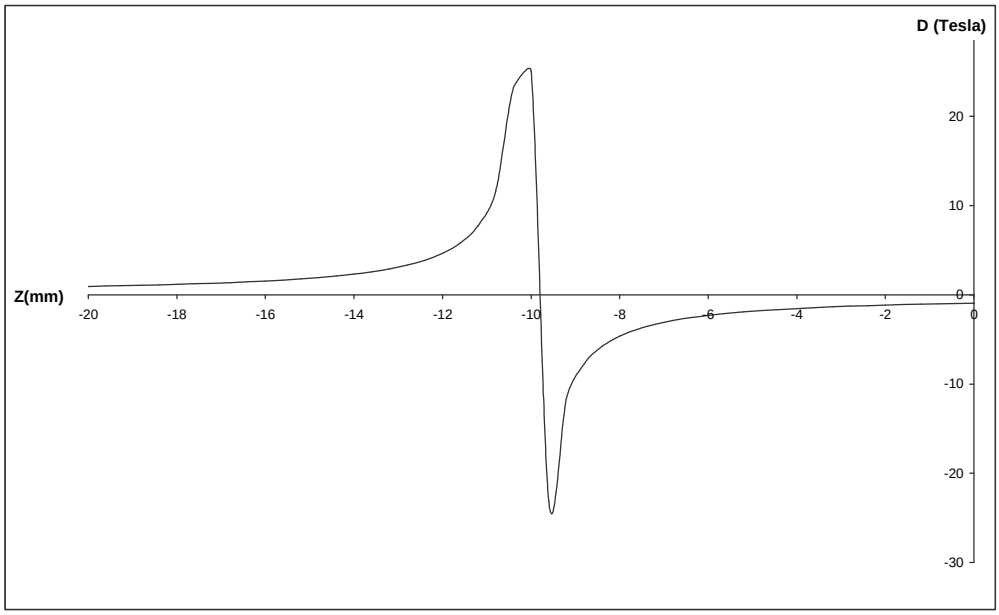

Figure (3-2): The axial deflection flux density distribution *D(z)* calculated with Glaser model.

3-2-1 Infinite magnification condition

3-2-1-1 effects of changing the angle

Both spherical and chromatic aberrations are computed under this operating condition. The following angles ø = 30^{o}, 45^{o}, 50^{o} and 60^{o} of saddle yoke coil, with coil lengths H = 37mm, are used in the computations of the aberrations. Figure (3-3) shows the relation between relative spherical aberration coefficient Cs / fo and NI/SQRT (Vr). From this figure, one can show that ø = 60^{o} gives the lower values of Cs / fo. Also, the relative spherical aberration coefficient Cs/fo increases with increasing NI/SQRT(Vr). The minimum value of Cs /fo = 0.2 at NI/SQRT (Vr) = 0.035.

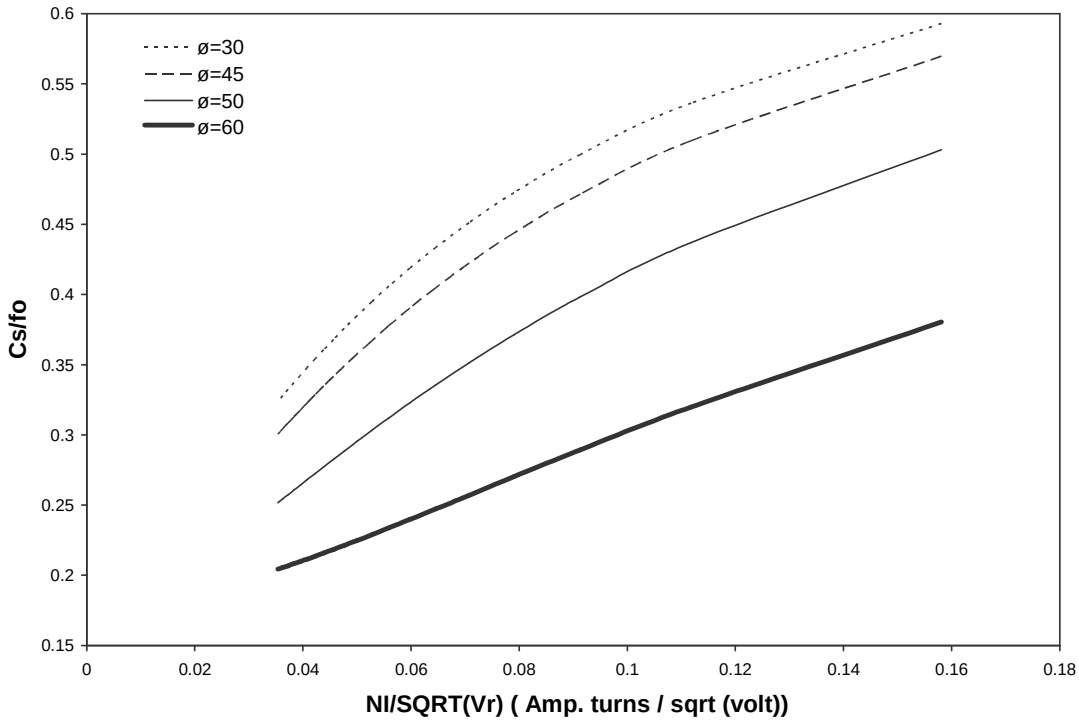

Figure (3-3): The relative spherical aberration coefficient as a function of NI / SQRT(Vr) for ø = 30^{o}, 45^{o}, 50^{o} and 60^{o} when H = 37mm.

Figure (3-4) shows the relation between Cc/fo and NI/SQRT(Vr). From the figure all cases appear to have the same behavior, and ø = 60^{o} gives us the minimum value of Cc/fo and the NI/SQRT(Vr) = 0.035 gives us the lower value of Cc/fo for all cases. From our calculations two parameters can be used to reduce the spherical and chromatic aberrations by selection the best angle and the best value of the ratio NI/SQRT(Vr) (by changing NI and Vr).

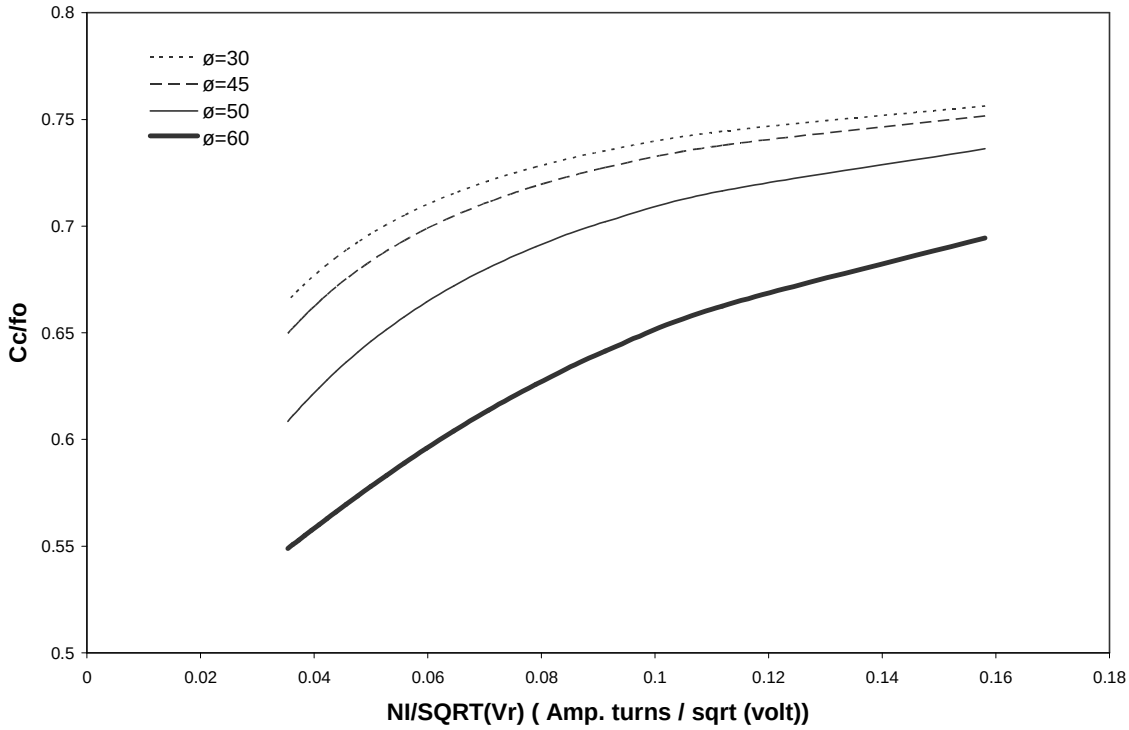

Figure (3-4): The relative chromatic aberration coefficient as a function of NI / SQRT(Vr) for ø = 30^{o}, 45^{o}, 50^{o} and 60^{o} when H = 37mm.

The relation between Cs/fo and Cc/fo with the angle of saddle deflection coil ø is shown in figures (3-5) - (3-6), respectively at NI/SQRT(Vr) = 0.05 . both cases have the same behavior, where Cs/fo and Cc/fo decrease as the angle increases.

The pole piece shape is found by using the reconstruction method, where equation (2-12) is used to achieve this task.

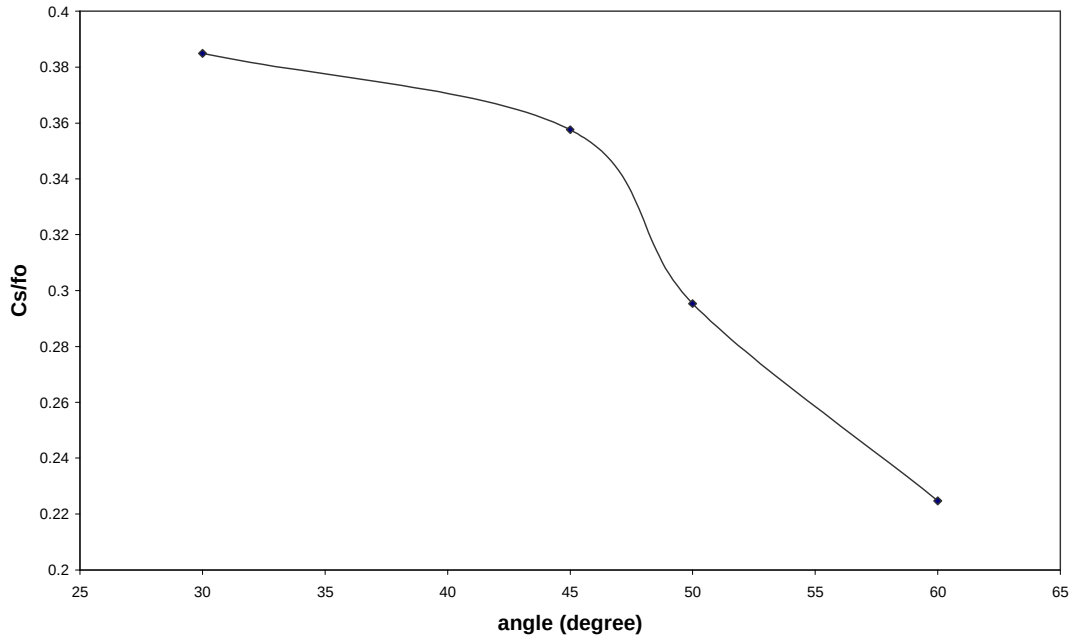

Figure (3-5): The relative spherical aberration coefficient as a function of the angle ø at NI/SQRT(Vr) = 0.05.

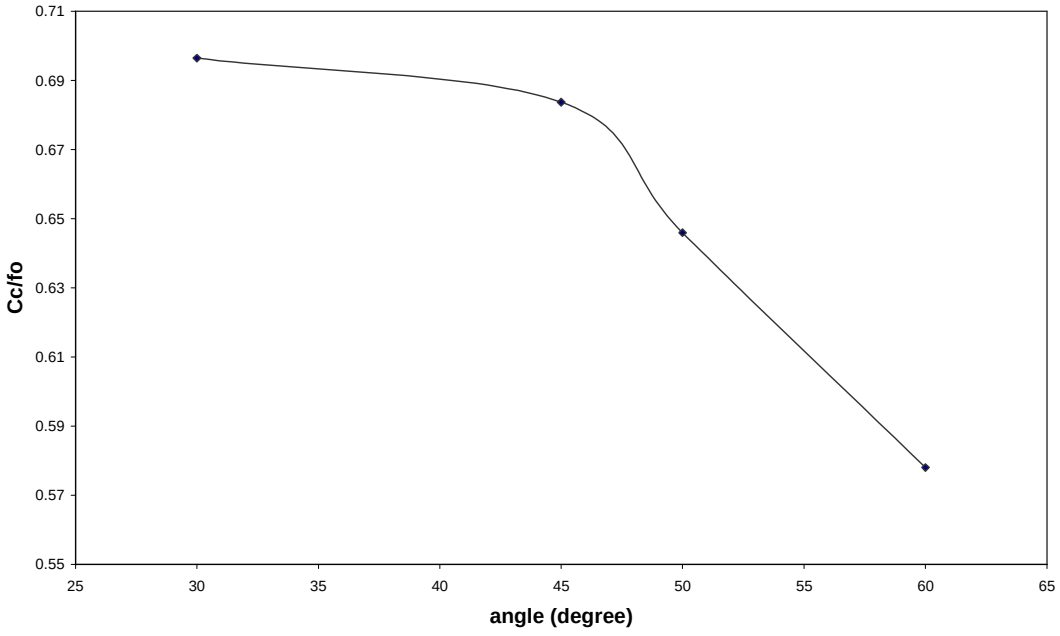

Figure (3-6): The relative chromatic aberration coefficient as a function of the angle ø at NI/SQRT(Vr) = 0.05 .

Figure (3-7) shows the shape of the upper half part of the pole piece for ø = 60^{o} and H = 37mm.

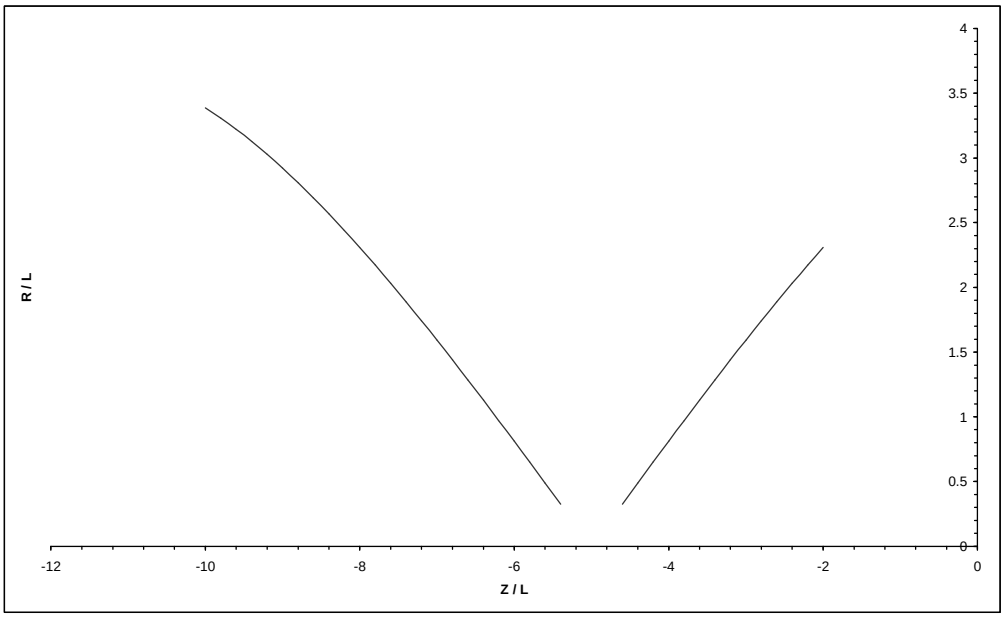

Figure (3-7): The pole piece shape when ø = 60^{o} and H = 37mm.

3-2-1-2 effects of changing the length of coil

To study the effects of variation of the length of the coil H on the Cs/fo and Cc/fo we take different values of H, where H=27, 37, 47, 57 and 67mm with ø = 60^{o} are taken into account. Figure (3-8) shows this effect on a spherical aberration. This figure shows that the length H=27mm gives the lower value of Cs/fo which is equal to 0.19 at NI/SQRT(Vr) = 0.035.

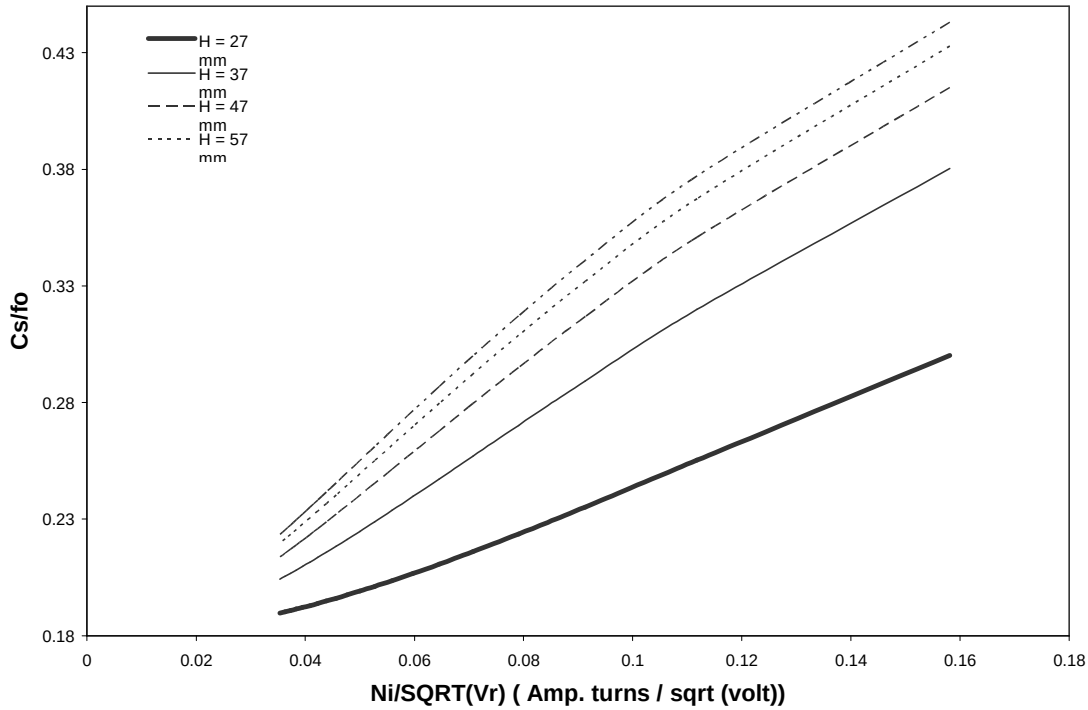

Figure (3-8): The relative spherical aberration coefficient as a function of NI / SQRT(Vr) for ø = 60^{o} and H = 27, 37, 47, 57 and 67mm.

Figure (3-9) shows the effect of variation of the length on the Cc/fo . Figure (3-9) shows that the length H=27mm gives the best value of Cc/fo which is equal to 0.515 at NI/SQRT(Vr) = 0.035. In both spherical and chromatic aberrations one can find that the values of relative aberration coefficient increase as the ratio of NI/SQRT(Vr) increase. Also, at the lower

values of NI/SQRT(Vr) one has the best values of both spherical and chromatic aberrations, and one can select the values of NI and Vr to keep this ratio small.

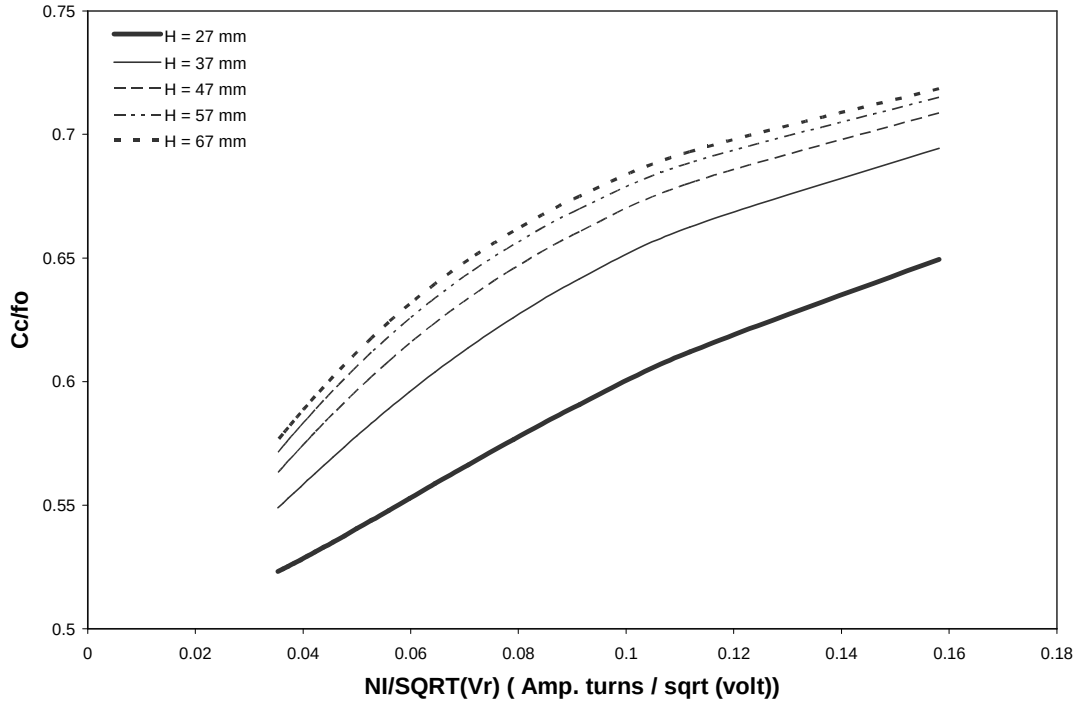

Figure (3-9): The relative chromatic aberration coefficient as a function of NI / SQRT(Vr) for ø = 60^{o} and H =27, 37, 47, 57 and 67mm.

The relation between Cs/fo and Cc/fo and the length of the coil H is shown for NI/SQRT(Vr) =0.05 in figures (3-10) and (3-11), respectively. The values of Cs/fo and Cc/fo increase when the length of the coil H increases and at the length H=27mm one can have a better result. Therefore, to reduce the values of relative spherical and chromatic aberrations the designer can use the shorter lengths to design the saddle deflection coil. Figure (3-12) shows the shape the upper half part of pole piece which is found by using the reconstruction method for ø = 60 and H=27mm.

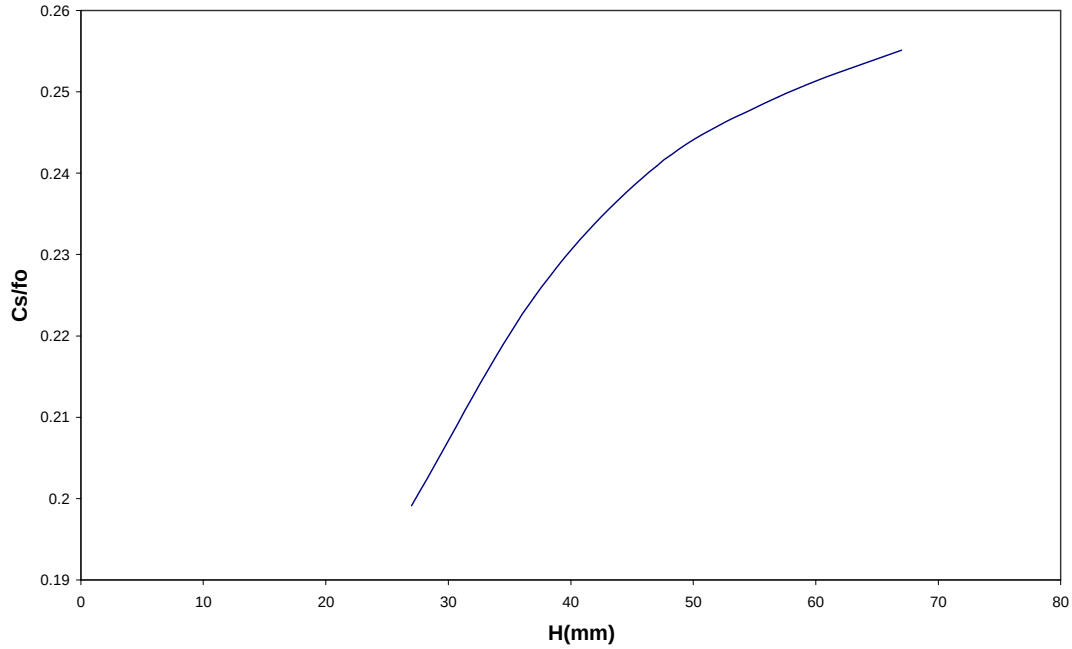

Figure (3-10): The relative spherical aberration coefficient as a function of the length of the coil H at NI/SQRT(Vr) = 0.05 .

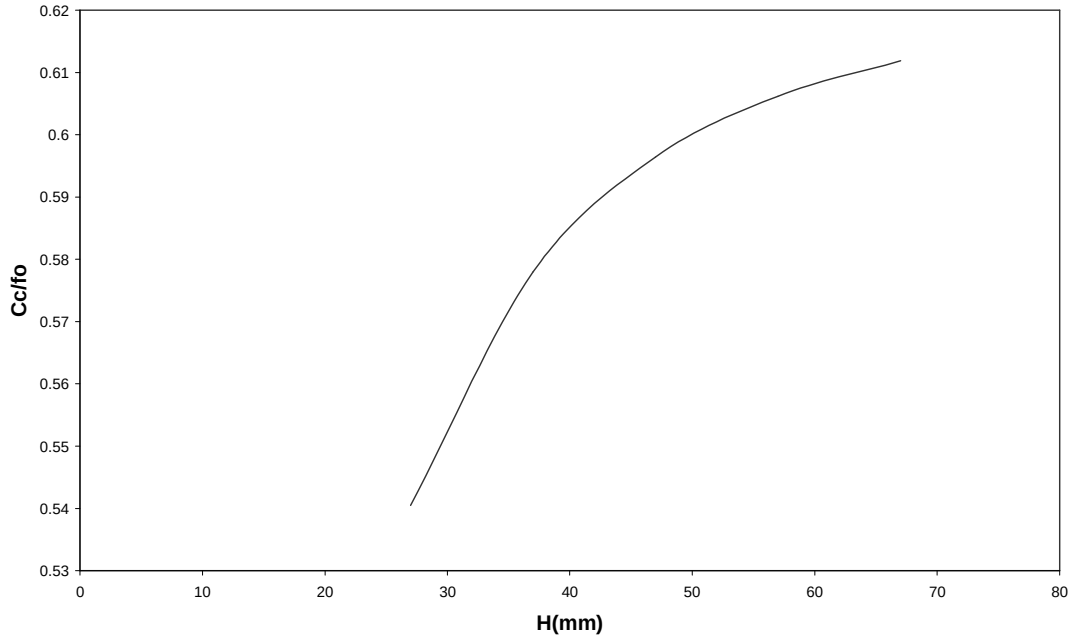

Figure (3-11): The relative chromatic aberration coefficient as a function of the length of the coil H at NI/SQRT(Vr) = 0.05 .

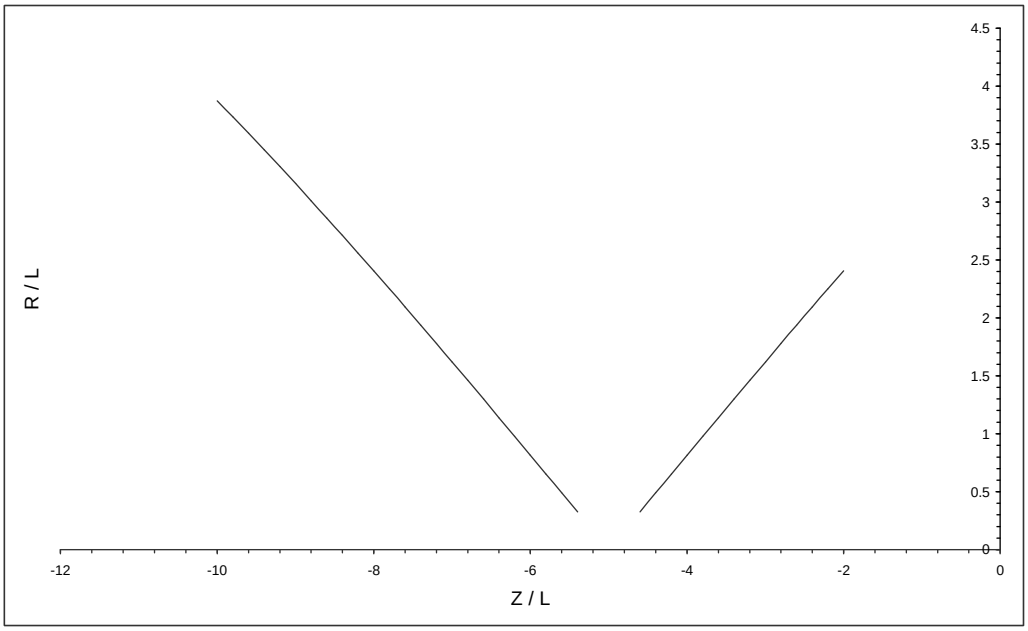

Figure (3-12): The pole piece shape when ø = 60^{o} and H = 27mm.

3-2-2 Zero magnification condition

3-2-2-1 effects of changing the angle

Both spherical and chromatic aberrations are computed using this operating condition. Different angles of saddle yoke coil, ø = 30^{o}, 45^{o}, 60^{o} and 75^{o} with constant length of coil H=37mm, are used in calculations. Figure (3-13) shows the relation between Cs/fo and NI/SQRT(Vr). In this figure, we find that at ø = 75^{o} the lower value of aberrations can be found. From the figure one can also see that the quotient Cs/fo increase when the ratio NI/SQRT(Vr) increases and the minimum value of Cs/fo = 0.31 is at NI/SQRT(Vr) = 0.035 .

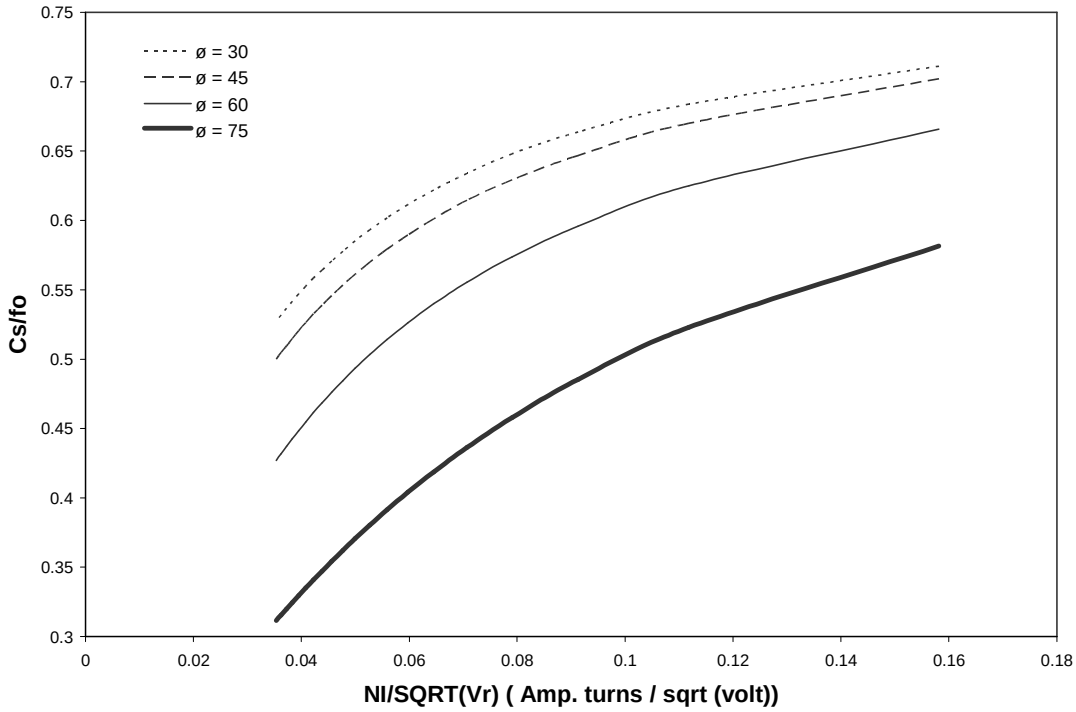

Figure (3-13): The relative spherical aberration coefficient as a function of NI / SQRT(Vr) for ø = 30^{o}, 45^{o}, 60^{o} and 75^{o} when H = 37mm.

Figure (3-14) shows the relation between Cc/fo and NI/SQRT(Vr). In this figure, we find that ø = 75^{o} give us the best value of Cc/fo which is equal to 0.655 at NI/SQRT(Vr) = 0.035. The values of relative chromatic aberrations has the same behavior as relative spherical aberrations in figure (3-13). At the smaller values of NI/SQRT(Vr) one can find the minimum values of both spherical and chromatic aberrations and by choosing the values of NI and Vr one can keep the aberration coefficients small. The relation between Cs/fo and Cc/fo with the angle of saddle deflection coil ø is shown in figures (3-15) and (3-16), respectively with NI/SQRT(Vr) =0.05. In both cases the Cs/fo and Cc/fo decrease as value of (ø) increases. The optimum values of Cs/fo and Cc/fo at are ø =75^{o} .

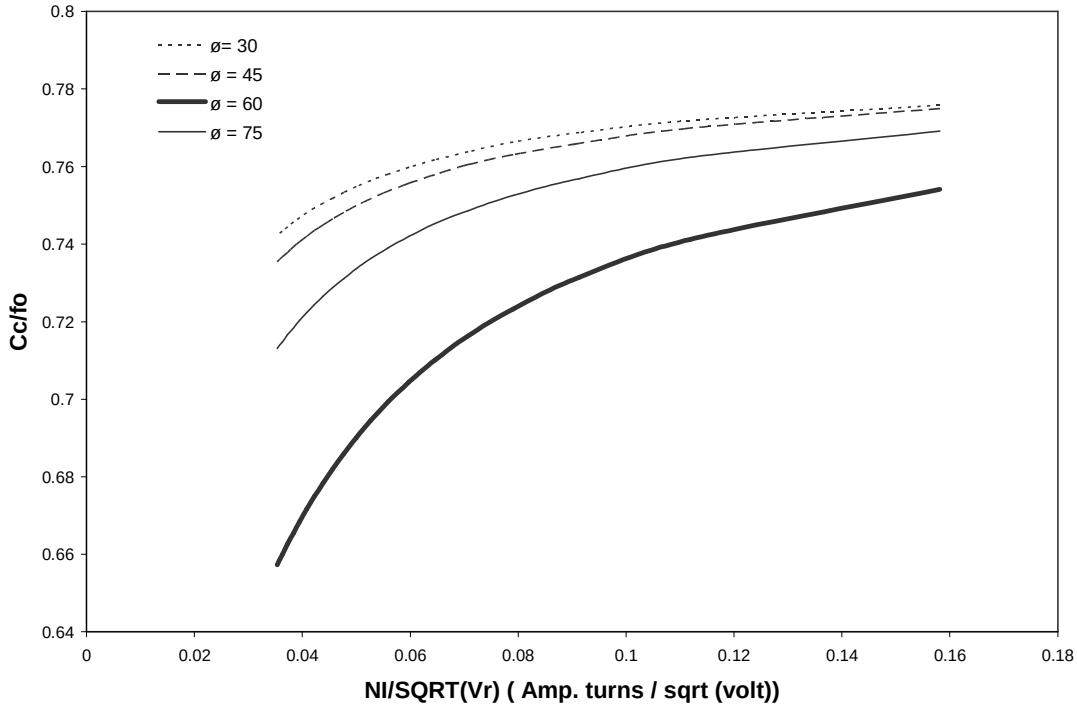

Figure (3-14): The relative chromatic aberration coefficient as a function of NI / SQRT(Vr) for ø =30^{o}, 45^{o}, 60^{o} and 75^{o} when H = 37mm.

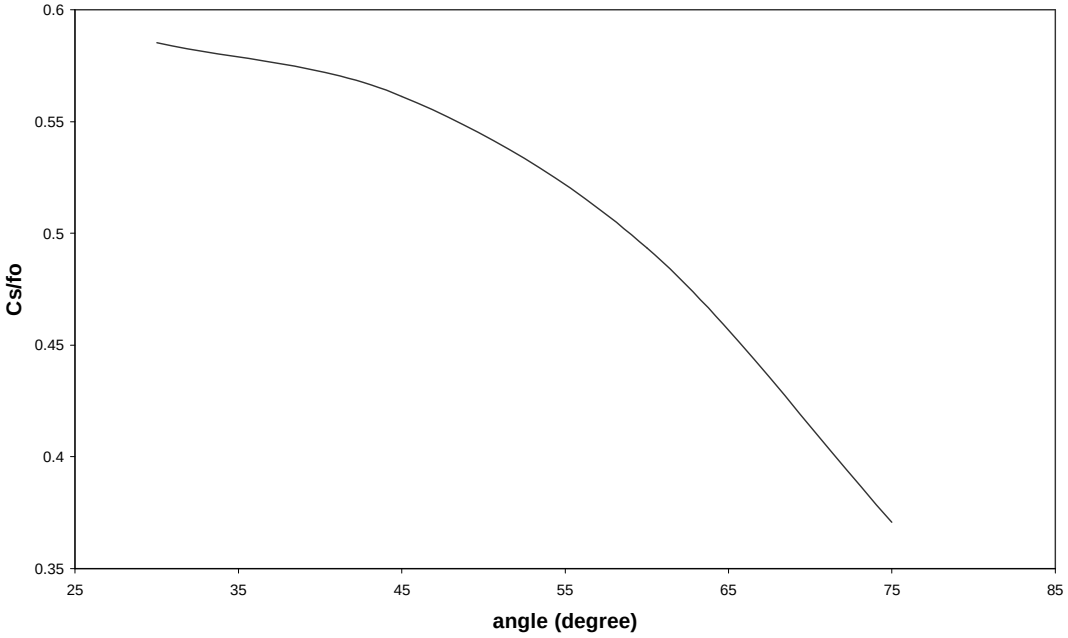

Figure (3-15): The relative spherical aberration coefficient as a function of the angle ø for H = 37mm at NI/SQRT(Vr) =0.05.

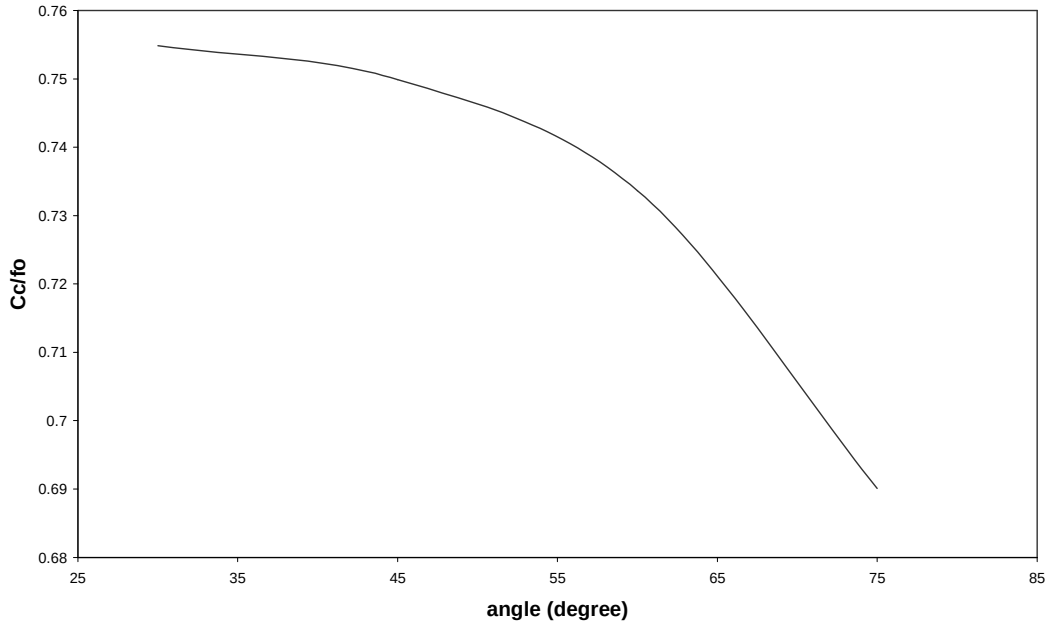

Figure (3-16): The relative chromatic aberration coefficient as a function of the angle ø for H = 37mm at NI/SQRT(Vr) =0.05.

The shape of the upper half part of pole piece for ø = 75^{o} and H=37mm is shown in figure (3-17), where it is determined by using the reconstruction method.

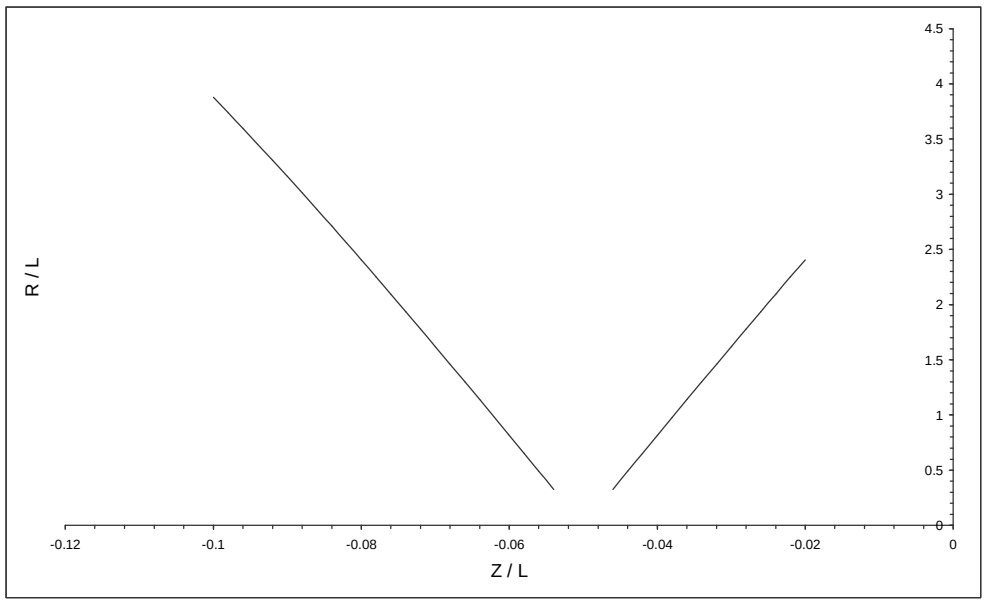

Figure (3-17): The pole piece shape when ø = 75^{o} and H = 37mm.

3-2-2-2 effects of changing the length of coil

The variation of the length of the coil has been studied to find the optimum length which gives us the minimum values of spherical and chromatic aberrations. The calculations for different values of the length of the coil,

H = 27,37,47,57 and 67mm, are made for ø = 75^{o}. Figure (3-18) shows the results of spherical aberration. In this figure we find that the H = 27mm gives the lower values of Cs/fo which is equal to 0.434 at NI/SQRT(Vr)=0.035. From the calculation of all lengths we find that the all cases have the same behavior, where the relative aberration coefficient increases as the ratio NI/SQRT(Vr) increases.

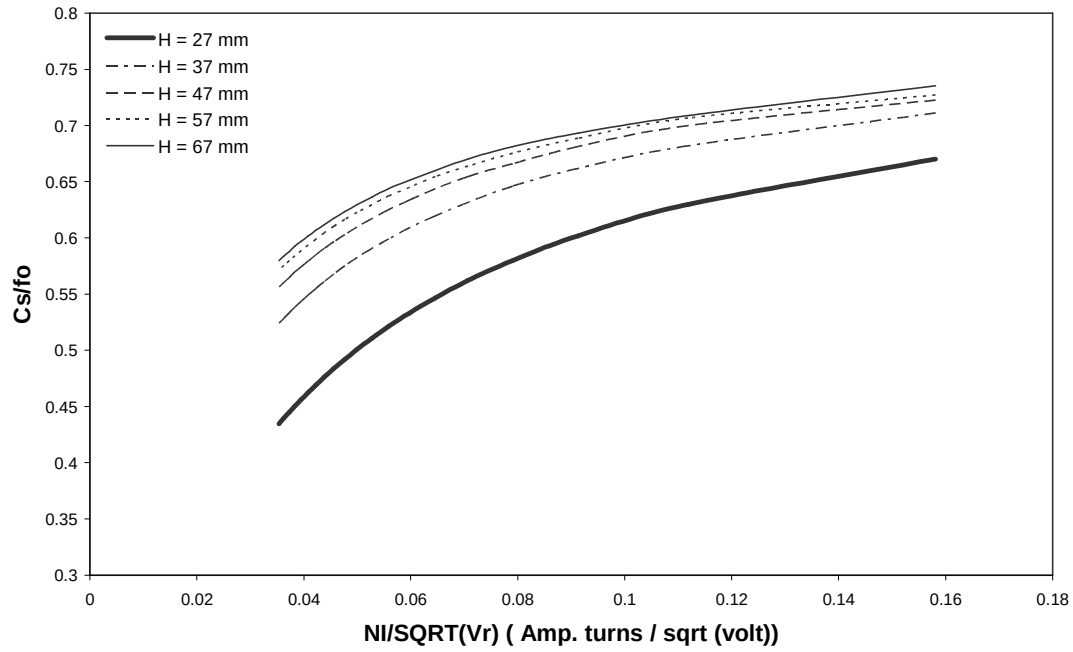

Figure (3-18): The relative spherical aberration coefficient as a function of NI / SQRT(Vr) for ø = 75^{o} and H = 27, 37, 47, 57 and 67mm.

The effect of variation of the coil length on the relative chromatic aberration coefficient is shown in figure (3-19). One finds that at the length H=27mm the best value of Cc/fo which is equal to 0.715 at NI/SQRT(Vr) = 0.035 is found. In all calculations of Glaser model we find that the spherical aberrations give smaller values than that of the chromatic aberrations.

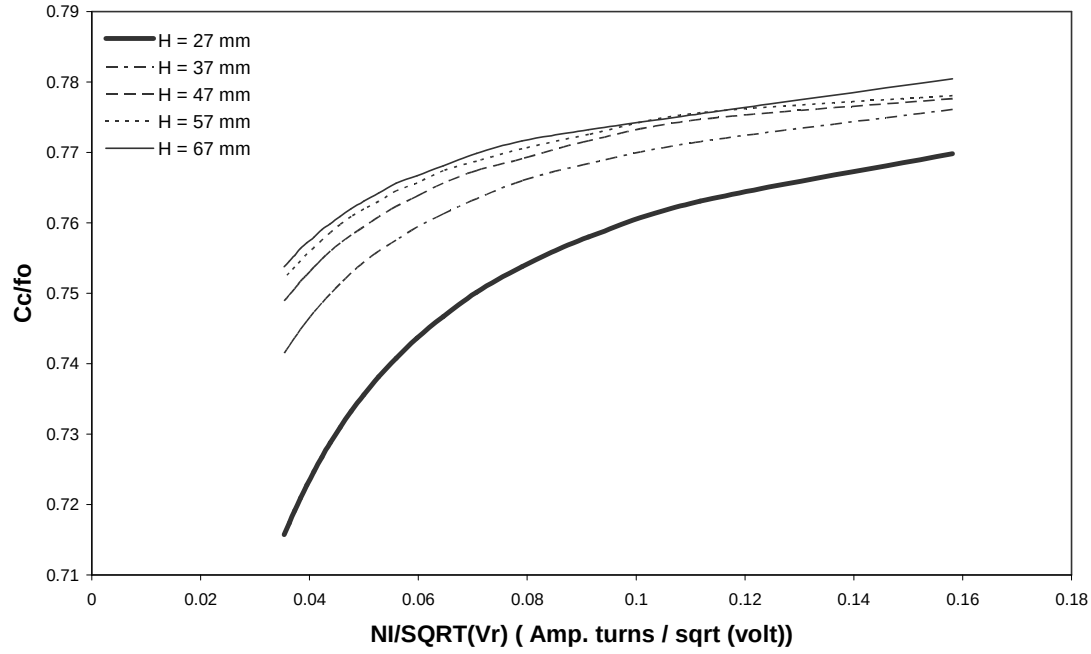

Figure (3-19): The relative chromatic aberration coefficient as a function of NI / SQRT(Vr) for ø = 75^{o} and H =27, 37, 47, 57 and 67mm.

The relation between Cs/fo and Cc/fo with the length of the coil H is shown in figure (3-20) and (3-21), respectively at constant NI/SQRT(Vr) = 0.05. the values of Cs/fo and Cc/fo increase when the length of the coil increases and H = 27mm gives us the lower values.

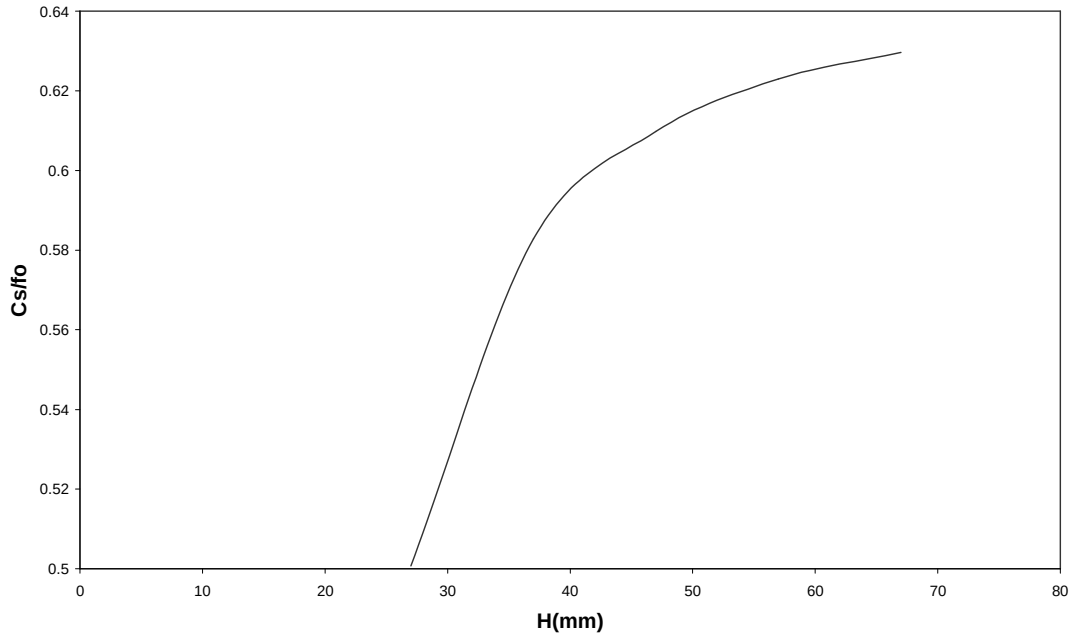

Figure (3-20): The relative spherical aberration coefficient as a function of the length of the coil H **at** NI/SQRT(Vr) = 0.05.

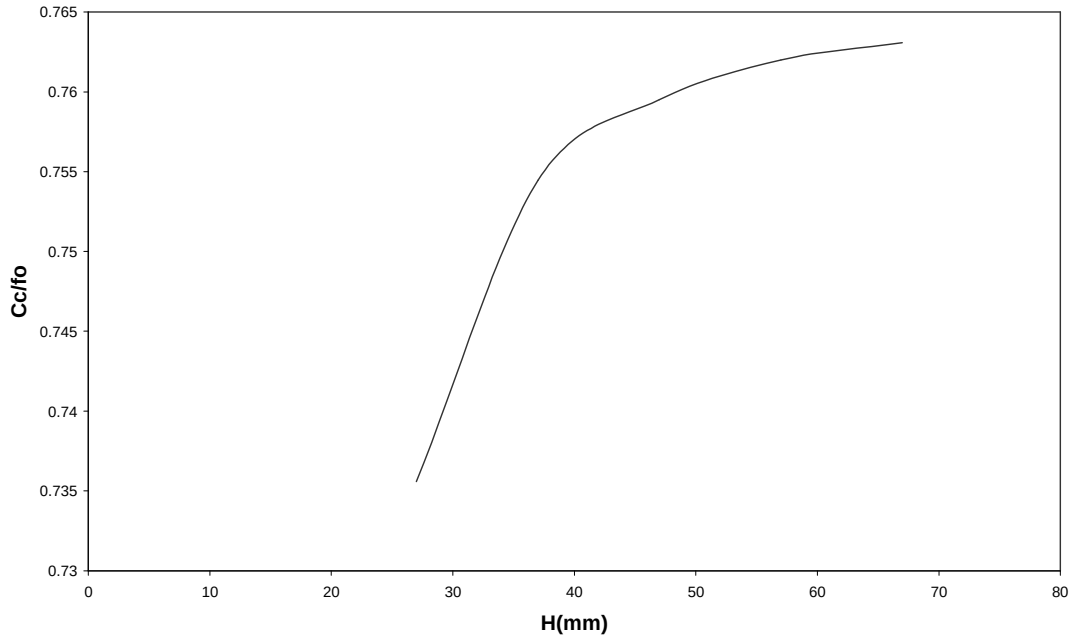

Figure (3-21): The relative chromatic aberration coefficient as a function of the length of the coil H NI/SQRT(Vr) = 0.05.

The shape of the upper part of the pole piece of ø = 75^{o} and H = 27mm appear in figure (3-22).

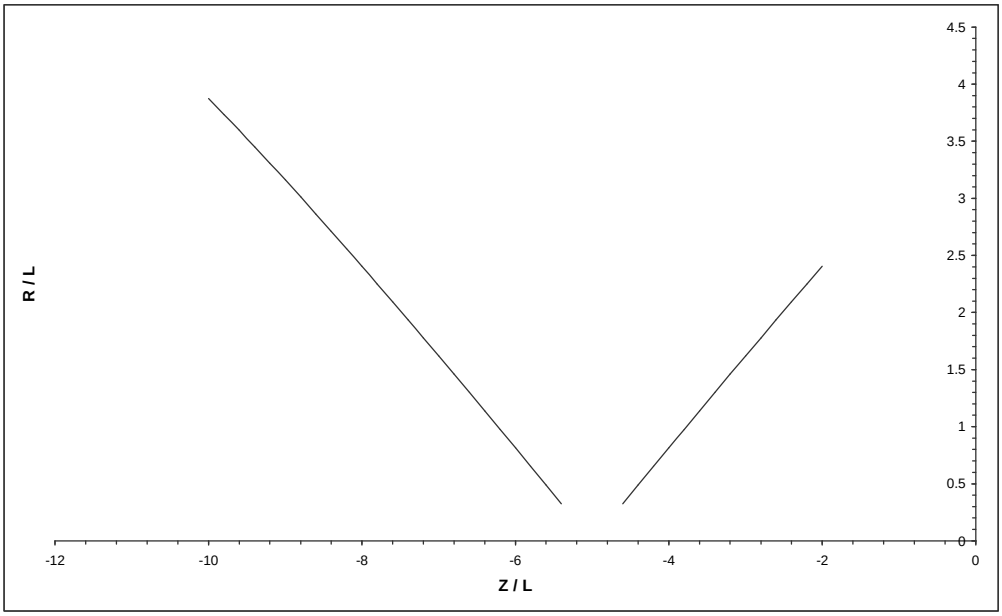

Figure (3-22): The pole piece shape when ø = 75^{o} and H = 27mm.

3-3 The Design By Using Grivet-Lenz Model

The axial flux density distribution for Grivet-Lenz model is given by the following [Szilagyi 1988]:

$$B(z) = B_m \; Sech(\frac{z}{b}) \qquad (3-2)$$

where B_m is the maximum value of the magnetic field and it is calculated by using equation (2-10), $b = 0.7593\ a$ where a is the field width at half maximum ($B_m / 2$).

The shapes of axial flux density distribution B(z) and axial deflection flux distribution D(z) are shown in figure (3-23) and (3-24), respectively.

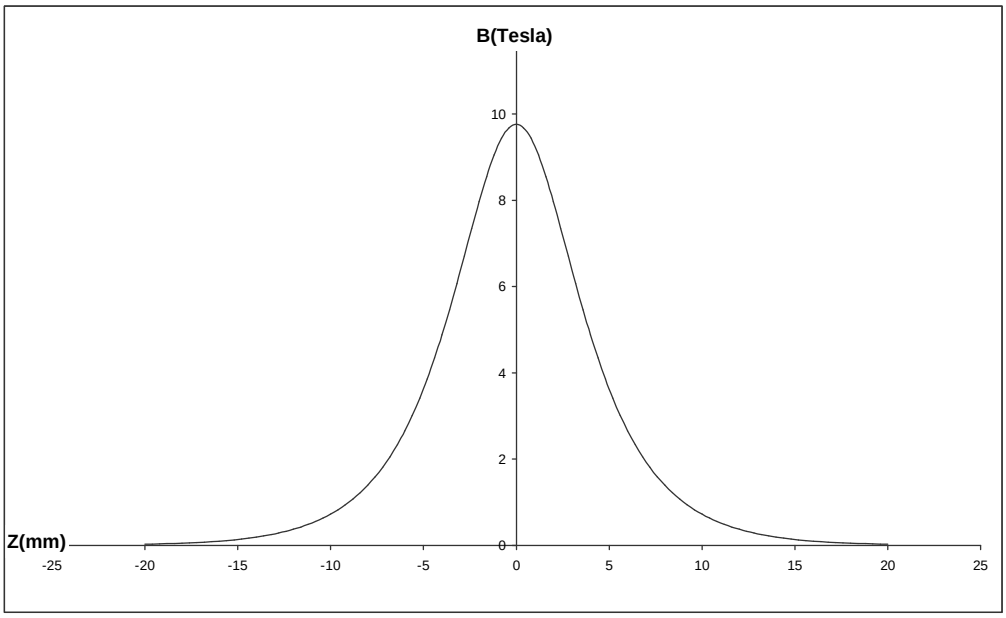

Figure (3-23): The axial flux density distribution *B(z)* of Grivet-Lenz model

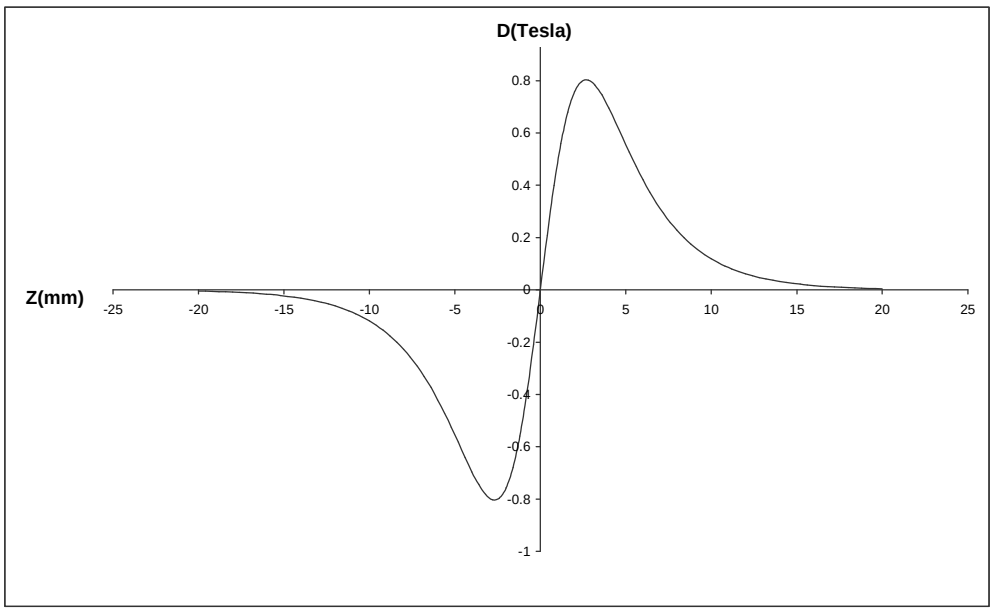

Figure (3-24): The axial deflection flux density distribution *D(z)* calculated with Grivet-Lenz model.

3-3-1 Infinite magnification condition

3-3-1-1 effects of changing the angle of the coil

The different angle of saddle yoke coil, ø = 30^{o}, 45^{o} and 75^{o} with constant coil length H =37mm, are studied. Figure (3-25) shows the relation between Cs/fo and NI/SQRT(Vr). In this figure, we find that the angle ø = 30^{o} gives the optimum value of Cs/fo. Also, we find that the ratio Cs/fo decreases as NI/SQRT(Vr) increases. As the ratio NI/SQRT(Vr) increases the all values the curves of quotient Cs /fo at different angles are closer to each other. Also, both results of the two angles ø =30^{o} and ø =75^{o} take the same value at the ratio NI/SQRT(Vr) = 0.16 .

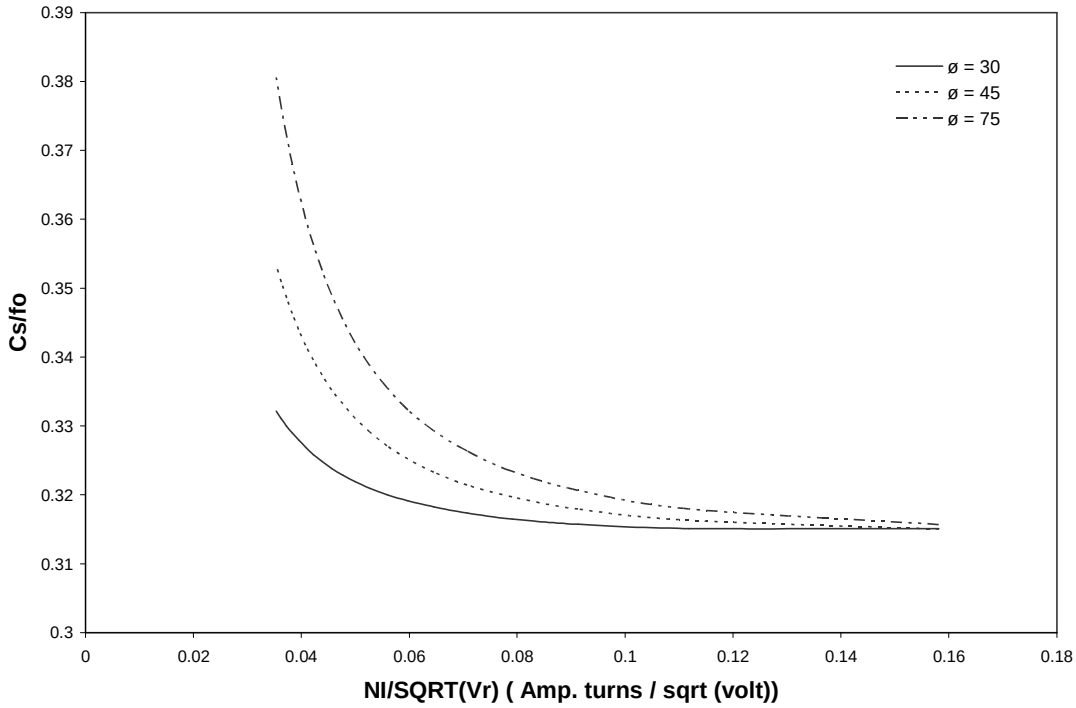

Figure (3-25): The relative spherical aberration coefficient as a function of NI / SQRT(Vr) for ø = 30^{o}, 45^{o} and 75^{o} when H = 37mm.

Figure (3-26) shows the relation between Cc/fo and NI/SQRT(Vr) for different angle ø = 30^{o}, 45^{o} and 75^{o}, respectively. In this figure, the values of Cc/fo are reduced when NI/SQRT(Vr) increases and the angle ø = 30^{o} gives the lower values of Cc/fo up to a certain values of NI/SQRT(Vr) = 0.11 and after this value the Cc/fo will increase and at the same time the two curves of ø = 45^{o} and 75^{o} will decrease and the values of Cc/fo for the two cases take the same value at NI/SQRT(Vr) =0.16 and this value is smaller than the value of ø =30^{o}. That means we have two optimum depending of the values of the ratio NI/SQRT(Vr).

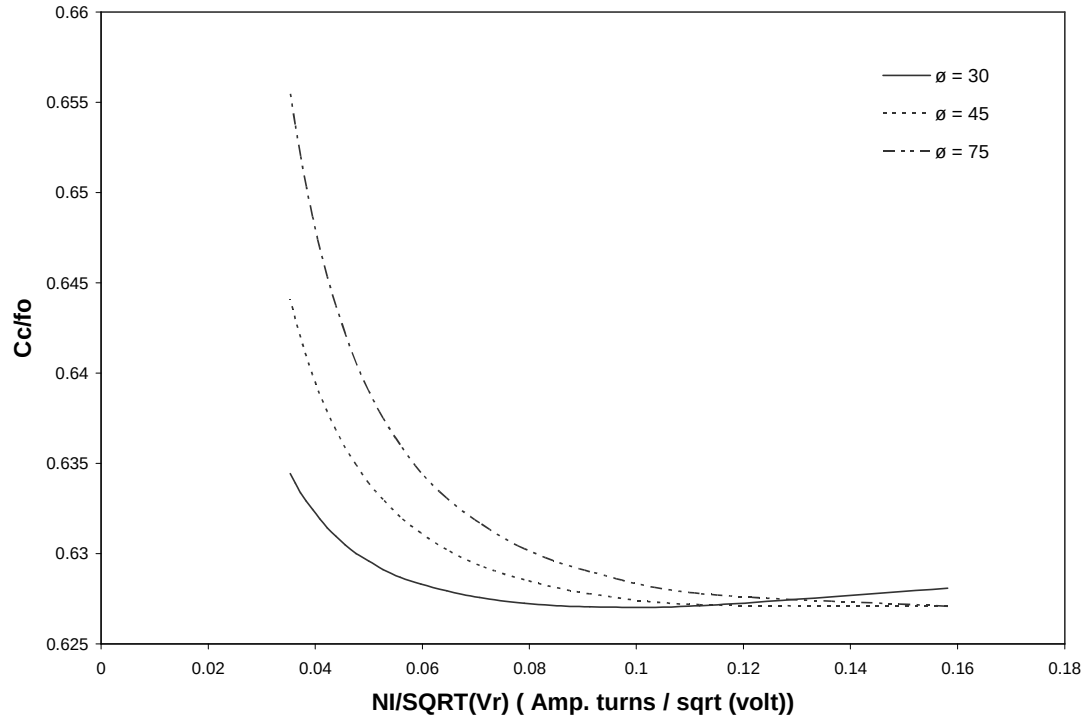

Figure (3-26): The relative chromatic aberration coefficient as a function of NI / SQRT(Vr) for ø = 30^{o}, 45^{o} and 75^{o} when H = 37mm.

The relation between Cs/fo and Cc/fo with the angle of saddle deflection coil ø is shown in figures (3-27) and (3-28), respectively at NI/SQRT(Vr) = 0.05. Both cases have the same behavior, where Cs/fo and Cc/fo are increased as the angle ø increases.

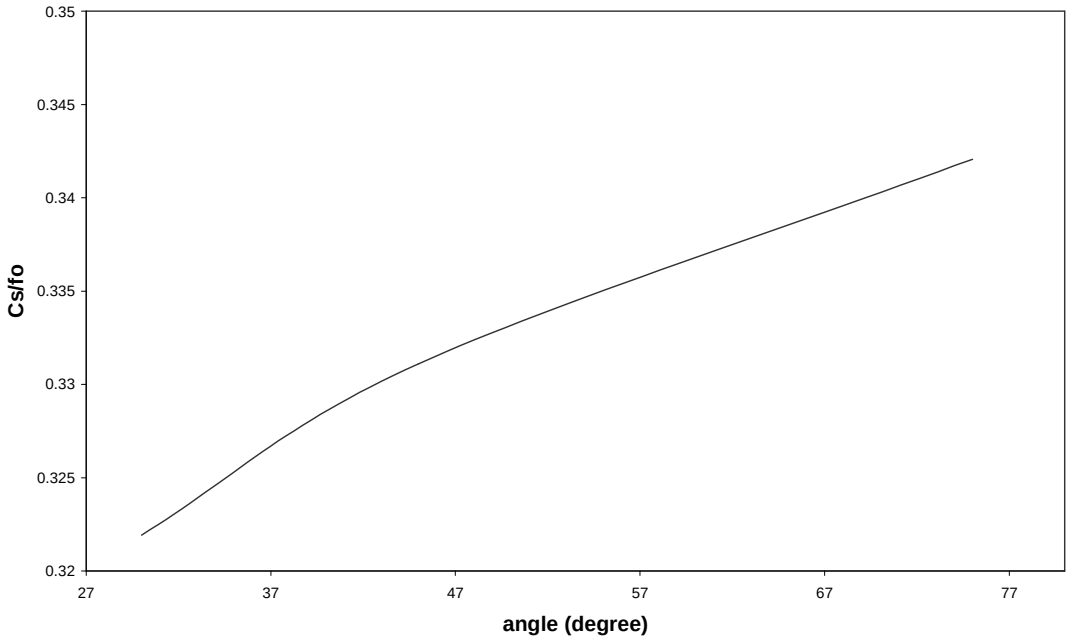

Figure (3-27): The relative spherical aberration coefficient as a function of the angle ø with H = 37mm at NI/SQRT(Vr) = 0.05.

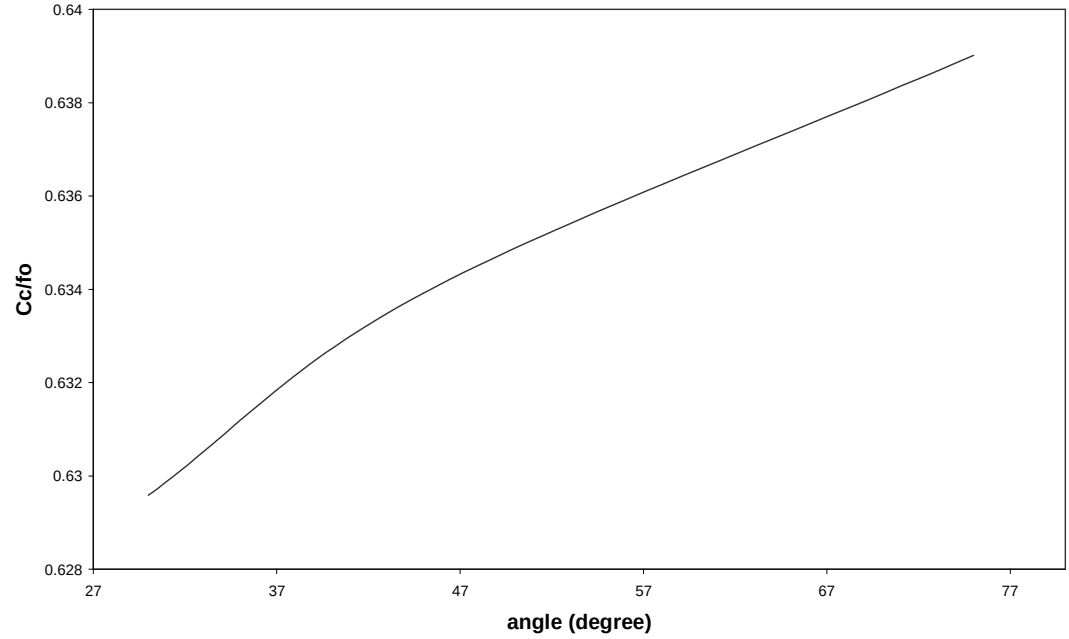

Figure (3-28): The relative chromatic aberration coefficient as a function of the angle ø with H = 37mm at NI/SQRT(Vr) = 0.05.

The shape of the upper half part of the pole piece is found by using reconstruction method for ø =30^{o} and H = 37mm is shown in figure (3-29).

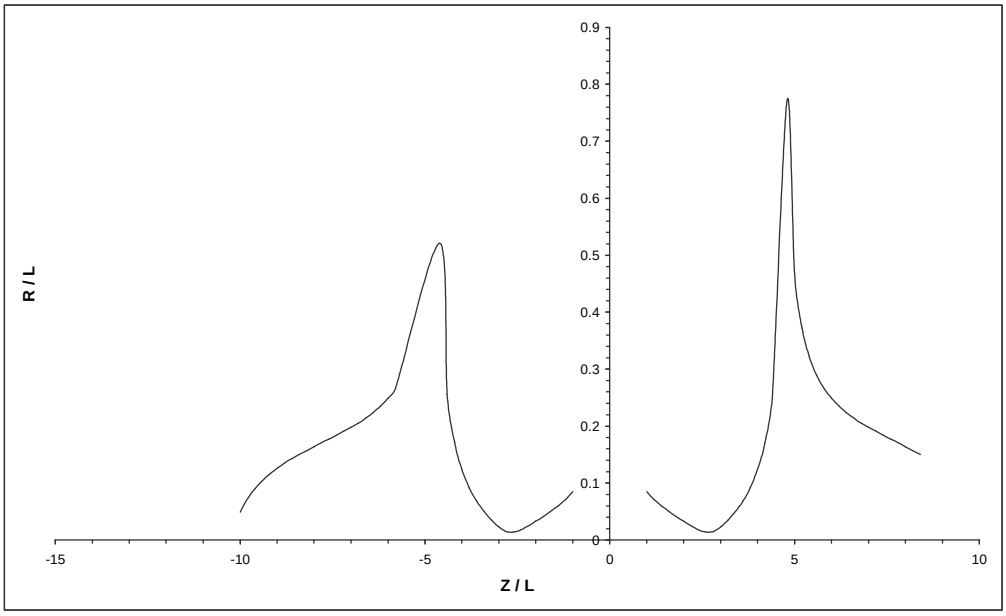

Figure (3-29): The pole piece shape when ø = 30^{o} and H = 37mm.

3-3-1-2 effects of changing the length of the coil

After finding that the angle ø = 30^{o} represents optimum angle which give us the minimum aberrations, we try to see the effect of changing the length of the coil. Therefore, we choose H= 37, 47 and 57mm and the results are shown in figure (3-30). From the figure one can find that the Cs/fo decrease as NI/SQRT(Vr) increase up to NI/SQRT(Vr) = 0.118 then the ratio Cs/fo will be increased as NI/SQRT(Vr) increases. All the curves intercept at NI/SQRT(Vr) = 0.118 and have the same value of Cs/fo. For coil length H = 57mm one can have the lower for Cs /fo up to NI/SQRT(Vr) = 0.118, while H =37mm represents the best length of the coil when NI/SQRT(Vr) > 0.118.

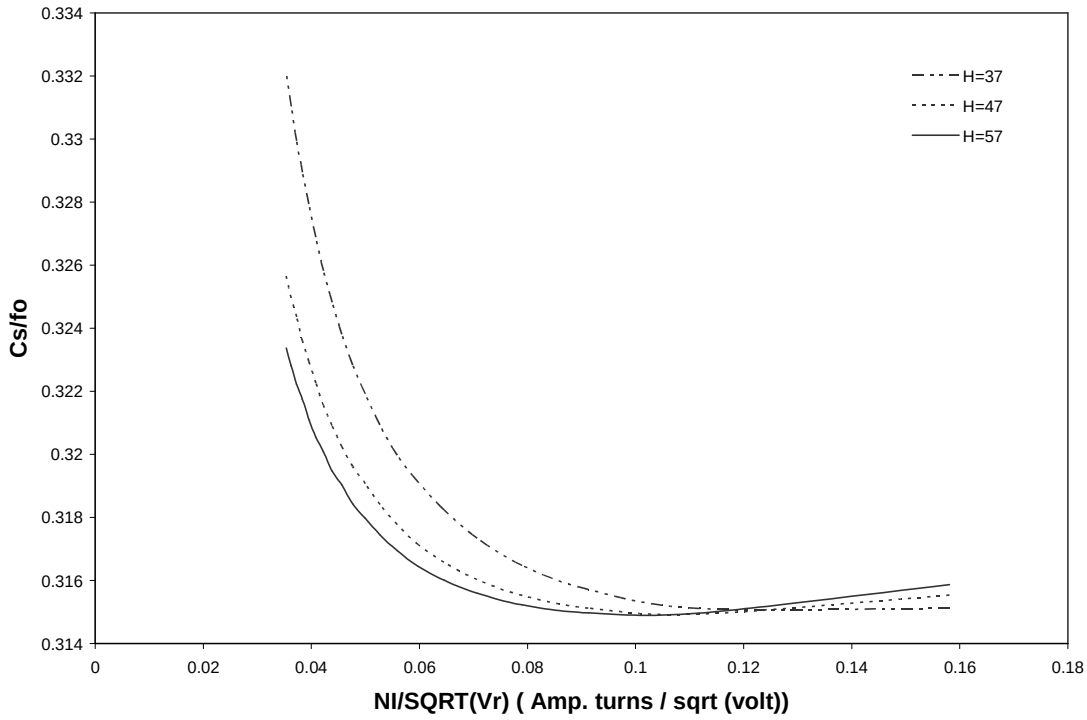

Figure (3-30): The relative spherical aberration coefficient as a function of NI / SQRT(Vr) for ø = 30^{o} with H = 37, 47 and 57mm.

Figure (3-31) shows the effect of variation of the coil length H on the Cc/fo. In this figure we find that the three curves take the same behavior of spherical aberration case. The relations between Cs/fo and Cc/fo with coil length H at NI/SQRT(Vr) = 0.05 are shown in figures (3-32) and (3-33), respectively. In the figures (3-30) and (3-31), the Cs/fo and Cc/fo very slightly decrease as H increases and this description is true up to NI/SQRT(Vr) = 0.118 for spherical case and up to 0.09 for chromatic case. Hence, when NI/SQRT(Vr) > 0.118 the behavior is reversed, i.e. Cs/fo and Cc/fo very slightly increase as coil length H increases.

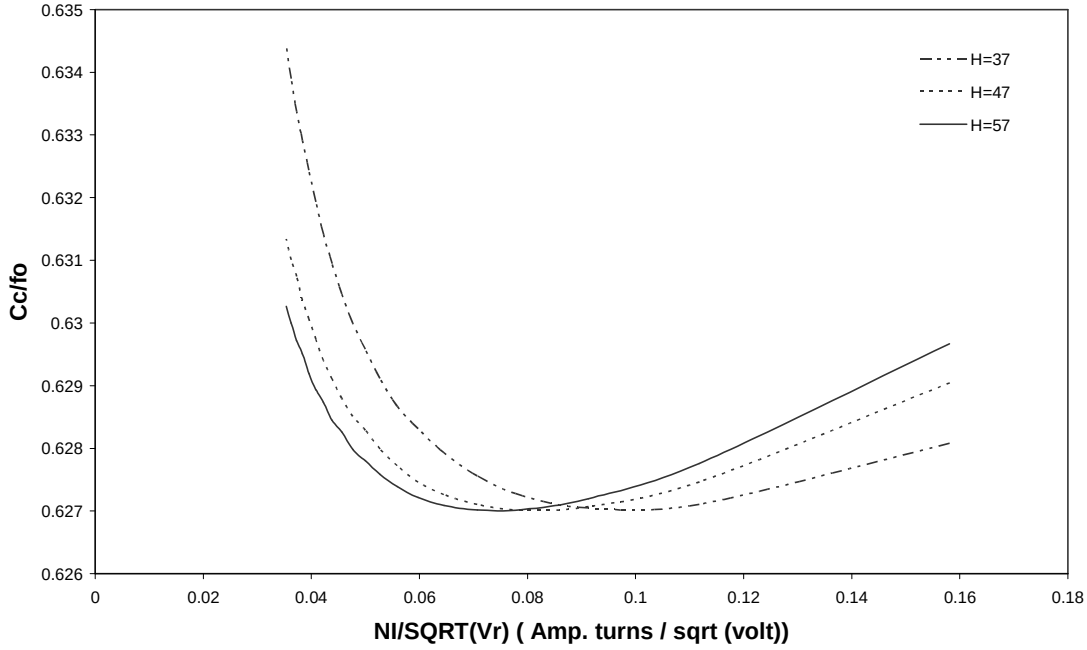

Figure (3-31): The relative chromatic aberration coefficient as a function of NI / SQRT(Vr) for ø = 30^{o} with H = 37, 47 and 57mm.

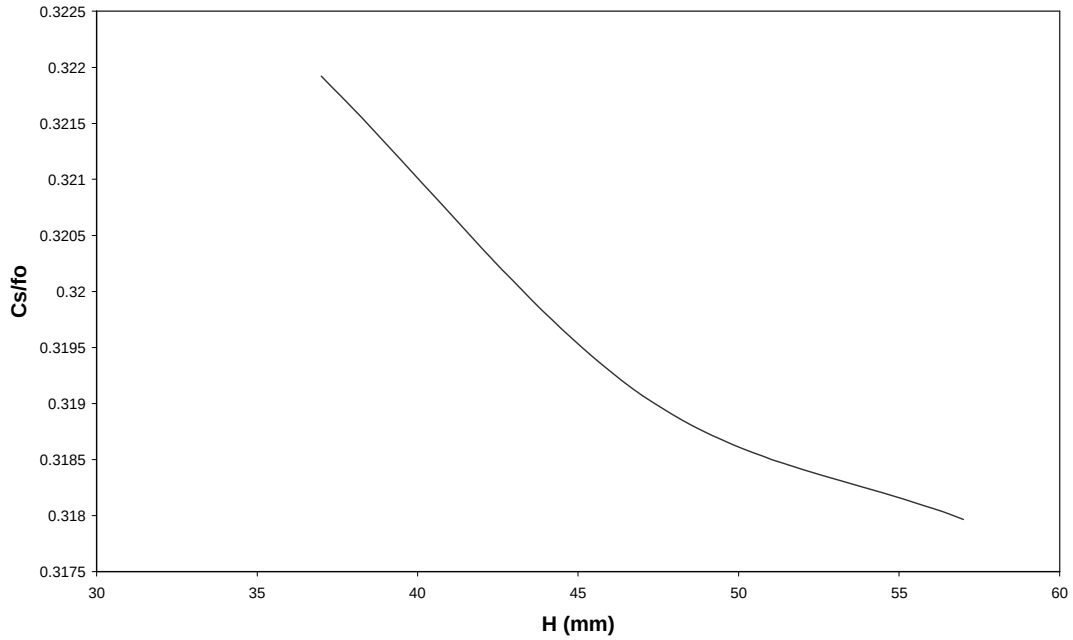

Figure (3-32): The relative spherical aberration coefficient as a function of the coil length H for $ø = 30^{o}$.

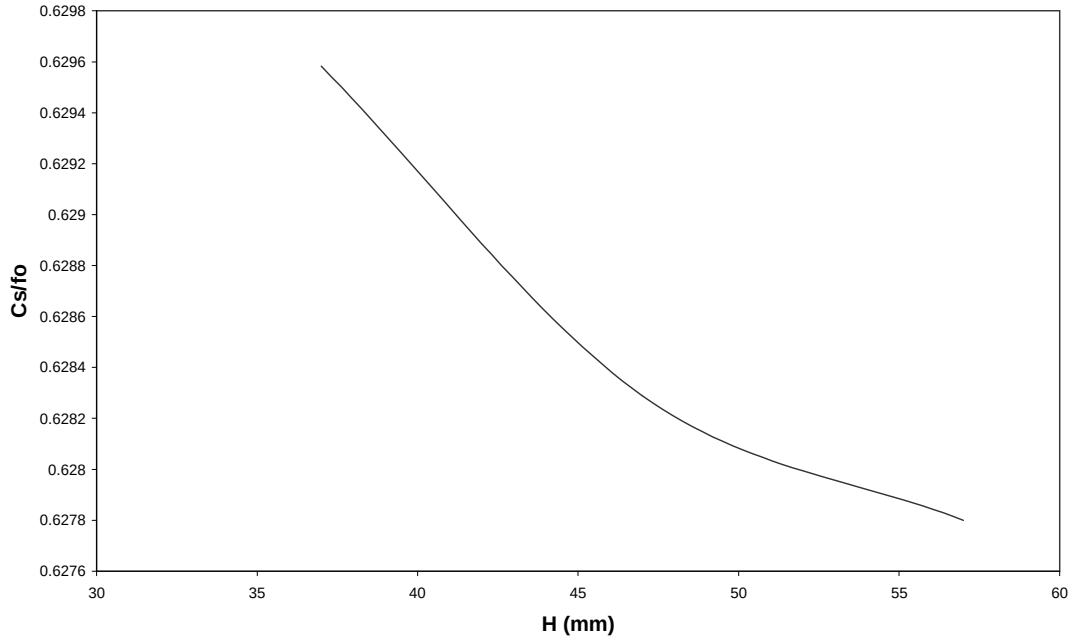

Figure (3-33): The relative chromatic aberration coefficient as a function of the coil length H for $ø = 30^{o}$.

The shape of the upper half part of the pole piece for ø = 30^{o} and H = 57mm shown in figure (3-34).

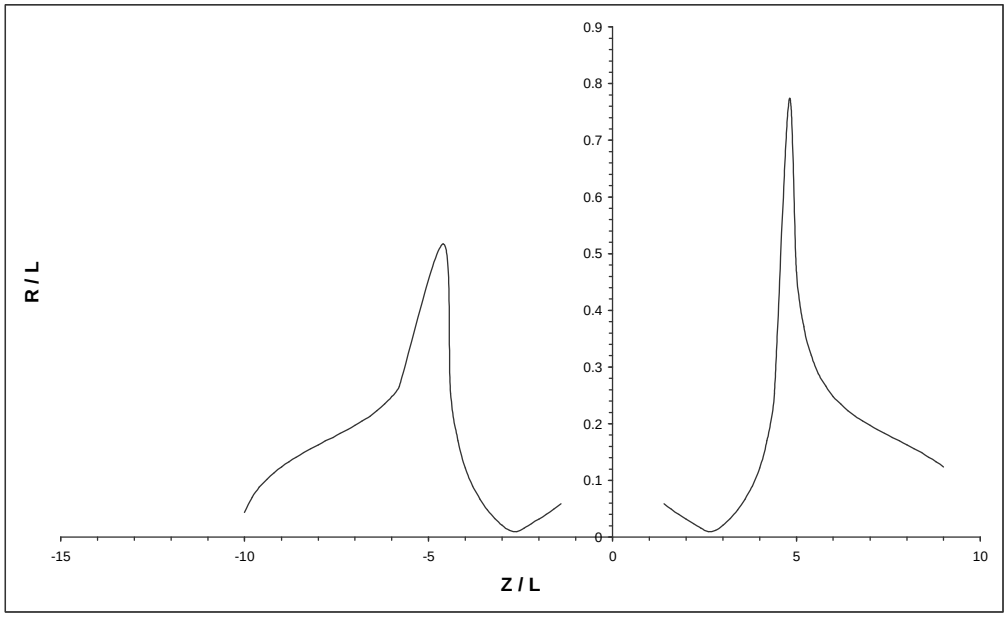

Figure (3-34): The pole piece shape when ø = 30^{o} and H = 57mm.

3-3-2 Zero magnification condition

3-3-2-1 effects of changing the angle

The spherical and chromatic aberrations are studied in this operating condition. Different angles, ø = 45^{o}, 50^{o} and 60^{o}, of saddle yoke coil are taken into account. Figure (3-35) represents the results of these calculations. In this figure, we find that the Cs/fo decreases as NI/SQRT(Vr) increases and all curves are closed to each other at the value of NI/SQRT(Vr) higher than 0.1 . Also, we find that the ø = 45^{o} gives us the optimum angle and the values of Cs/fo of ø = 45^{o} for wide range of NI/SQRT(Vr) appear to be constant.

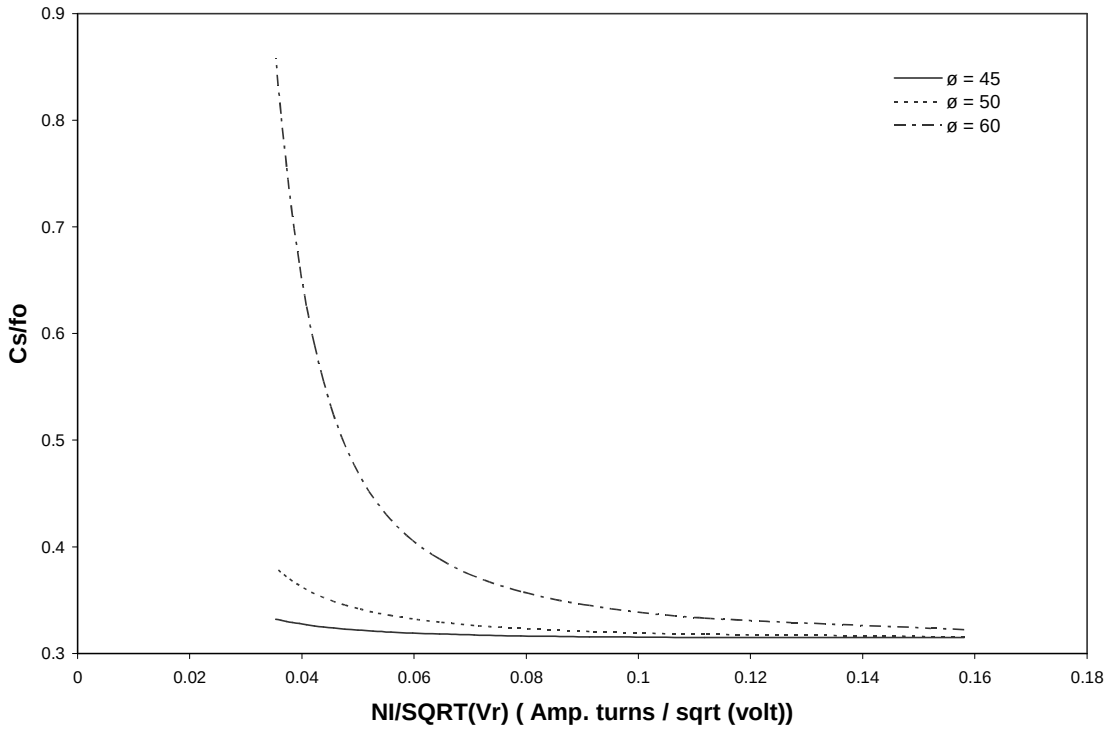

Figure (3-35): The relative spherical aberration coefficient as a function of NI / SQRT(Vr) for ø = 45^{o}, 50^{o} and 60^{o} when H = 37mm.

Figure (3-36) represents the results of chromatic aberration. From the calculations of three angles we find that the three curves take the same behavior of spherical aberration case. The relation between Cs/fo and Cc/fo with the angle of saddle deflection coil is shown in figures (3-37) and (3-38), respectively with NI/SQRT(Vr) = 0.05. In both cases the Cs/fo and Cc/fo increase as the angle increases.

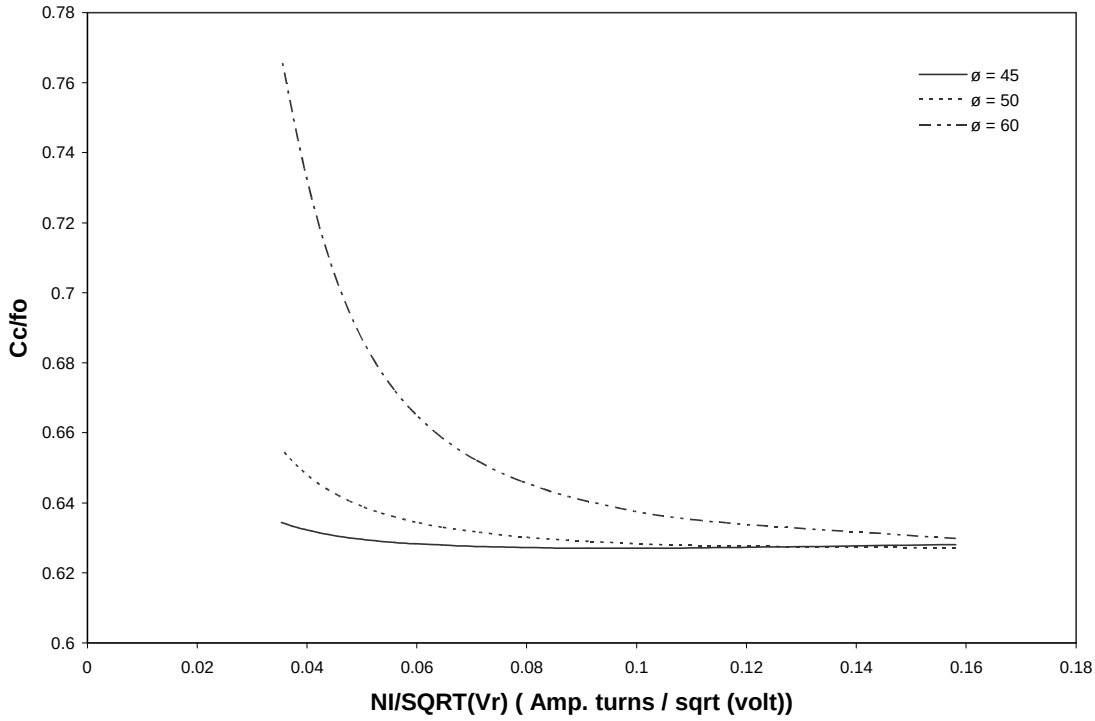

Figure (3-36): The relative chromatic aberration coefficient as a function of NI / SQRT(Vr) for ø = 45^{o}, 50^{o} and 60^{o} when H = 37mm.

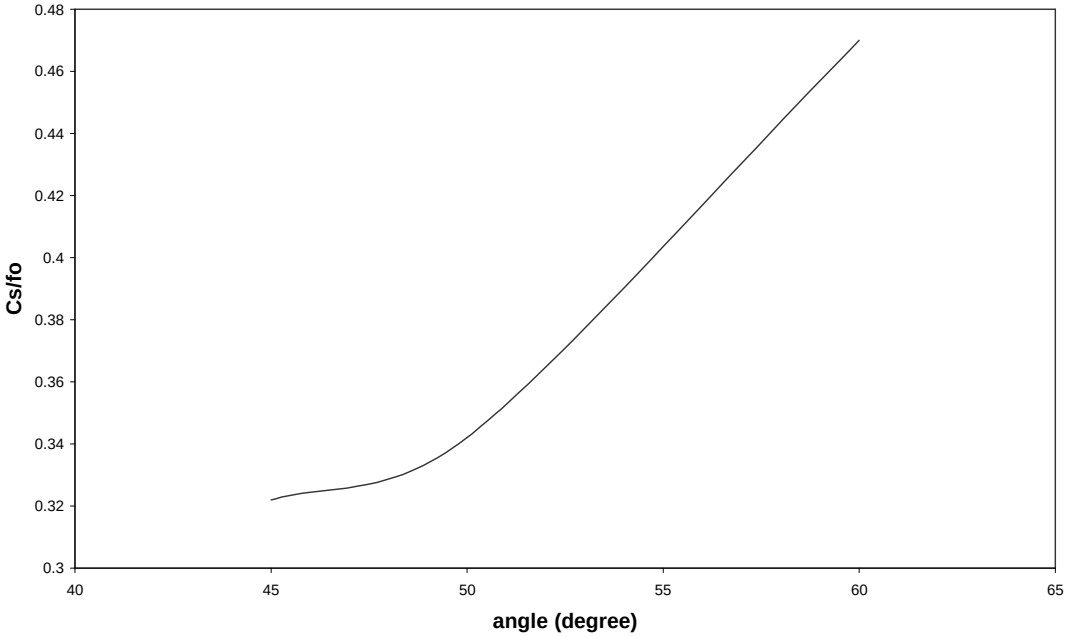

Figure (3-37): The relative spherical aberration coefficient as a function of the angle ø with H = 37mm.

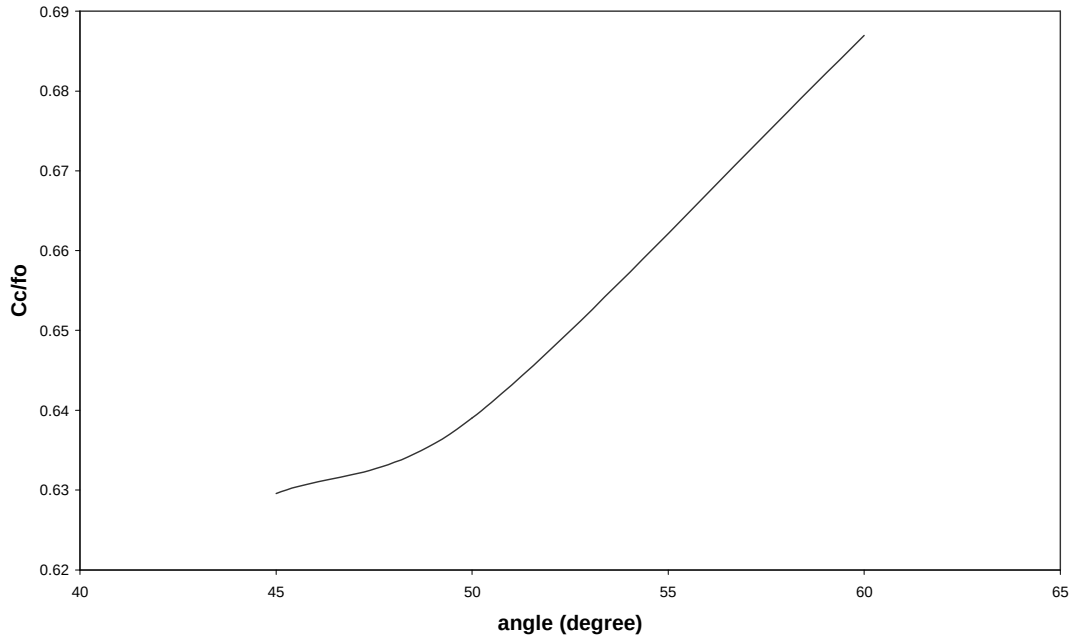

Figure (3-38): The relative chromatic aberration coefficient as a function of the angle ø with H = 37mm.

The shape of the upper half part of the pole piece for ø = 45^{o} and H = 37mm is shown in figure (3-39), where it is found by using the reconstruction method.

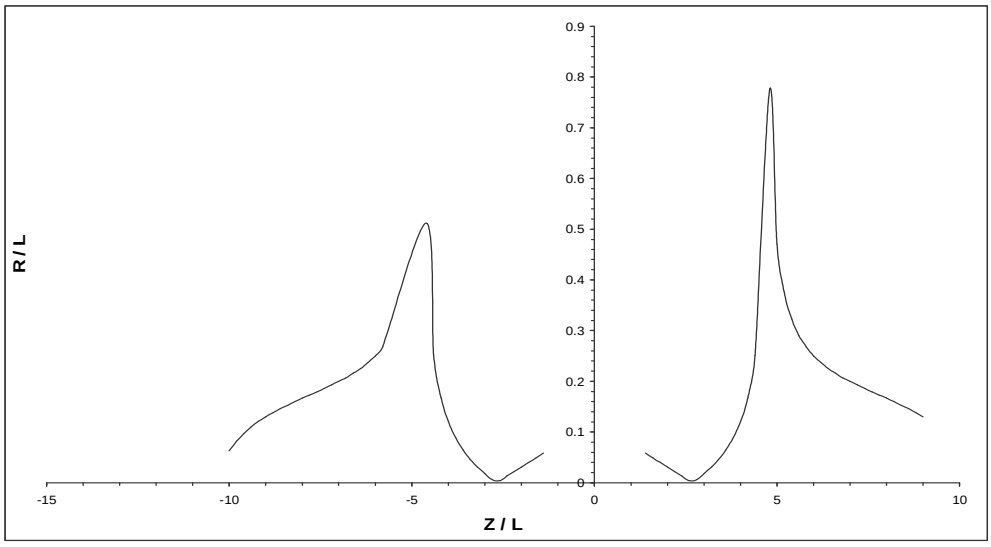

Figure (3-39): The pole piece shape when ø = 45^{o} and H = 37mm.

3-3-2-2 effects of changing the length of coil

Different value of length of the coil, H = 37, 57 and 67mm with ø = 45^{o}, are studied to find the optimum length which give us the best values of Cs/fo and Cc/fo. The results of spherical aberration are shown in figure (3-40). In this figure, we find that the H = 67mm represents the optimum length. The effect of changing the length of the coil on chromatic aberration is shown in figures (3-41). In this figure it appears that the H = 67mm gives the best result up to NI / SQRT(Vr) = 0.09, while H = 37mm represent the best length of the coil when NI / SQRT(Vr) > 0.09 .

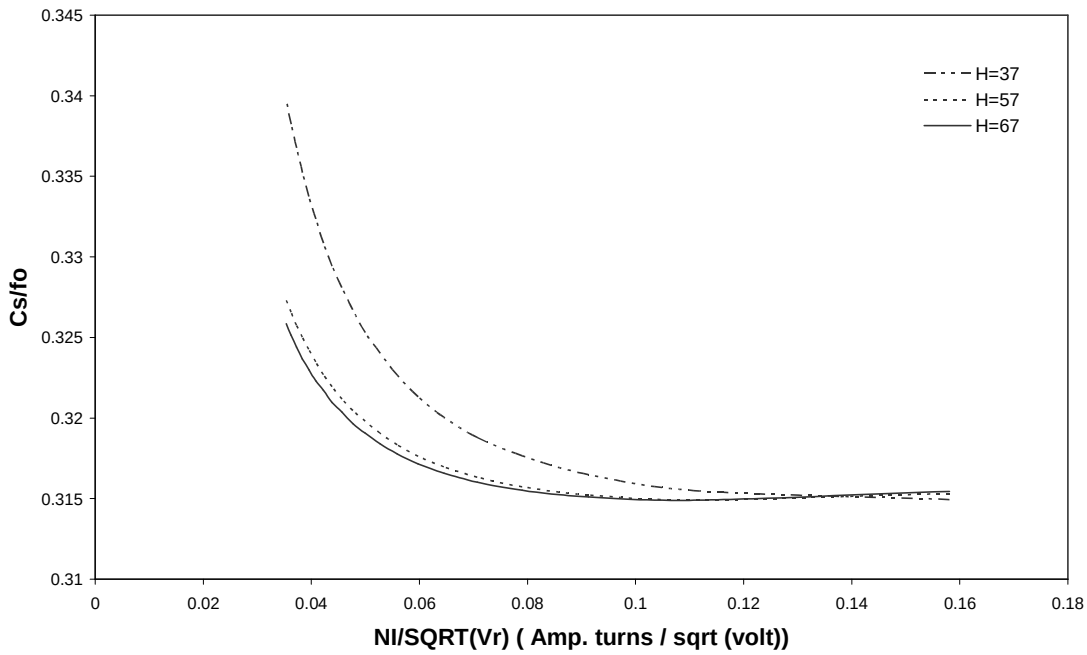

Figure (3-40): The relative spherical aberration coefficient as a function of NI / SQRT(Vr) for ø = 45^{o} with H = 37, 57 and 67mm.

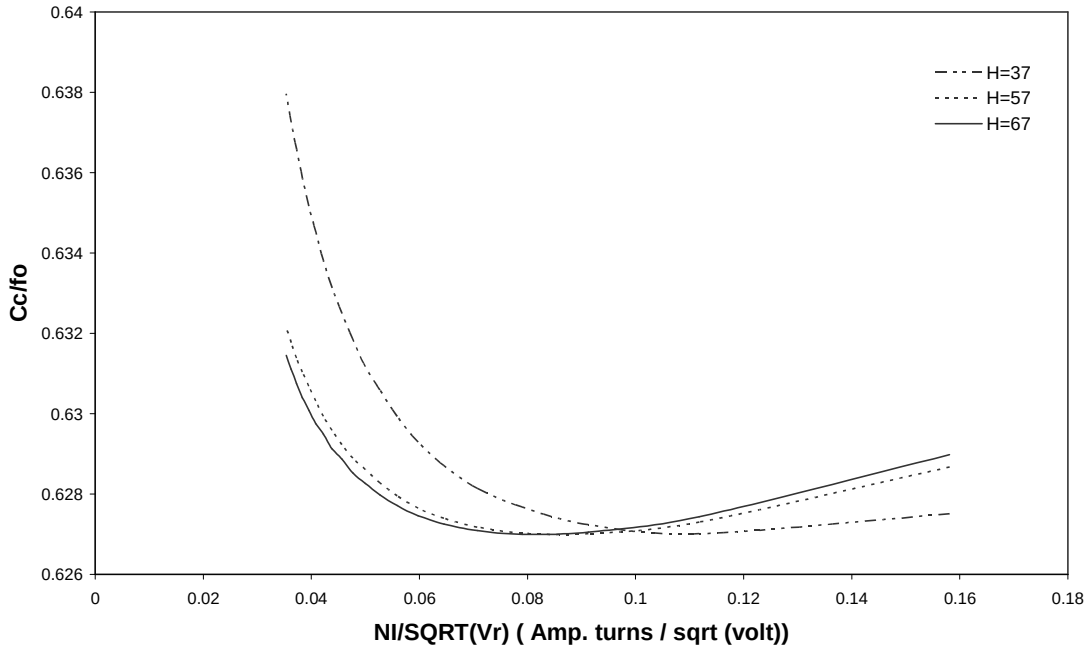

Figure (3-41): The relative chromatic aberration coefficient as a function of NI / SQRT(Vr) for ø = 45^{o} with H = 37, 57 and 67mm.

The relation between Cs/fo and Cc/fo with the length of the coil is shown in figures (3-42) and (3-43), respectively for NI/SQRT(Vr) = 0.05. The Cs/fo and Cc/fo decrease as the length of the coil increases. This behavior is true up to NI/SQRT(Vr) = 0.13 for spherical aberration and up to 0.095 for chromatic aberration and the values of Cs/fo and Cc/fo will increase as NI/SQRT(Vr) > 0.13 for spherical and 0.095 for chromatic aberration.

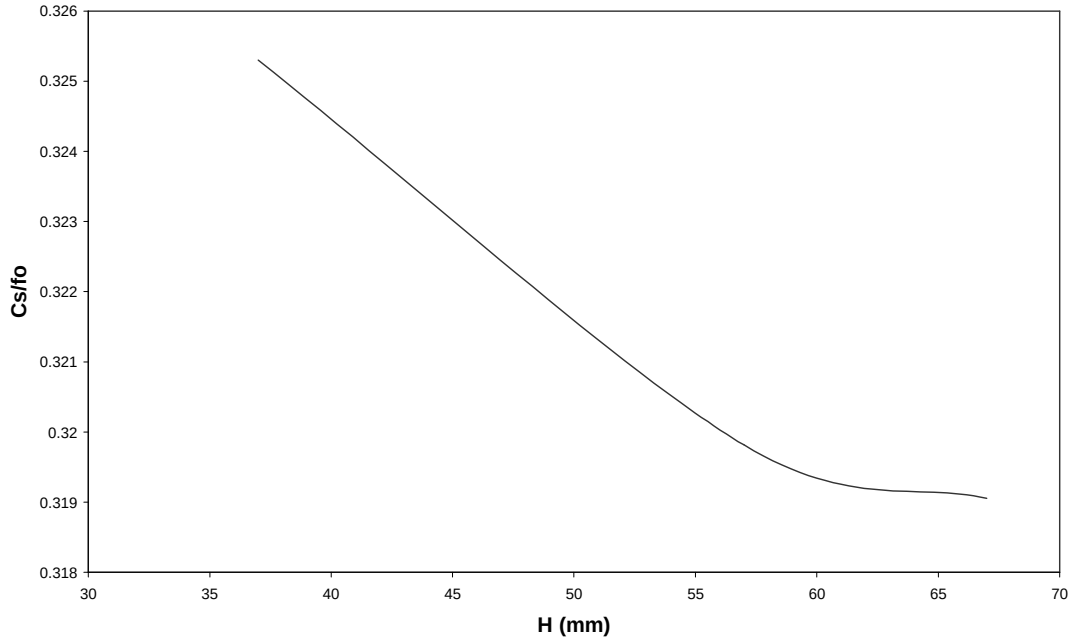

Figure (3-42): The relative spherical aberration coefficient as a function of the coil length with constant angle $\phi = 45^{o}$.

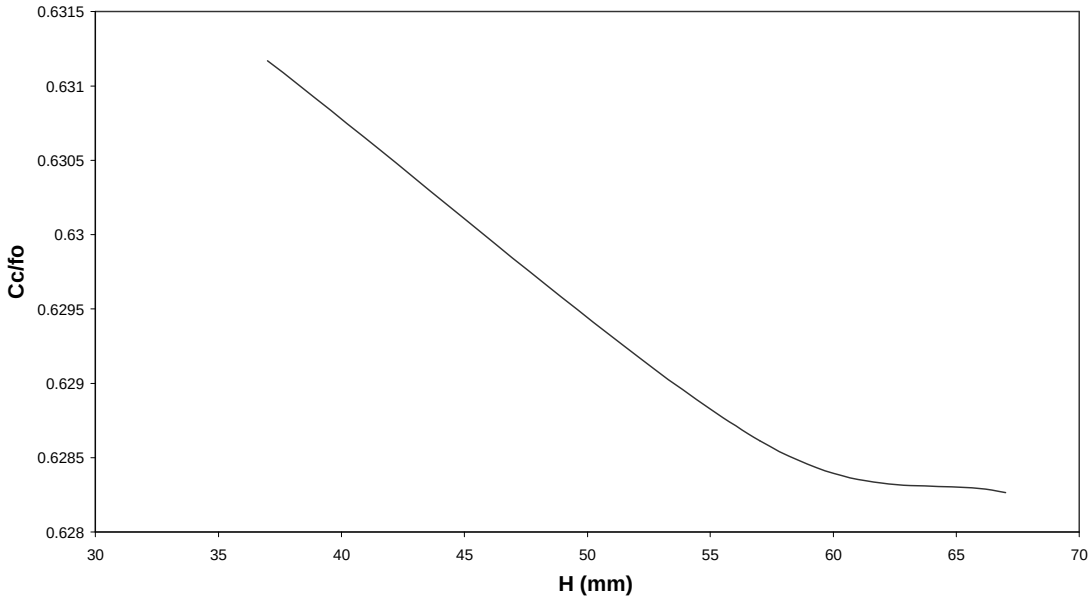

Figure (3-43): The relative chromatic aberration coefficient as a function of the coil length with constant angle $\phi = 45^{o}$.

The shape of the upper half part of the pole piece of ø = 45^{o} and H = 67mm is given in figure (3-44).

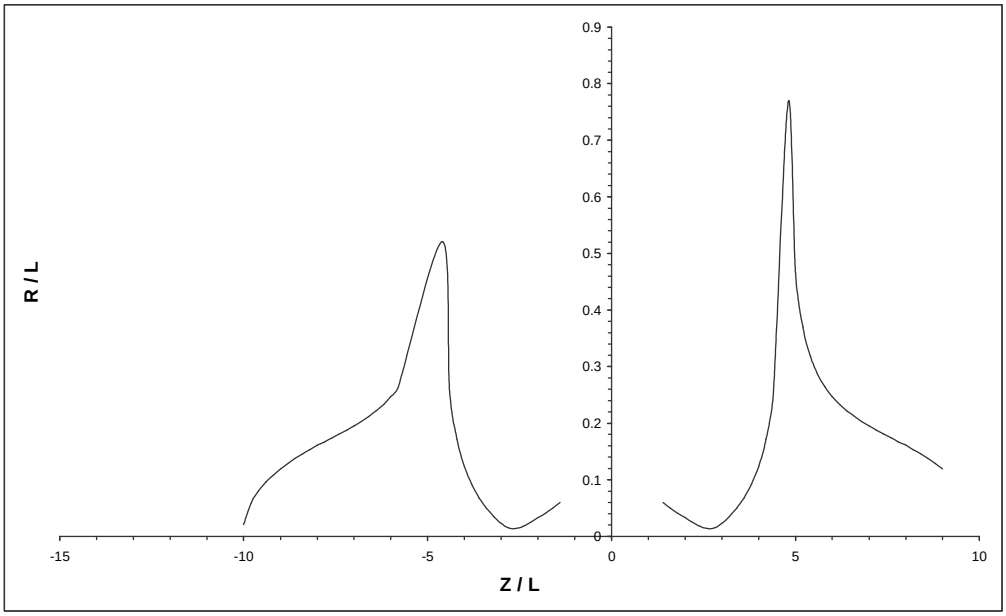

Figure (3-44): The pole piece shape when ø = 45^{o} and H = 67mm.

3-4 The Design By Using New Suggestion Field Distribution

In order to reduce the spherical and / or chromatic aberrations we have suggested new deflection field distribution and we have studied both spherical and chromatic aberrations. We choose the geometrical shape of the deflection yoke coil which gives us optimum properties in both Glaser and Grivet-Lenz models. We find that the spherical and chromatic aberrations can be reduced in many cases.

The suggestion deflection field distribution is given by:

$$D(z) = -B_m\,(z-10)\,\exp[-5(z+5)^2] \qquad (3-3)$$

The shape of axial deflection field distribution of suggestion field distribution is shown in figure (3-45).

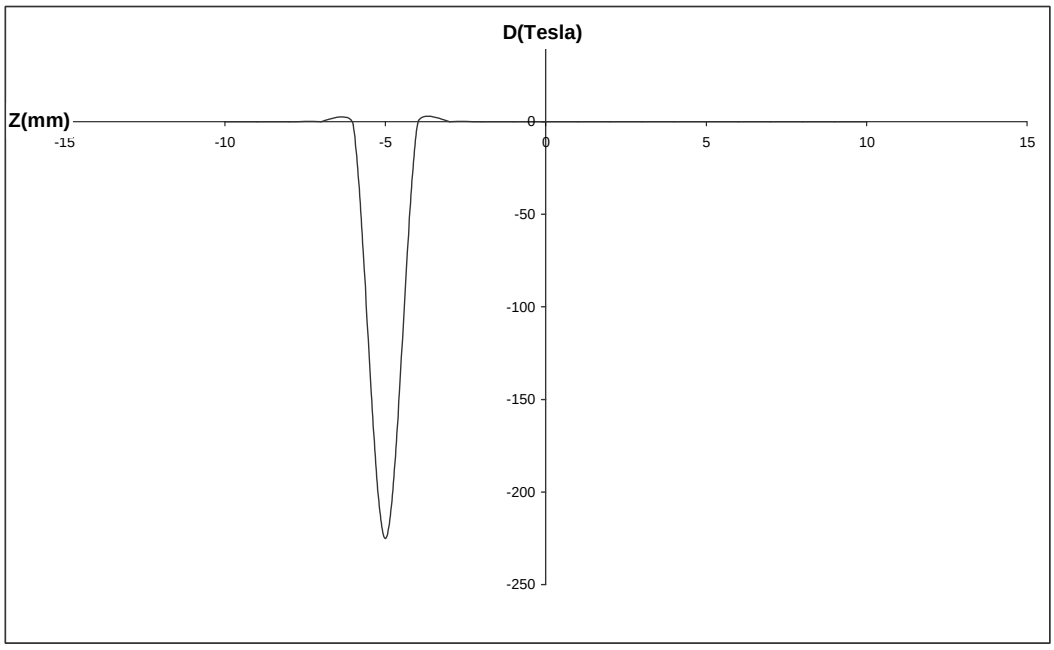

Figure (3-45): The axial deflection flux density distribution *D(z)* calculated with suggestion new field distribution model.

3-4-1 Comparison with Glaser model

3-4-1-1 infinite magnification condition

In results of Glaser model we find that the best result due to the geometrical shape of coil angle ø = 60^{o} and the coil length H = 27mm. This dimension is used in the present field distribution and the results of spherical and chromatic aberration are shown in figures (3-46) and (3-47), respectively. Under this operating condition, the new field distribution failure to reduce the spherical and chromatic aberrations. The shape of the upper quarter part of the pole piece for ø = 60^{o} and H = 27mm which is calculated by using the present new field distribution is shown in figure (3-48).

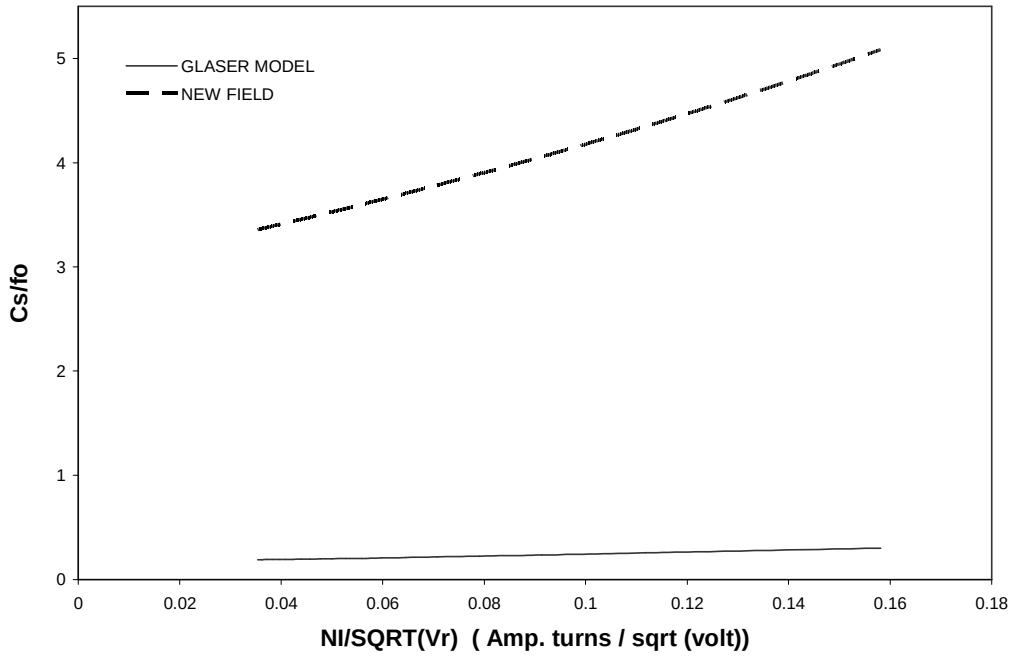

Figure (3-46): Comparison between the relative spherical aberration coefficient calculations for Glaser model and new suggestion field for ø = 60^{o} and H = 27mm.

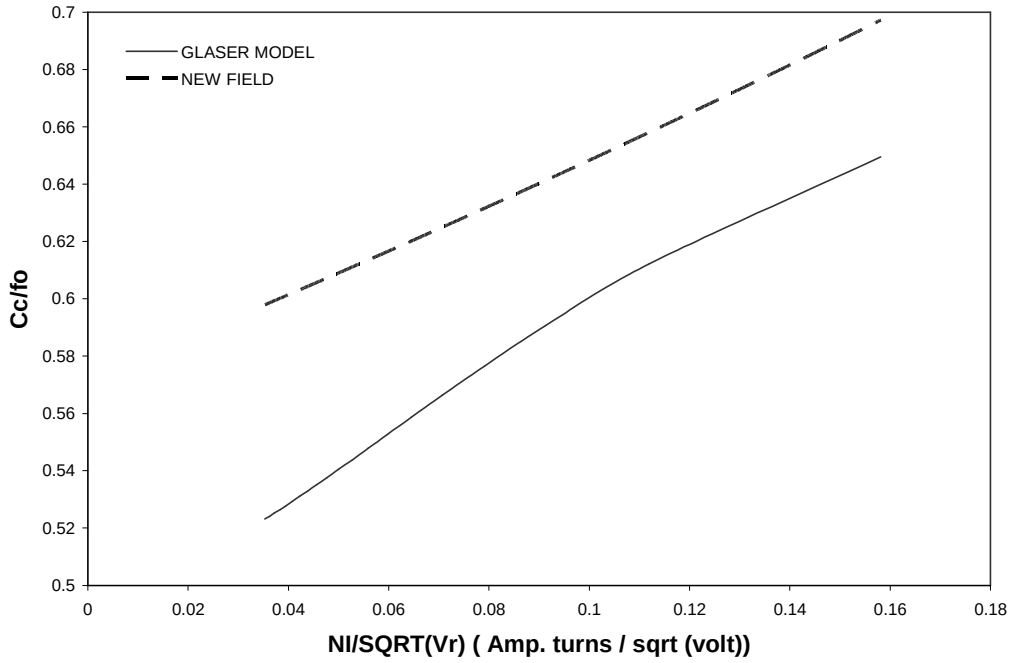

Figure (3-47): A comparison between the relative chromatic aberration coefficient calculations for Glaser model and the new suggestion field for ø = 60^{o} and H = 27mm.

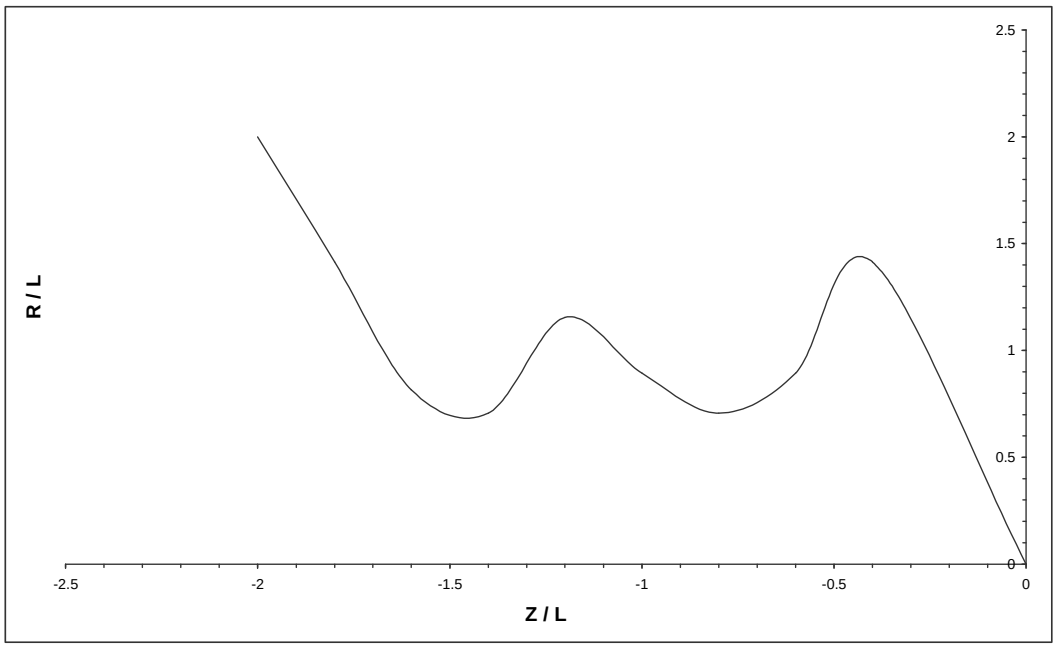

Figure (3-48): The pole piece shape when ø = 60^{o} and H = 27mm.

3-4-1-2 zero magnification condition

In this operating condition, the geometrical shape of the saddle deflection yoke coil of angle ø = 75^{o} and H = 27mm, which gives us the best result in Glaser model, is taken into account. The calculation by using the new field distribution shows that both spherical and chromatic aberrations can be reduced under this operating condition and one can optimized the result by using the new deflection field distribution as is shown in figures (3-49) and (3-50) and the upper quarter part of the pole piece is shown in figure (3-51).

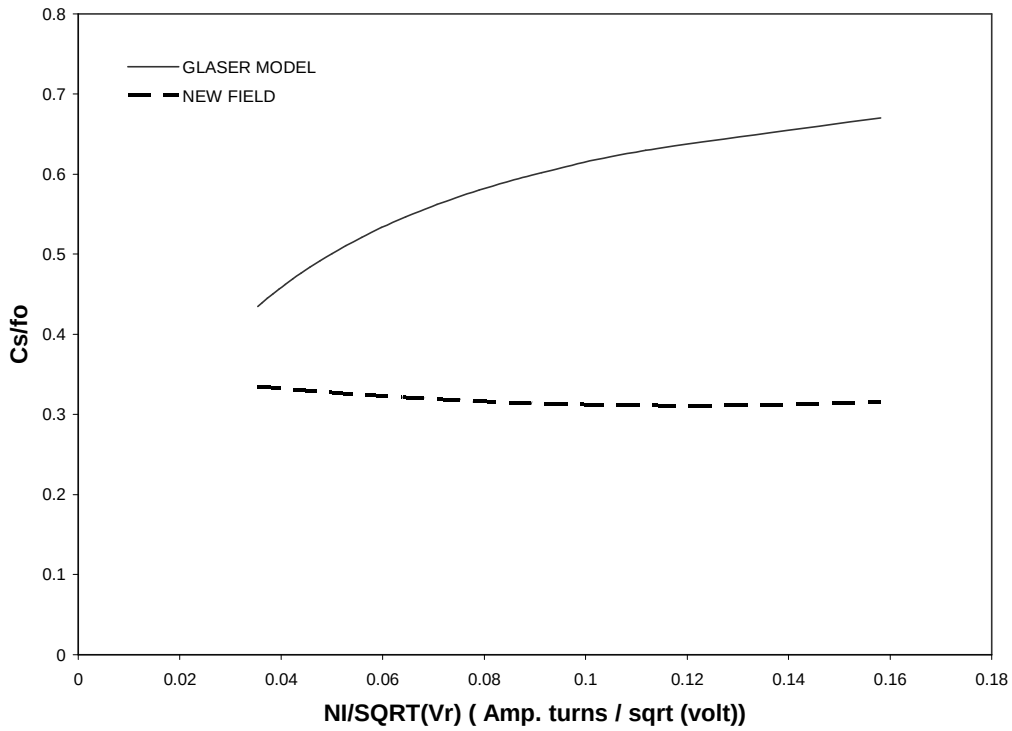

Figure (3-49): A comparison between the relative spherical aberration coefficient calculations for Glaser model and the new suggestion field for ø = 105^{o} and H = 27mm.

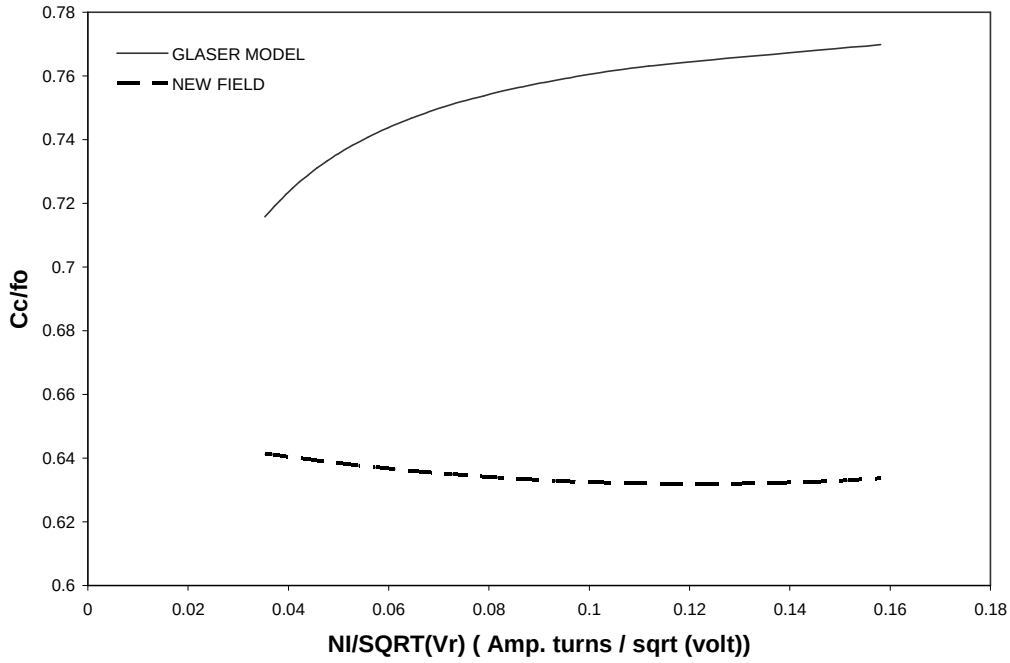

Figure (3-50): A comparison between the relative chromatic aberration coefficient calculations for Glaser model and the new suggestion field for ø = 75^{o} and H = 27mm.

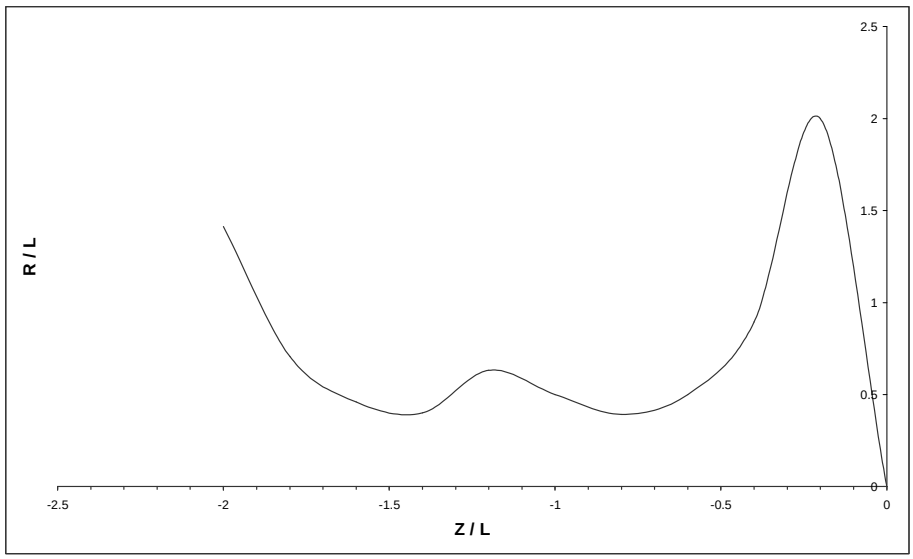

Figure (3-51): The pole piece shape when ø = 75^{o} and H = 27mm.

3-4-2 Comparison with Grivet-Lenz model

3-4-2-1 infinite magnification condition

In this operating condition, the two best dimensions of optimum result in Grivet-Lenz model are taken into account. Firstly, the angle $ø = 30^{o}$ and the length of coil H = 37mm are studied and the results of spherical and chromatic aberrations are shown in the figures (3-52) and (3-53). From the two figures, one can find that our new field distribution succeeds in reducing only the spherical aberration, giving us a good result for a spherical aberration case in comparison to Grivet-Lenz calculations. Also, the results for chromatic aberrations stile acceptable with very small increasing. Secondly, the angle $ø = 30^{o}$ and the length of coil H = 57mm are used to calculate the spherical n and chromatic aberrations and the results are shown in figures (3-54) and (3-55). Also, the new field distribution calculations succeeds in reducing the value of spherical aberration and the results for chromatic aberrations stile acceptable with slightly increasing.

Finally, we find that the new field distribution can be used successfully in the calculation of both spherical and chromatic aberrations and it gives us a very acceptable result in this case.

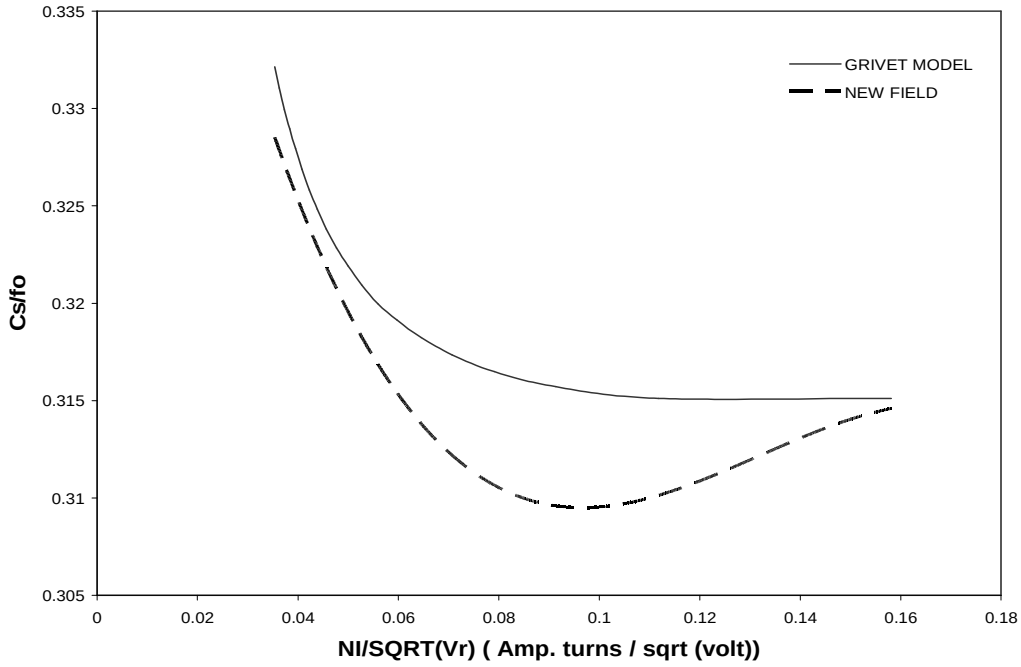

Figure (3-52): A comparison between the relative spherical aberration coefficient calculations of Grivet-Lenz model and a new suggestion field for ø = 30^{o} and H = 37.

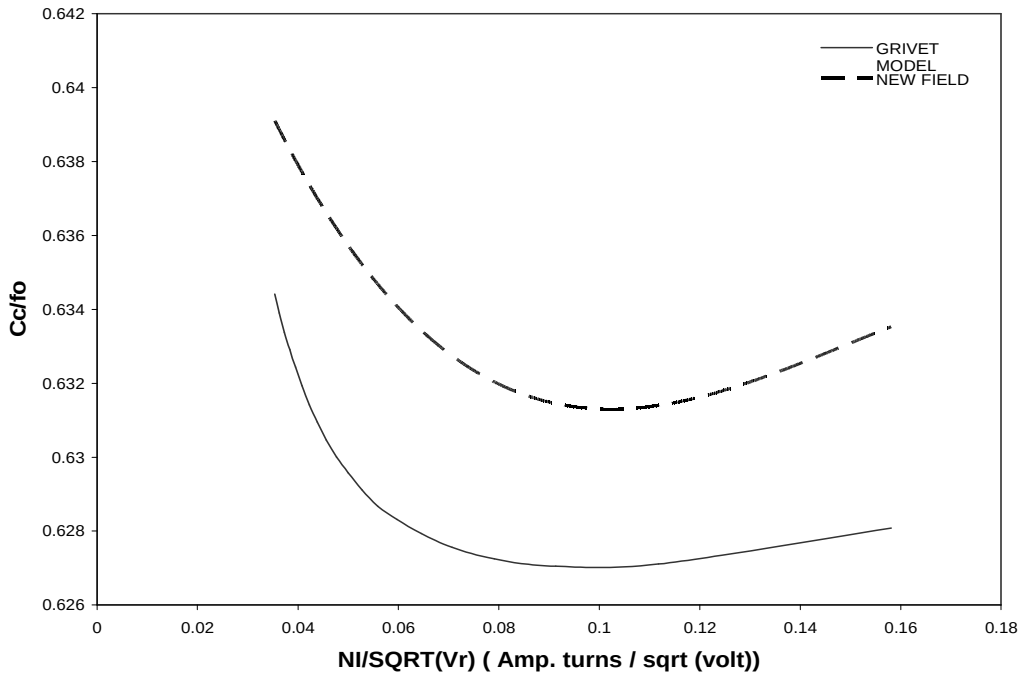

Figure (3-53): A comparison between the relative chromatic aberration coefficient calculations of Grivet-Lenz model and a new suggestion field for ø = 30^{o} and H = 37.

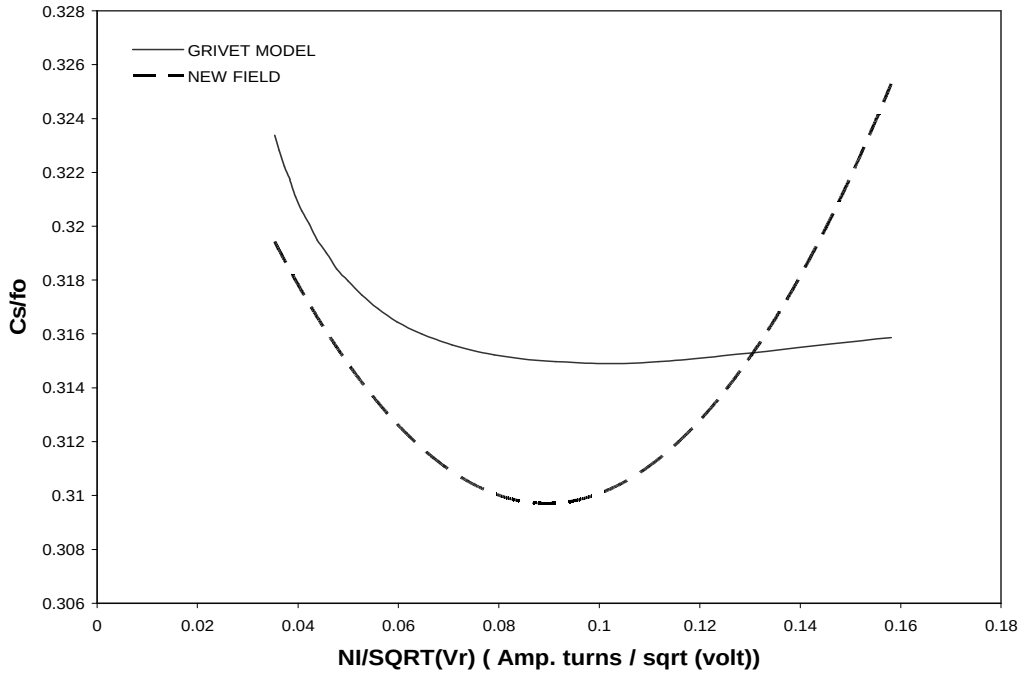

Figure (3-54): A comparison between the relative spherical aberration coefficient calculations of Grivet-Lenz model and a new suggestion field for ø = 30^{o} and H = 57.

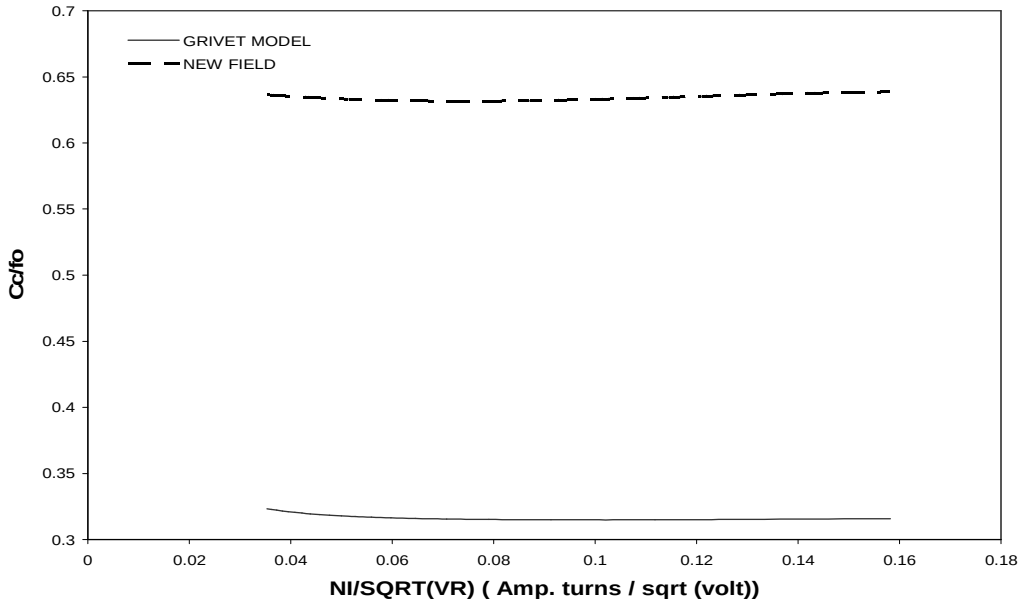

Figure (3-55): Comparison between the relative chromatic aberration coefficient calculations for Grivet-Lenz model and new suggestion field for ø = 30^{o} and H = 57.

The shape of upper quarter part of the pole piece for ø = 30^{o} with H = 37mm is shown in figure (3-56).

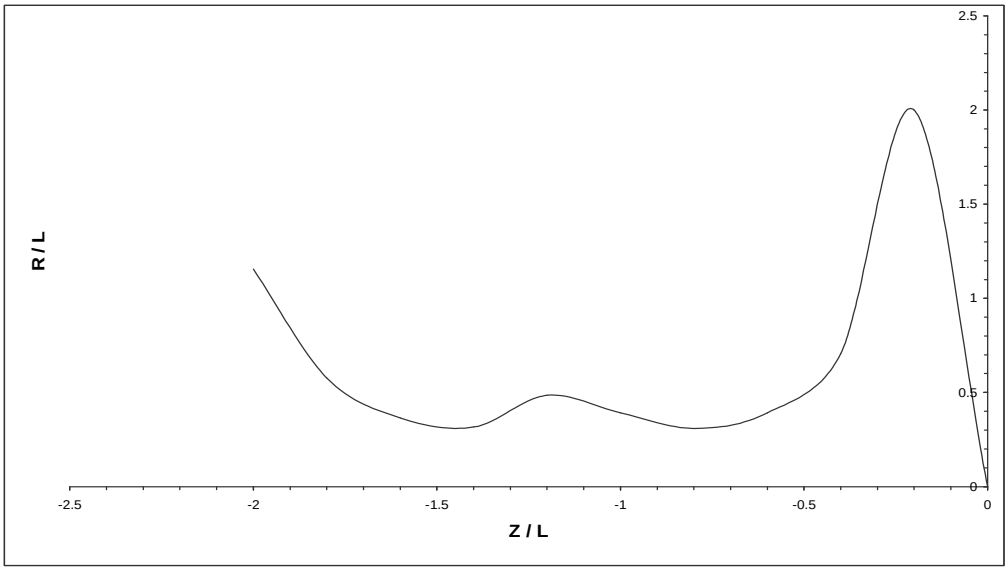

Figure (3-56): The pole piece shape when ø = 30^{o} and H = 37mm.

The shape of the upper quarter part of the pole piece for ø = 30^{o} with H = 57mm is shown in figure (3-57).

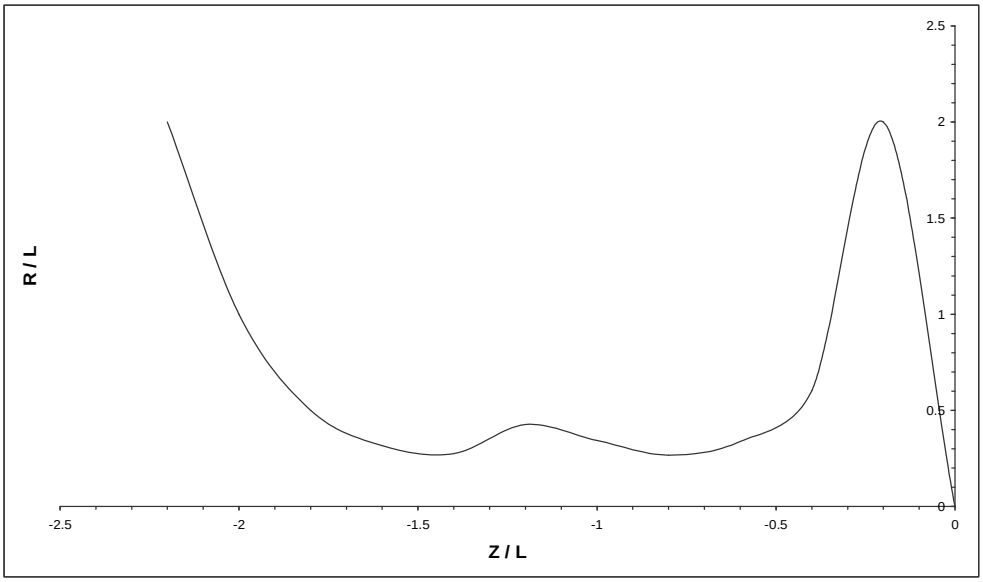

Figure (3-57): The pole piece shape when ø = 30^{o} and H = 57mm.

3-4-2-2 zero magnification condition

In this operating condition, the optimum two cases of Grivet-Lenz model have been studied. Firstly, the case of ø = 45^{o} and H = 37mm are studied and the results of spherical and chromatic aberrations are shown in figures (3-58) and (3-59). Spherical aberration can be reduced by new field distribution calculation. In figure (3-58), the values of Cs / fo for a new field distribution calculations is smaller than that of Grivet-Lenz model calculations and it gives best results up to NI / SQRT(Vr) = 0.12 and the two curves take the same value of Cs / fo at this point and after it the values of Cs / fo of new field distribution calculations have slightly increased in comparison with Grivet-Lenz model. Secondly, the case of ø = 45^{o} and H = 67mm are studied and both spherical and chromatic aberrations results are shown in figures (3-60) and (3-61). The new field distributions succeeds in reducing spherical aberration at the lower values of the ratio NI / SQRT(Vr) up to 0.1 and after this value the quotient Cs / fo is still acceptable with a slight increase in comparison with Grivet-Lenz model calculations as shown in figure (3-60). From figures (3-59) and (3-61), one can show that the values of quotient Cs / fo for a new field distribution calculations have a very small increase in comparison with Grivet-Lenz model calculations but this result is still acceptable and gives a better result.

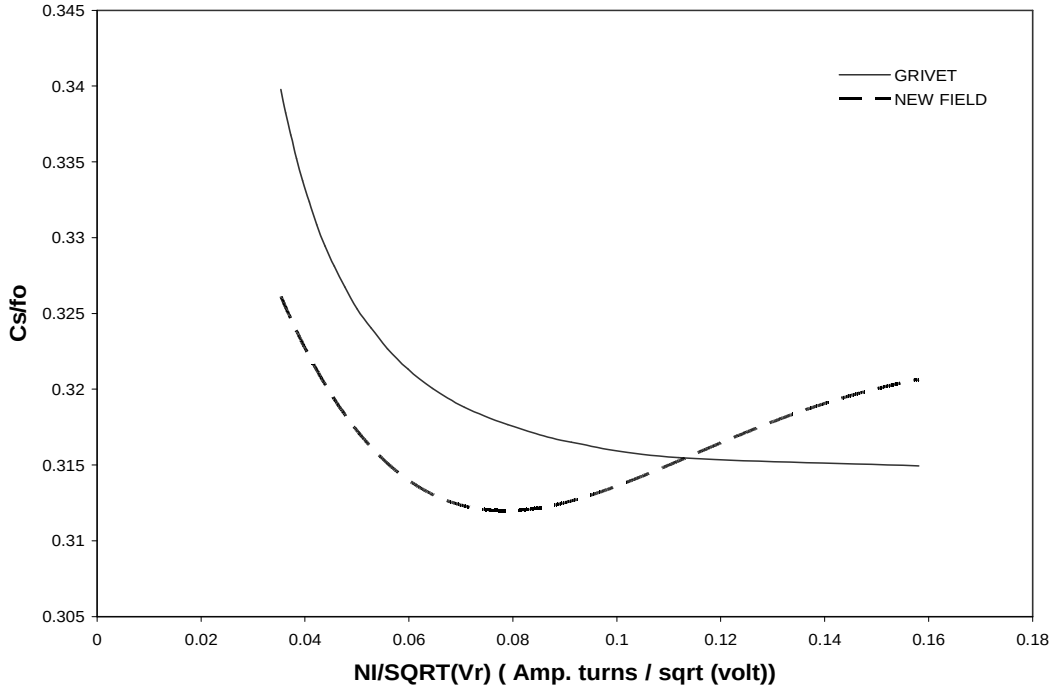

Figure (3-58): A comparison between the relative spherical aberration coefficient calculations of Grivet-Lenz model and a new suggestion field for ø = 45^{o} and H = 37.

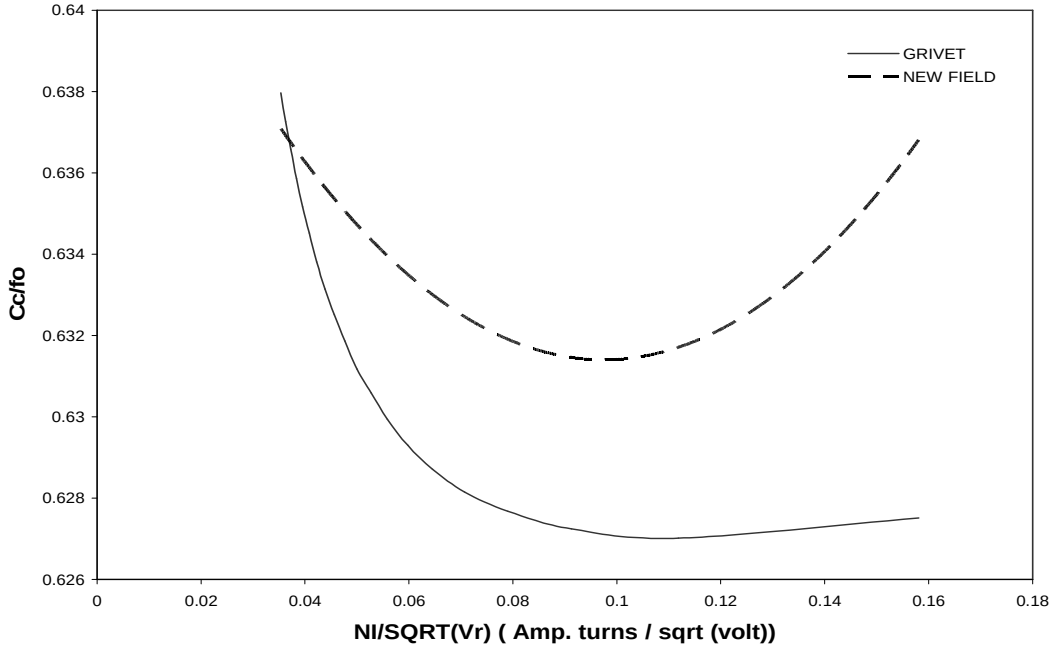

Figure (3-59): A comparison between the relative chromatic aberration coefficient calculations of Grivet-Lenz model and a new suggestion field for ø = 45^{o} and H = 37.

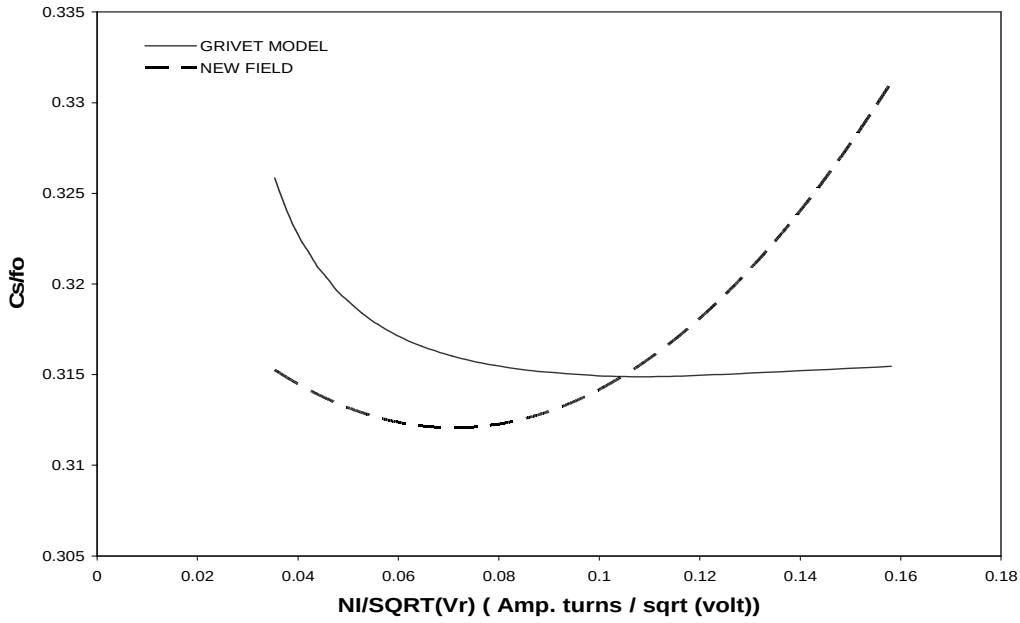

Figure (3-60): Comparison between the relative spherical aberration coefficient calculations for Grivet-Lenz model and new suggestion field for ø = 45^{o} and H = 67.

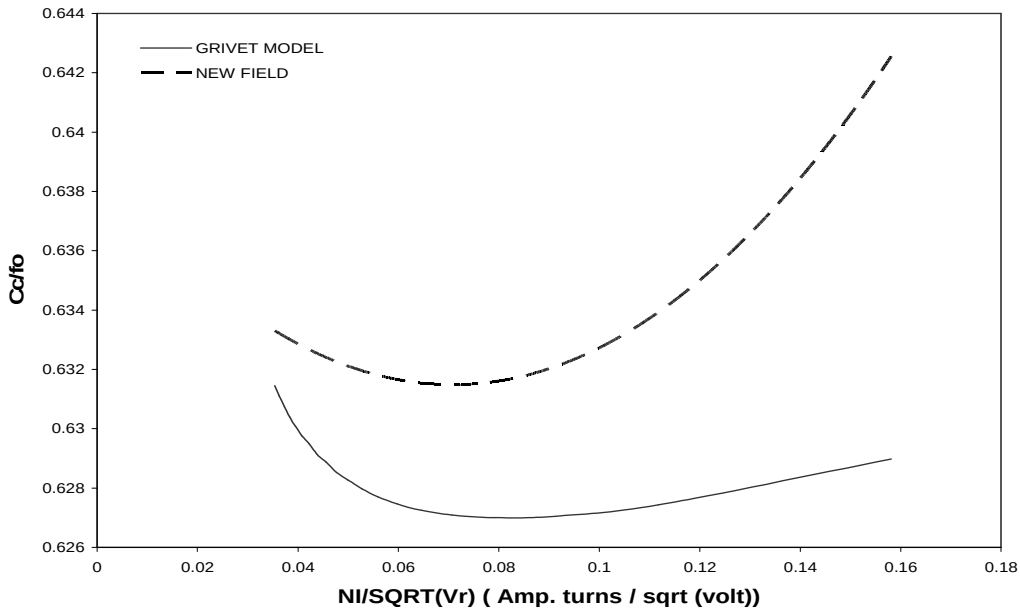

Figure (3-61): A comparison between the relative chromatic aberration coefficient calculations of Grivet-Lenz model and a new suggestion field for ø = 45^{o} and H = 67.

The upper half part of the pole piece for ø = 45^{o} and H = 37mm is shown in figure (3-62).

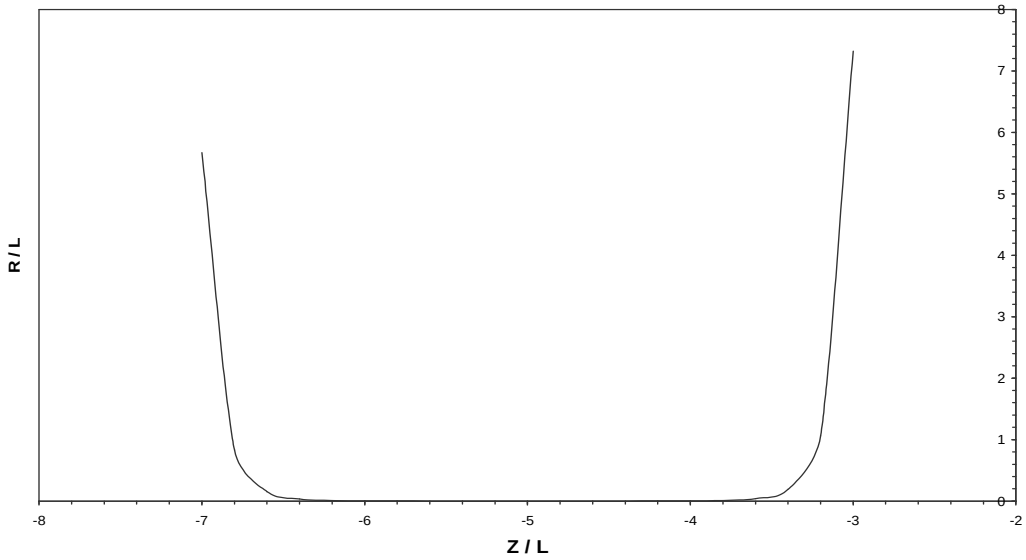

Figure (3-62): The pole piece shape when ø = 45^{o} and H = 37mm.

The upper half part of the pole piece for ø = 45^{o} and H = 37mm is shown in figure (3-63).

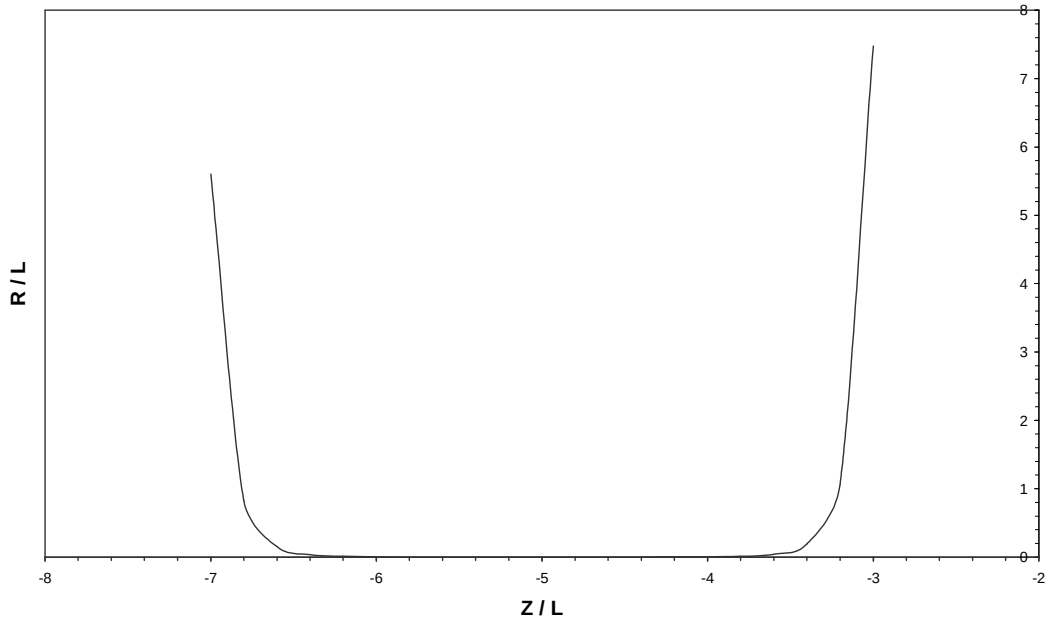

Figure (3-63): The pole piece shape when ø = 45^{o} and H = 67mm.

3-5 The Design By Using The Variable-Aperture Projection (V-AP) Arrangement

In the present section, we have determined the design of the deflector in a variable-aperture projection and the scanning system is based on the MOL concept [Goto 1978]. The axial field distribution *B(z)* is given by the following equation:

$$B(z)=\frac{A}{R}\exp\left\{-\left[\frac{(z-P)}{R}\right]^2\right\} \qquad (3-4)$$

where A, P and R are parameters specifying amplitude, position and radius of the coil, respectively.

The axial flux density distribution of the deflector *D(z)* is computed by using equation (2-11), where *B′* in equation (2-11) is computed by using equation (3-4). The general shape of axial field density distribution *B(z)* and deflection field density distribution *D(z)* are shown in figures (3-64) and (3-65) , respectively.

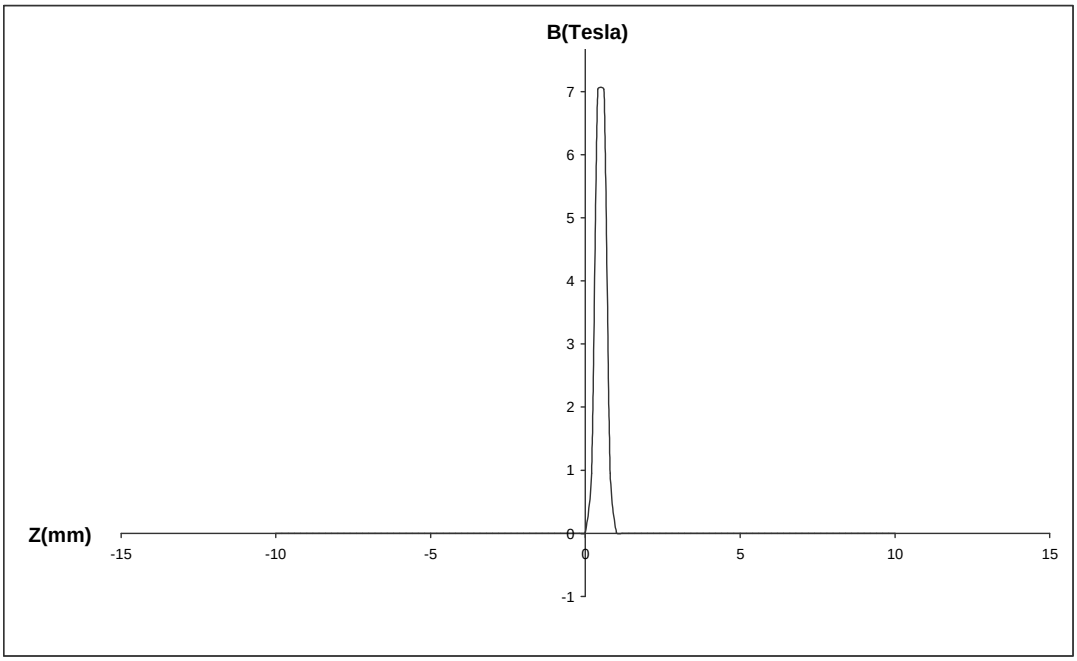

Figure (3-64): The axial flux density distribution *B(z)* of a VAP arrangement.

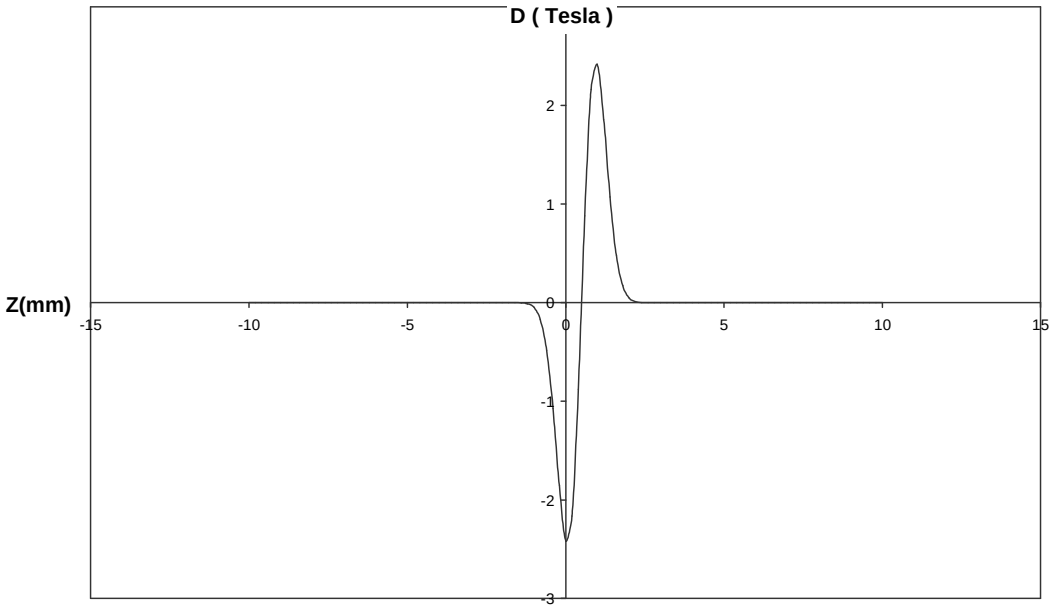

Figure (3-65): The axial deflection flux density distribution *D(z)* calculated with VAP arrangement.

3-5-1 Infinite magnification condition

In this part of the present work, we try to find the optimum values of spherical and chromatic aberrations as a function of changing the position of the coil P. The following coil positions P = 0.3, 0.4, 0.5, 0.6 and 0.7 are taken into account in the calculations; while the values of A and R are 1.80579 and 0.2, respectively[Goto 1978]. The results of spherical aberration in this operating condition are shown in figure (3-66). In this figure we find that the position of coil P = 0.7 give us the best values of Cs/fo for range of NI/SQRT(Vr). The results of calculations of chromatic aberrations shown in figure (3-67) coincide with the results in the spherical aberration.

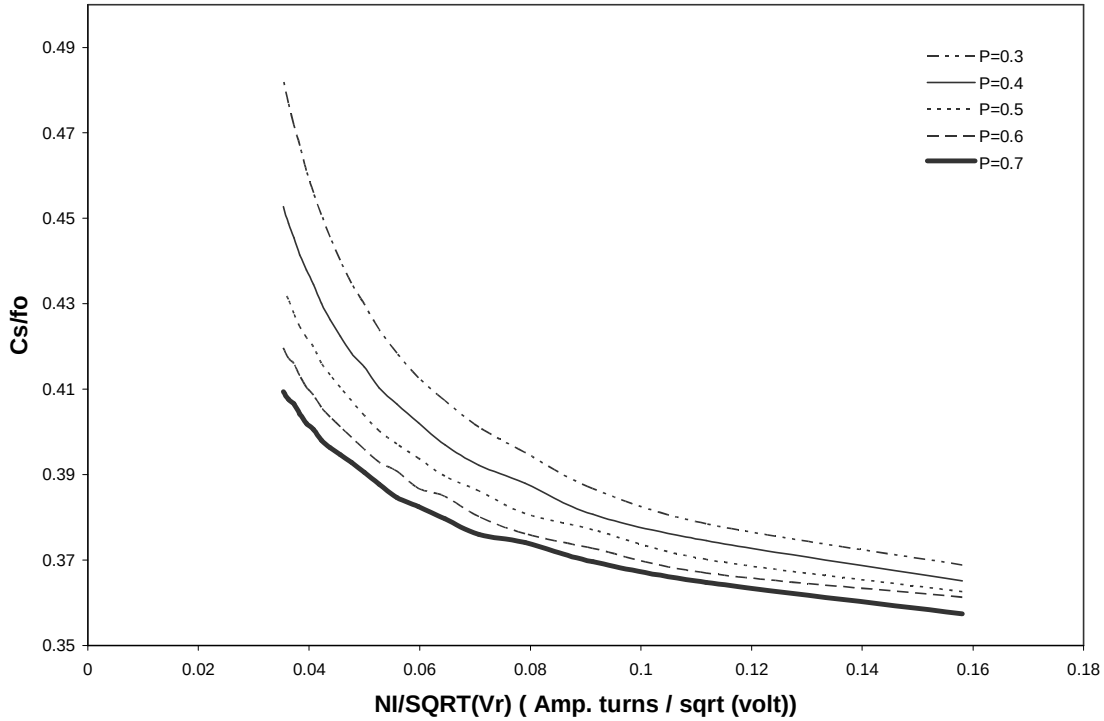

Figure (3-66): The relative spherical aberration coefficient as a function of NI / SQRT(Vr) for P = 0.3, 0.4, 05, 0.6 and 0.7 .

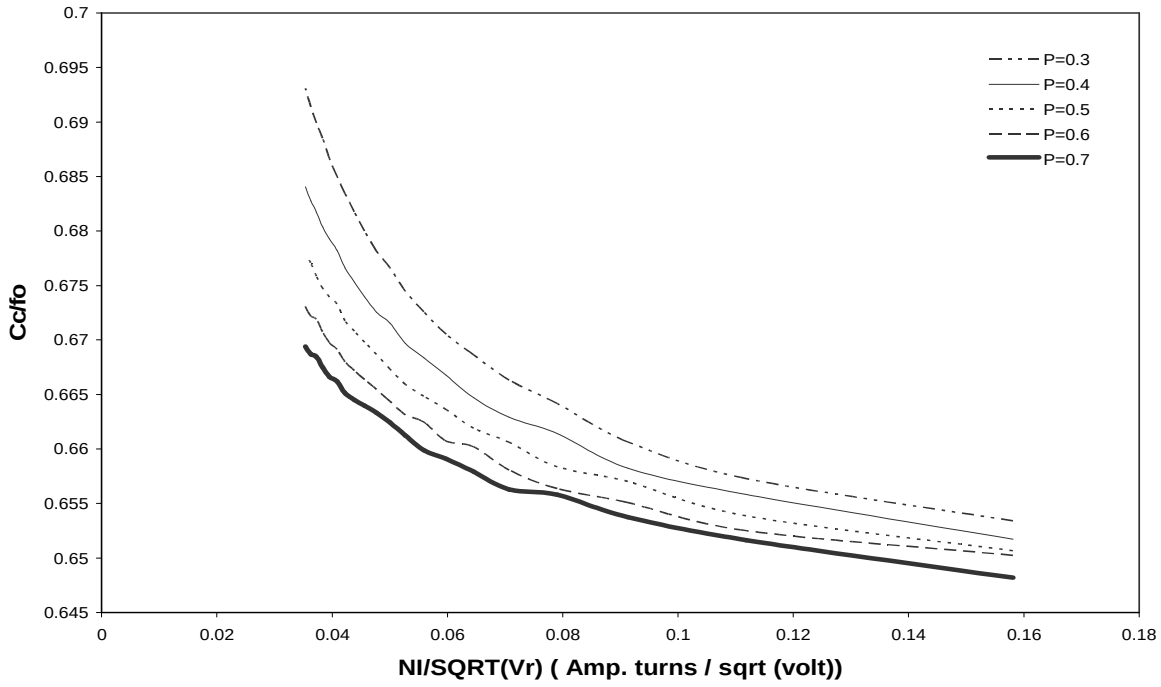

Figure (3-67): The relative chromatic aberration coefficient as a function of NI / SQRT(Vr) for P = 0.3, 0.4, 0.5, 0.6 and 0.7 .

The relation between Cs/fo and Cc/fo as a function of the position of the coil P is shown in the figures (3-68) and (3-69), respectively. In these two figures, we find that the values of Cs/fo and Cc/fo decrease as the position of the coil increases.

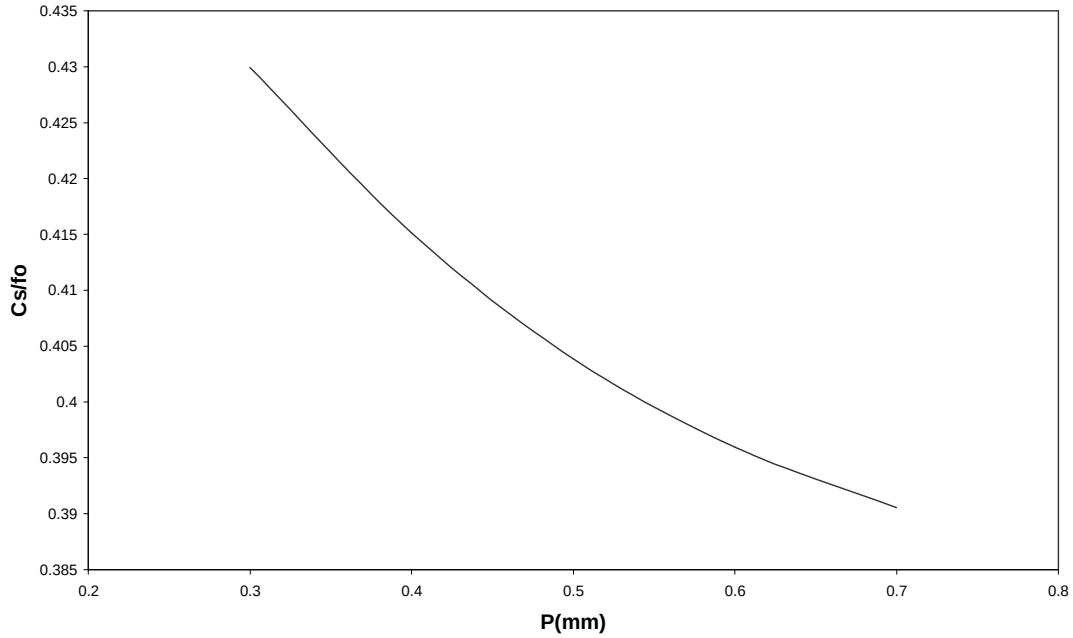

Figure (3-68): The relative spherical aberration coefficient as a function of the position of the coil P .

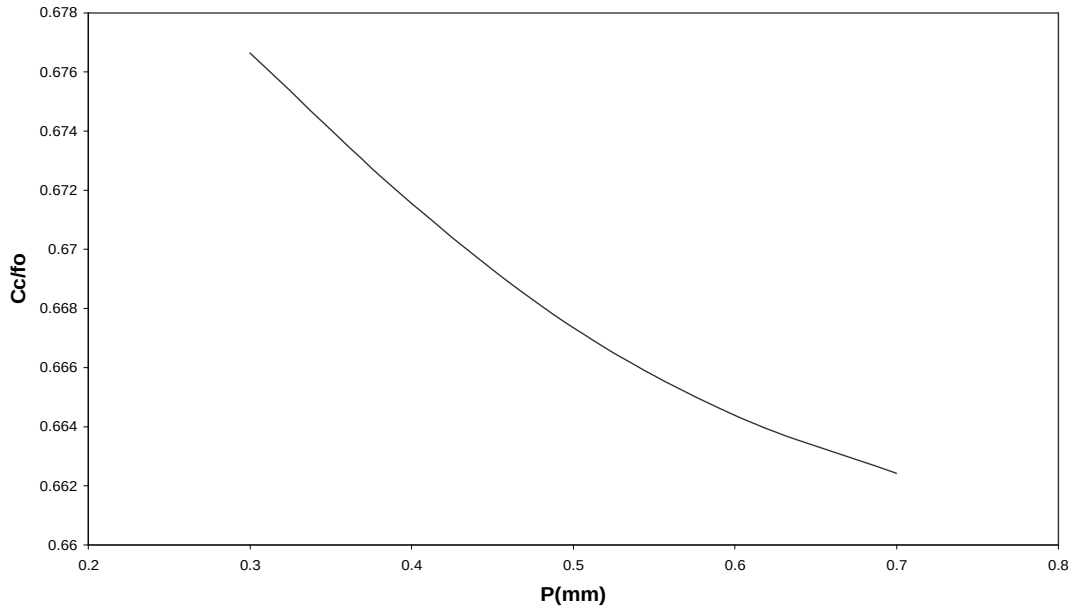

Figure (3-69): The relative chromatic aberration coefficient as a function of the position of the coil P .

The shape of the upper quarter part of the pole piece s of this case is shown in figure (3-70).

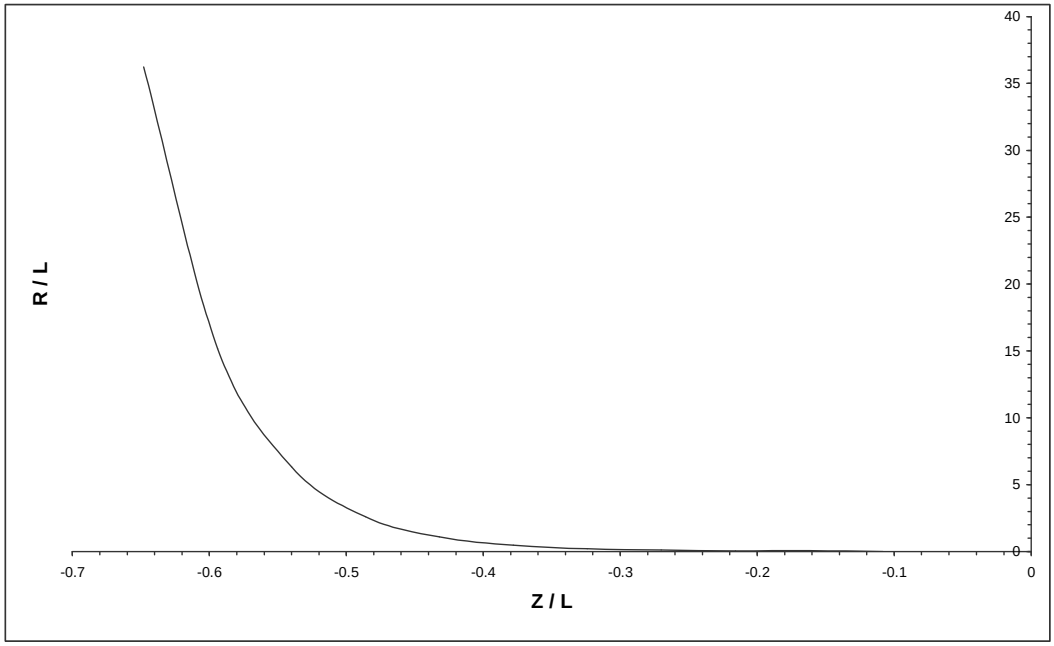

Figure (3-70): The pole piece shape for P = 0.7 .

3-5-2 Zero magnification condition

The same values of the position of the coil P which are used in infinite magnification condition are used. The results of the spherical calculations are shown in figure (3-71). From this figure we find that the position of the coil P = 0.3 gives the lower values for spherical aberration.

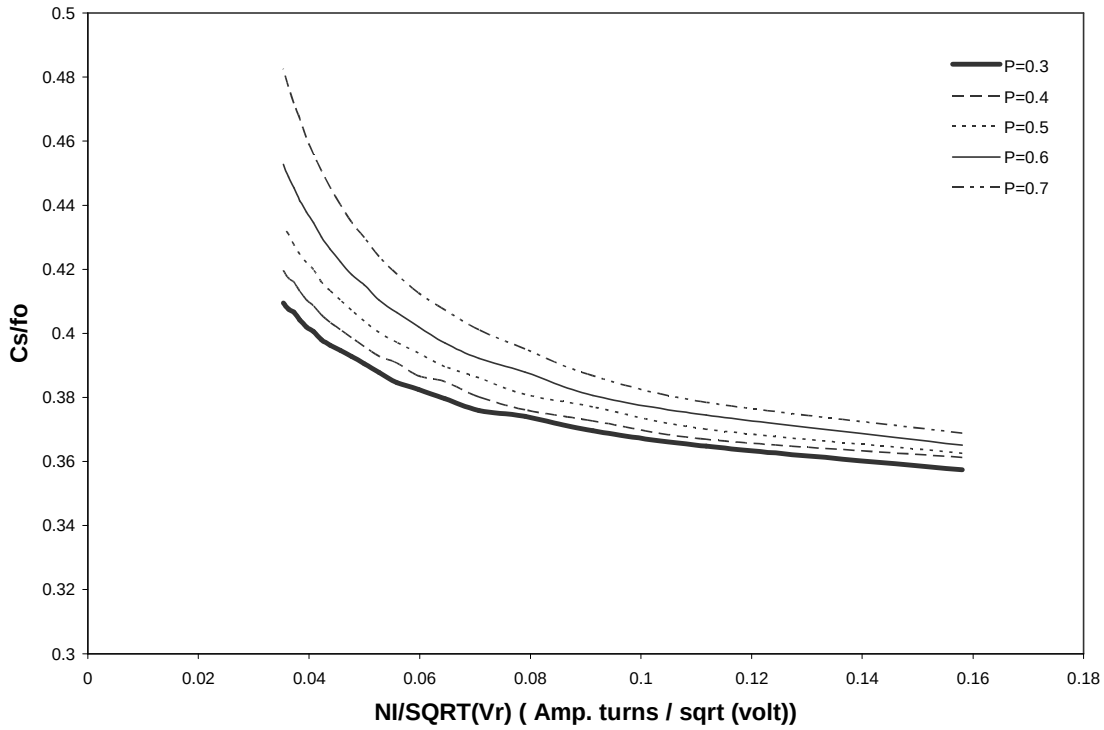

Figure (3-71): The relative spherical aberration coefficient as a function of NI / SQRT(Vr) for P = 0.3, 0.4, 0.5, 0.6 and 0.7 .

The results of the calculations of chromatic aberrations are shown in figure (3-72) and they coincide with the results in the spherical aberration case. The relation between Cs/fo and Cc/fo with the position of coil is shown in figures (3-73) and (3-74). In these two figures, we find that the values of Cs/fo and Cc/fo increase as the position of coil increases, except at the position between P = 0.5 and 0.6 where the Cs/fo and Cc/fo decrease.

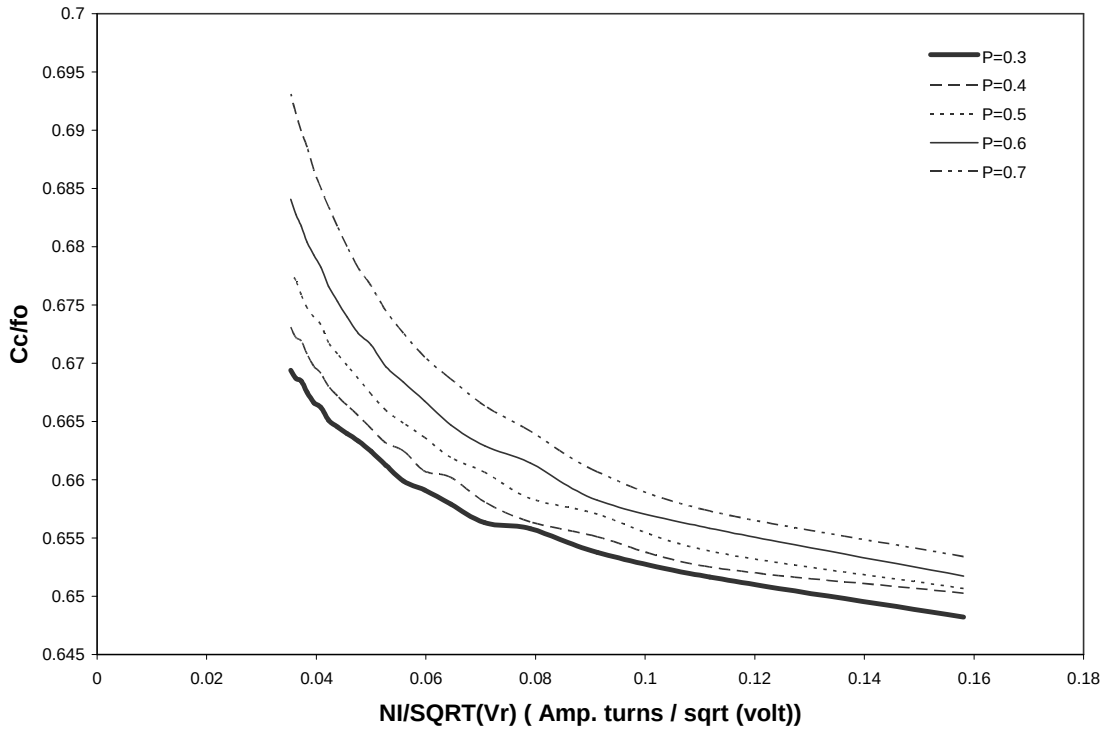

Figure (3-72): The relative chromatic aberration coefficient as a function of NI / SQRT(Vr) for P = 0.3, 0.4, 0.5, 0.6 and 0.7 .

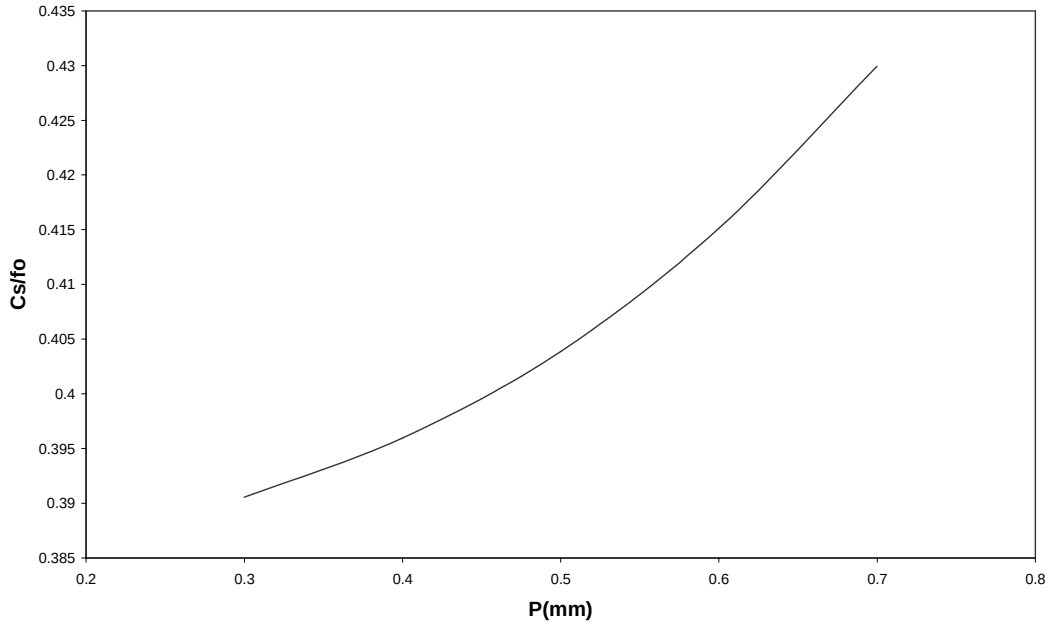

Figure (3-73): The relative spherical aberration coefficient as a function of the position of the coil P .

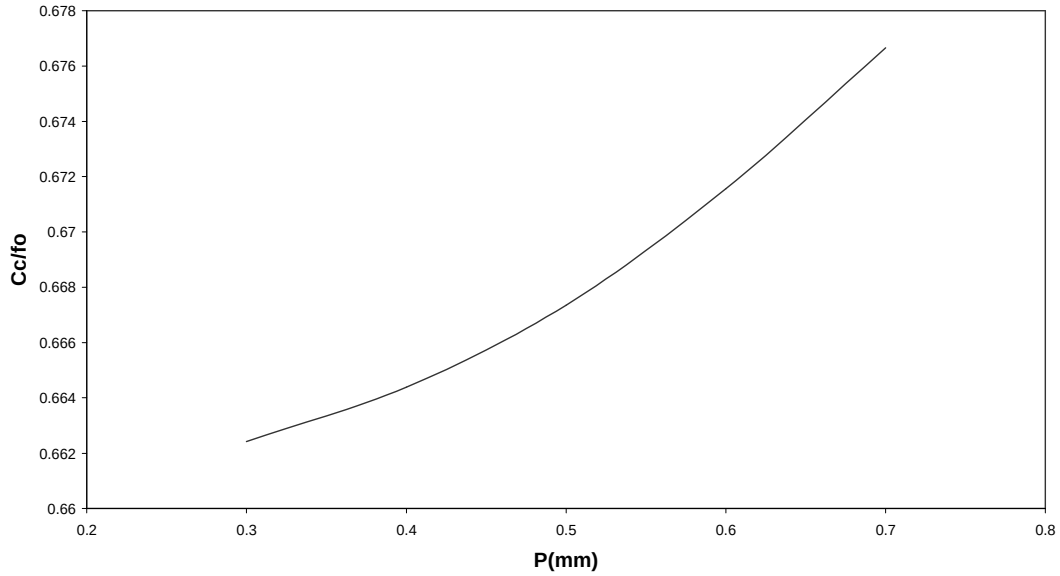

Figure (3-74): The relative chromatic aberration coefficient as a function of the position of the coil P.

The shape of the upper quarter part of the pole piece of this case is shown in figure (3-75).

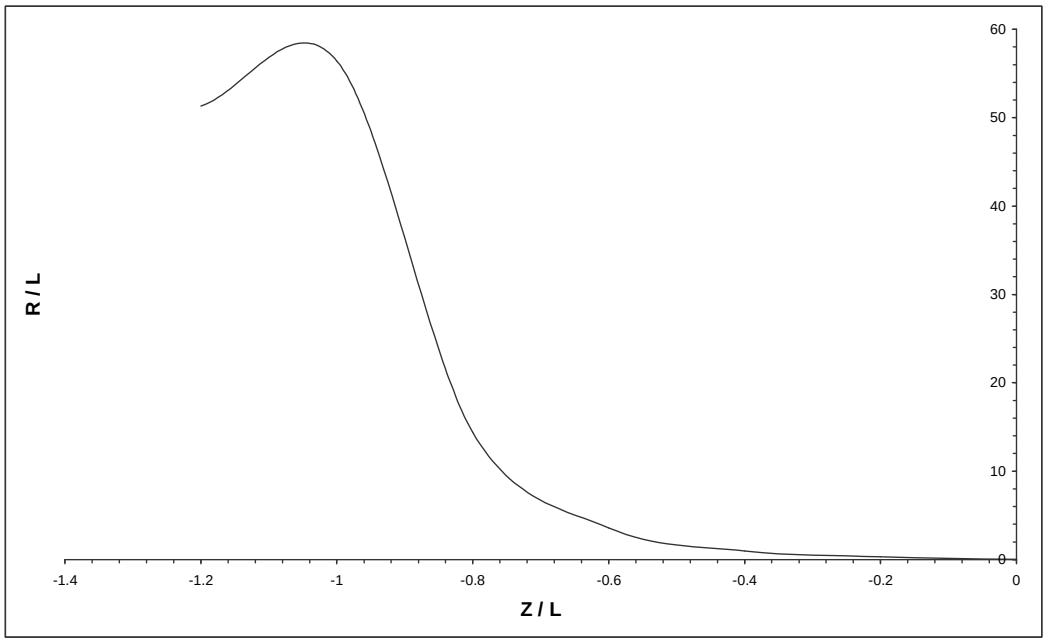

Figure (3-75): The pole piece shape for P = 0.3 .

Chapter Four

4- Results And Discussion Of Electrostatic Deflector

4-1 Introduction

In this part of the present work both analysis and synthesis approaches are used to find the optimum design of electrostatic deflectors which give us the minimum aberrations. In the analysis approach calculations we have studied the properties of asymmetrical and symmetrical electrostatic deflectors which consist of two parallel-plates have been studied. The optimization is made by changing the geometrical shape of the deflector, i.e. the variation of the vertical and horizontal dimensions of the deflector plates, to study its effects on the variation of the geometrical shape on the spherical and chromatic aberrations. The axial potential distributions of the symmetrical and asymmetrical deflectors are computed by using the finite element method (FEM).

After studying the properties of symmetrical electrostatic deflector by using the analysis approach we have tried to find the optimum design of this type of electrostatic deflector by using the synthesis approach. To achieve this we suggest an axial potential distribution which satisfies the solution of Laplace equation taken in the analytical approach. Then the shape of deflector is found by using the reconstruction method.

4-2 Asymmetrical Electrostatic Deflector

The asymmetrical electrostatic deflector, shape figure (4-1), is used in the present calculations. The horizontal dimension H is changed, as H=24, 30 and 40mm with constant vertical dimension V = 15mm , in order to find the optimum value of the spherical and chromatic aberrations. The axial potential distribution of these three cases which are computed by using the finite element method (FEM) are shown in figure (4-2).

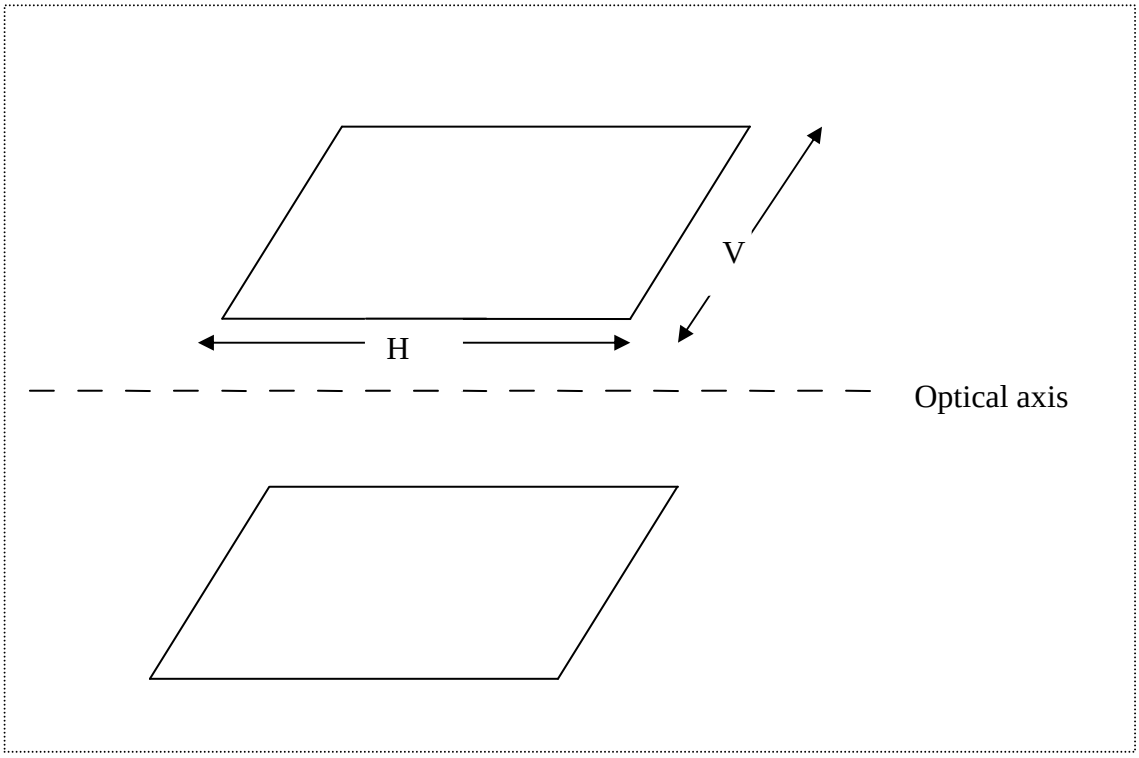

Figure (4-1): The shape of asymmetrical electrostatic deflector.

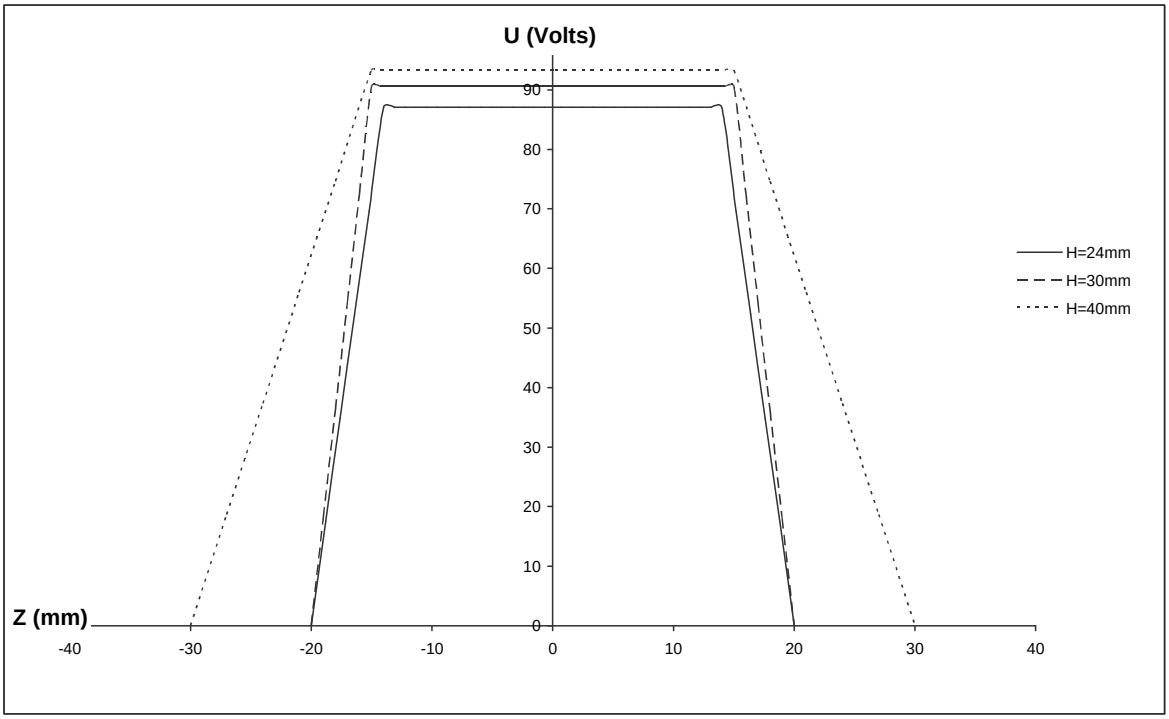

Figure (4-2): The axial potential distribution for asymmetrical electrostatic deflector with horizontal dimension H = 24, 30 and 40mm.

4-2-1 Infinite magnetic condition

The spherical and chromatic aberrations are computed in this operating condition. To find the optimum design we have tried to study the effect of variation the horizontal dimension H of the deflector. Different values of horizontal dimension, H=24, 30 and 40mm, are taken into account in the calculations of spherical and chromatic aberrations. The results of spherical aberration calculations are shown in figure (4-3). The optimum horizontal dimension which gives us the minimum value of spherical aberration is H = 24mm . In this figure we also find that the both H = 24 and 30mm have the same behavior where the values of Cs/fo decrease as Ui / Uo increase, while for H = 40mm the values of Cs/fo decrease as Ui / Uo increase up to Ui / Uo = 10 then the value of Cs/fo will be increased.

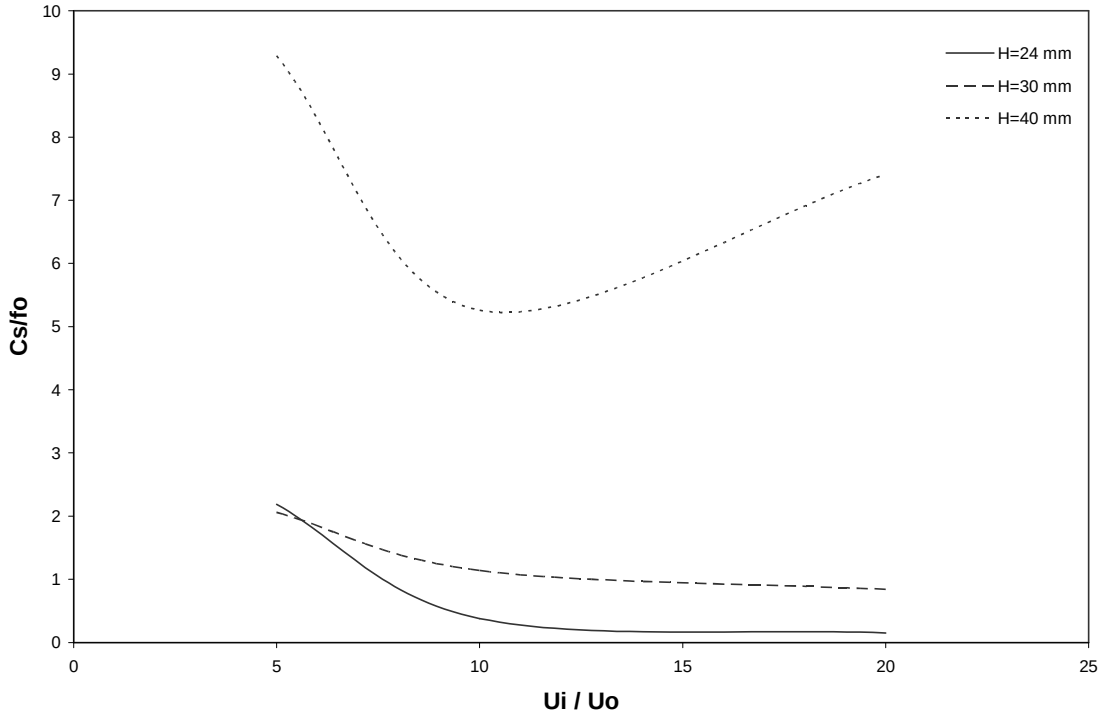

Figure (4-3): The relative spherical aberration coefficient as a function of Ui / Uo for H = 24, 30 and 40mm.

In chromatic aberration calculations we have found that the value of chromatic aberration can be reduced to very small values at Ui / Uo = 14 by choosing the horizontal dimension H = 24mm as is shown in figure (4-4). In this figure we find that the curve of H = 24mm has the opposite behavior to the curve of H = 40mm. In figures (4-5) and (4-6) one can see that the spherical and chromatic aberrations have the inverse proportion with the horizontal dimension. Therefore, according to the type of application the designer choose the horizontal dimension of the deflector.

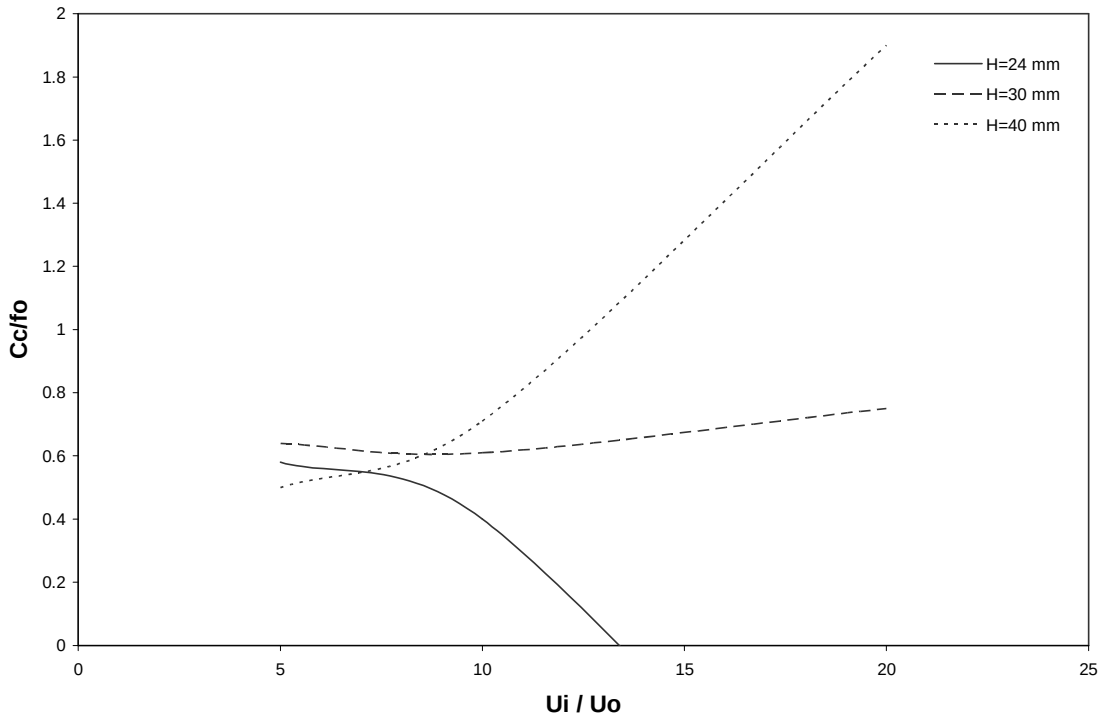

Figure (4-4): The relative chromatic aberration coefficient as a function of Ui / Uo for H = 24, 30 and 40mm.

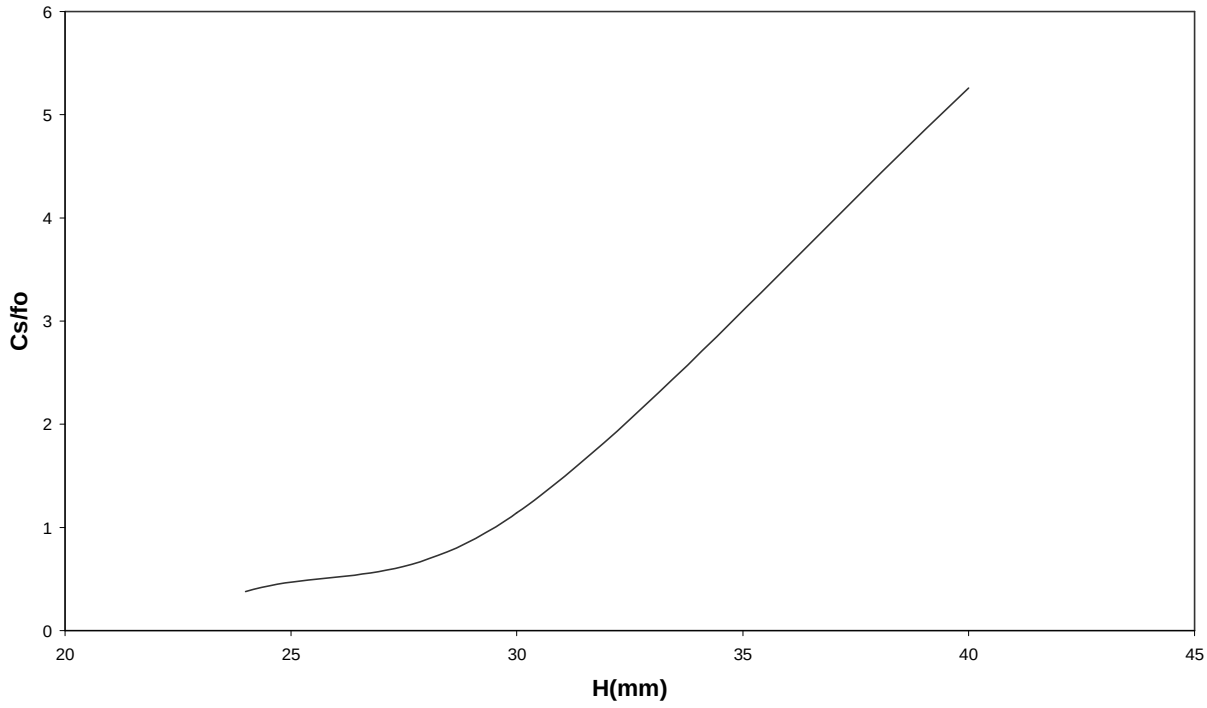

Figure (4-5): The relative spherical aberration coefficient as a function of the horizontal dimension H .

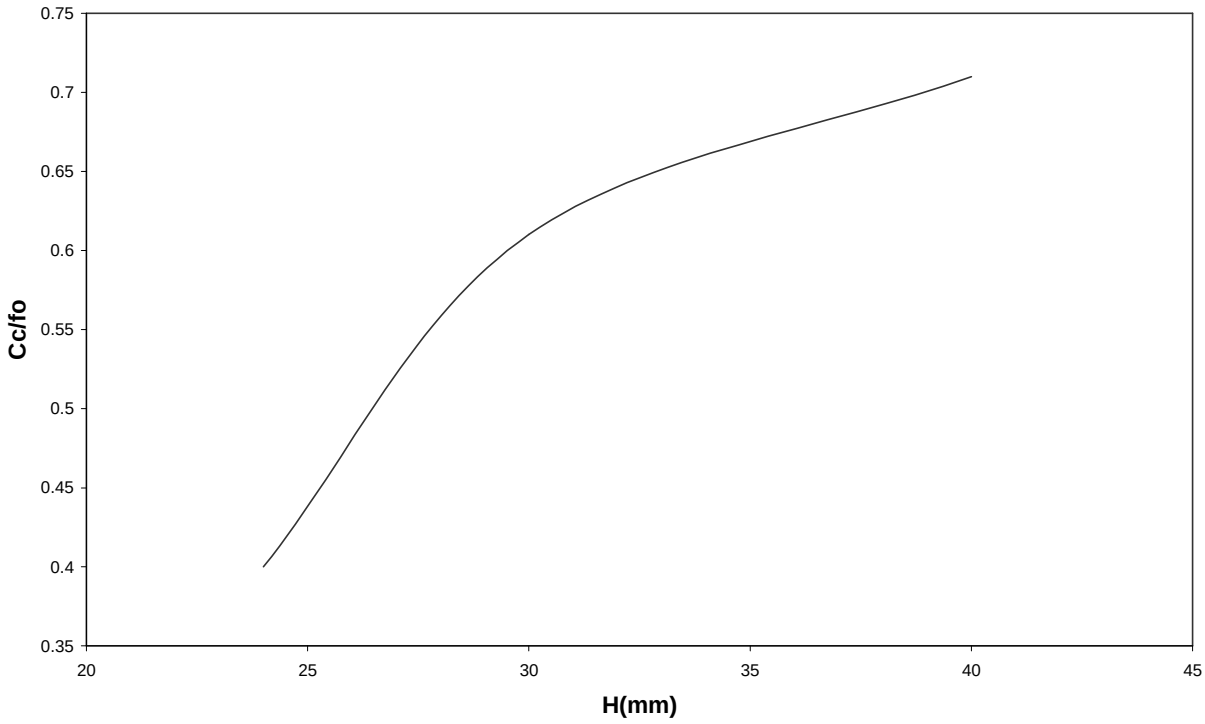

Figure (4-6): The relative chromatic aberration coefficient as a function of the horizontal dimension H .

4-2-2 Zero magnification condition

Under this operating condition the same values of horizontal dimension, H = 24, 30 and 40mm, are also tested to show its effects on spherical and chromatic aberrations. The results of the calculations of spherical aberration is shown in figure (4-7). The horizontal dimension H = 30mm gives us the best result in comparison with other cases as shown in this figure. The values Cs/fo appear to be slightly linear variation in all Ui / Uo range. While the other two dimensions H = 24 and 40mm have a minimum at Ui / Uo = 9 and relative high values of Cs/fo.

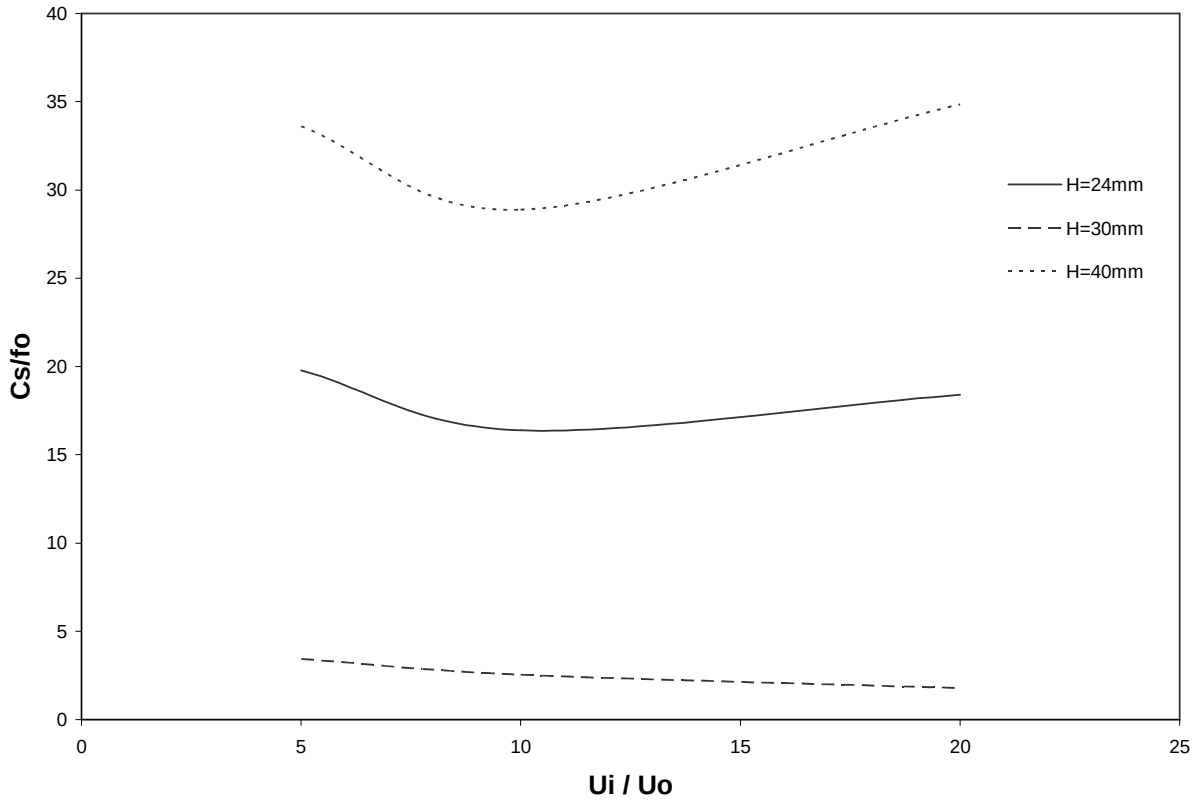

Figure (4-7): The relative spherical aberration coefficient as a function of Ui / Uo for H = 24, 30 and 40mm.

From figure (4-8) one can see that the horizontal dimension H = 40mm reduces the value of relative chromatic aberration to very small values at Ui / Uo =11.7 . The results of H = 24 and 30mm have the opposite behavior of the case of H = 40mm where the value of Cc/fo increases as Ui / Uo increases.

The relation between the relative spherical aberration and horizontal dimension (H) is shown in figure (4-9). The relative spherical aberration values decrease as the horizontal dimension increases up to H = 30mm then the value of Cs/fo will be increased. While in the chromatic aberration case we find the opposite behavior where we have the maximum value of Cc/fo at H = 30mm as is shown in figure (4-10).

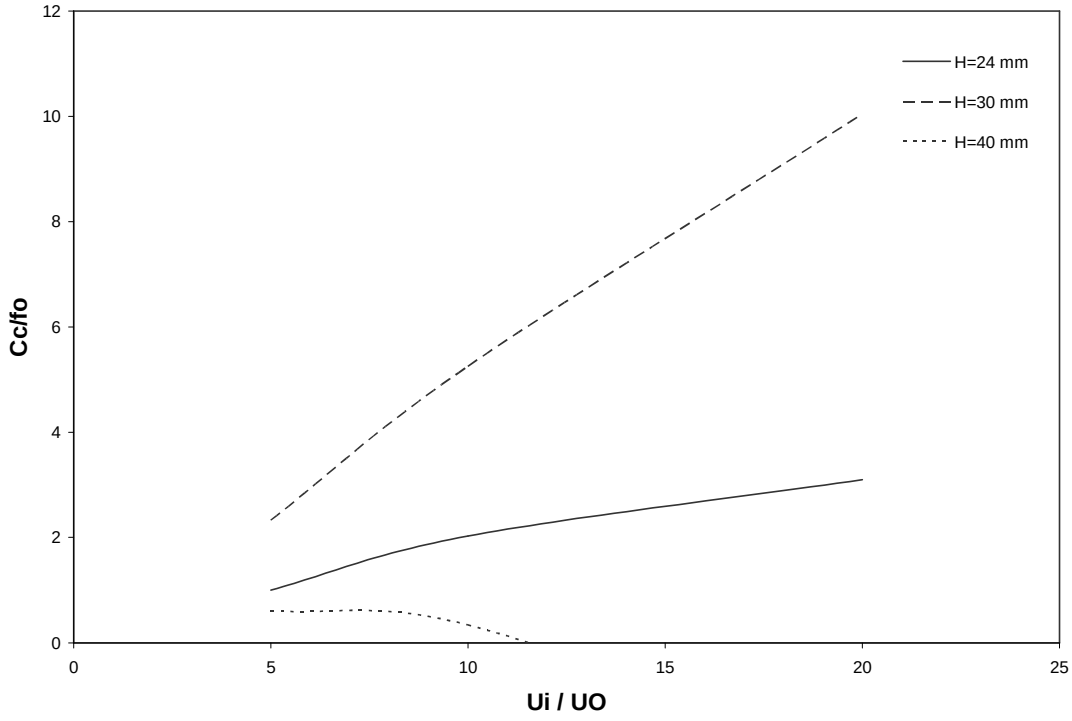

Figure (4-8): The relative chromatic aberration coefficient as a function of Ui / Uo for H = 24, 30 and 40mm.

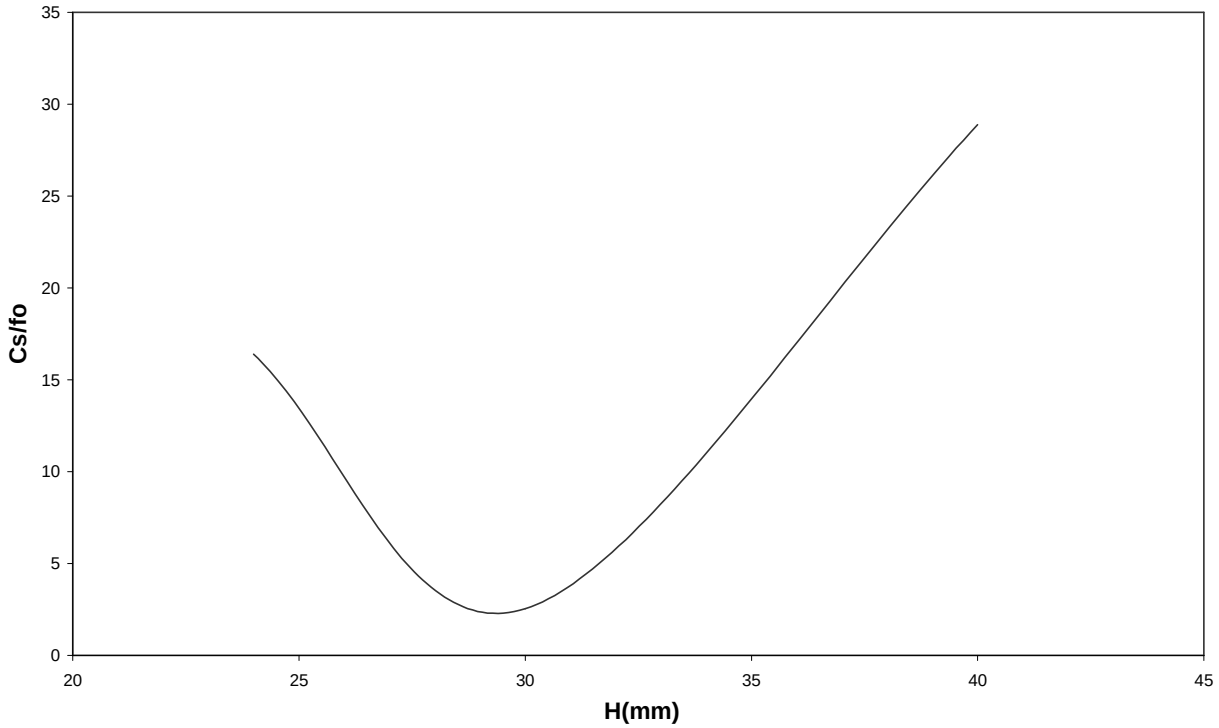

Figure (4-9): The relative spherical aberration coefficient as a function of horizontal dimension H .

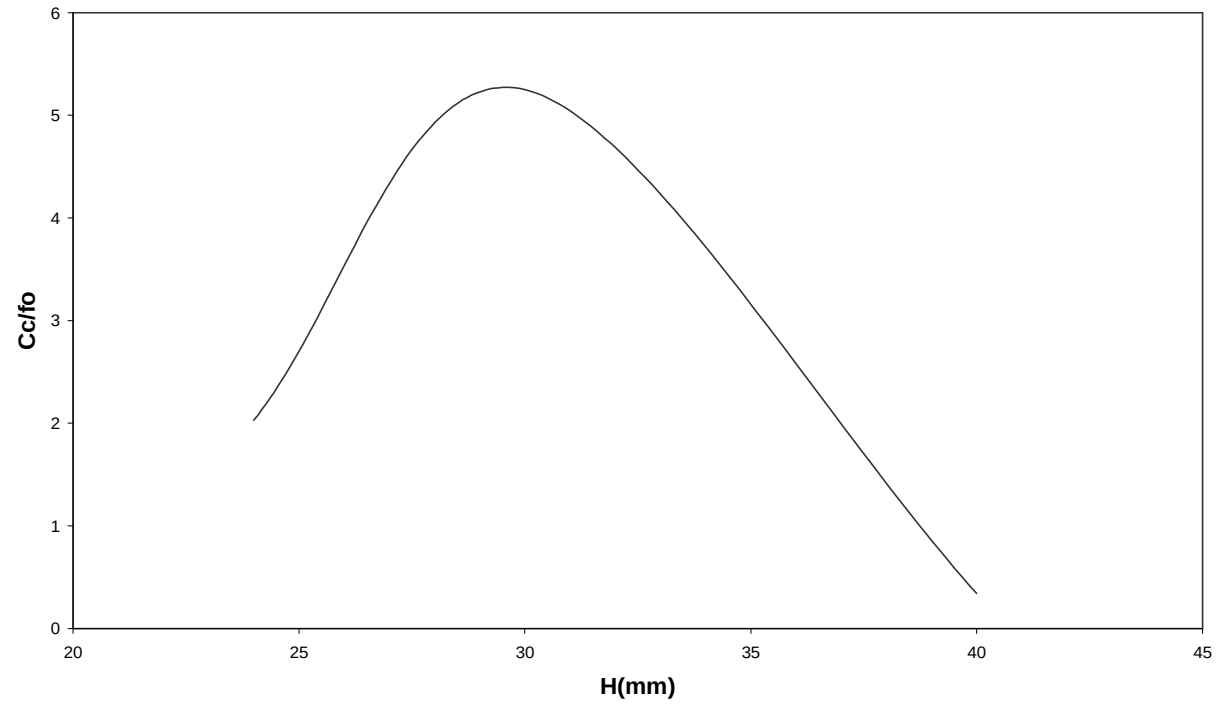

Figure (4-10): The relative chromatic aberration coefficient as a function of horizontal dimension H.

4-3 Symmetrical Electrostatic Deflector

The symmetrical electrostatic deflector whose shape is shown in figure (4-11) is used with different geometrical dimensions to study the effect of the different vertical dimension V on both spherical and chromatic aberrations. Three values of vertical dimensions V, V = 60, 55 and 50mm, are studied. The axial potential distributions of these cases are computed by using the finite element method (FEM) which is shown in figure (4-12).

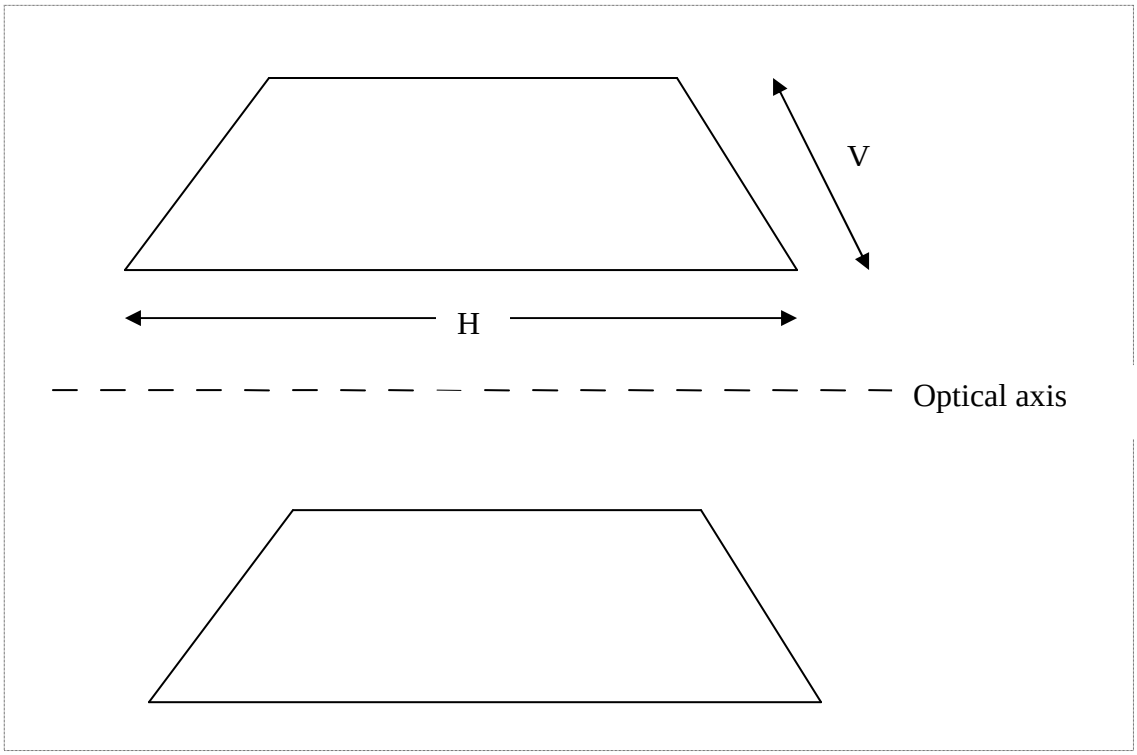

Figure (4-11): The shape of symmetrical electrostatic deflector.

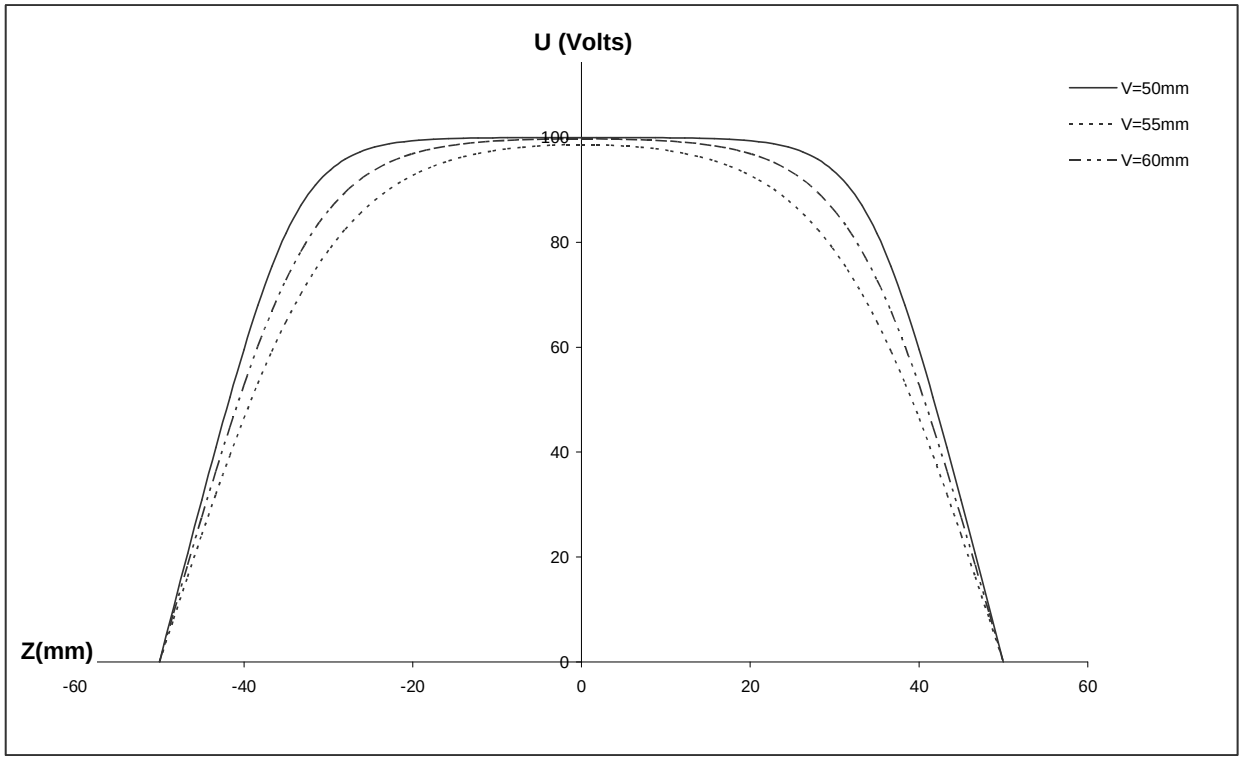

Figure (4-12): The axial potential distribution for symmetrical electrostatic deflector with horizontal dimension V = 50, 55 and 60mm.

4-3-1 Infinite magnification condition

The effect of changing the vertical dimension V on spherical and chromatic aberrations under this operating condition is shown with a different value, V = 60, 55 and 50mm, in figures (4-13) and (4-14). The calculations show that the vertical dimension V = 50mm gives us the lower value of relative spherical and chromatic aberrations. The values of relative spherical and chromatic aberrations increase as the values of Ui / Uo increase of all states which have the same behavior as is shown in figures (4-13) and (4-14). Both spherical and chromatic aberrations have the same relation with the vertical dimension V, where the relative spherical and chromatic aberrations increase as the vertical dimensions increase and this relation appears in figures (4-15) and (4-16).

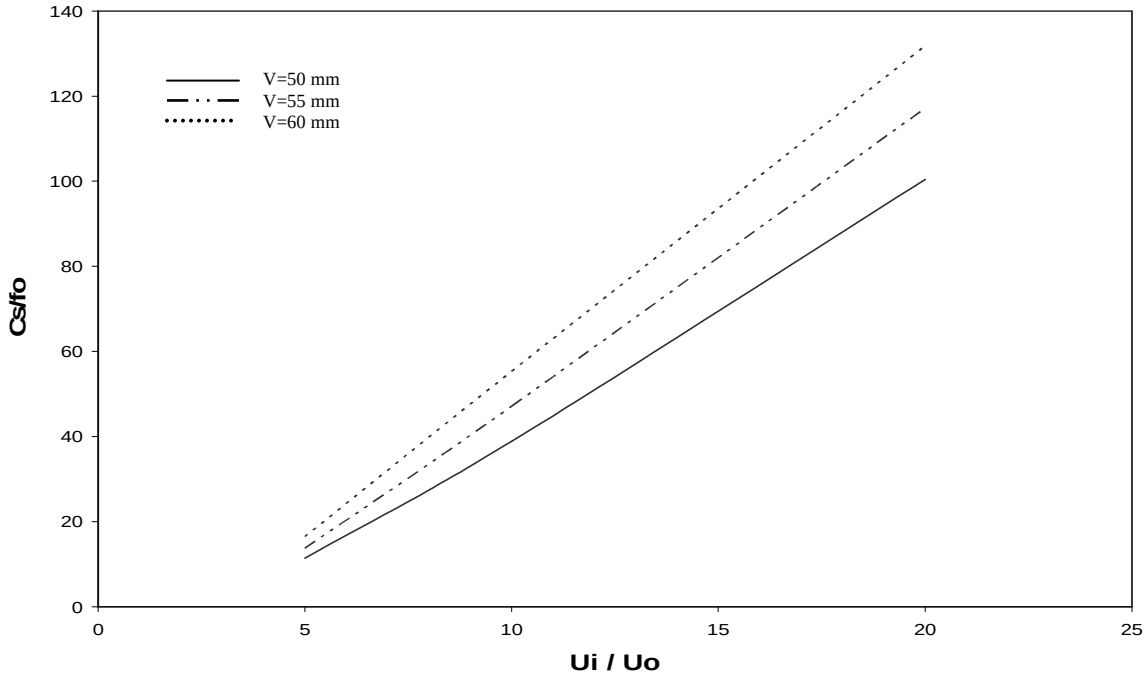

Figure (4-13): The relative spherical aberration coefficient as a function of Ui / Uo for V = 50, 55 and 60mm.

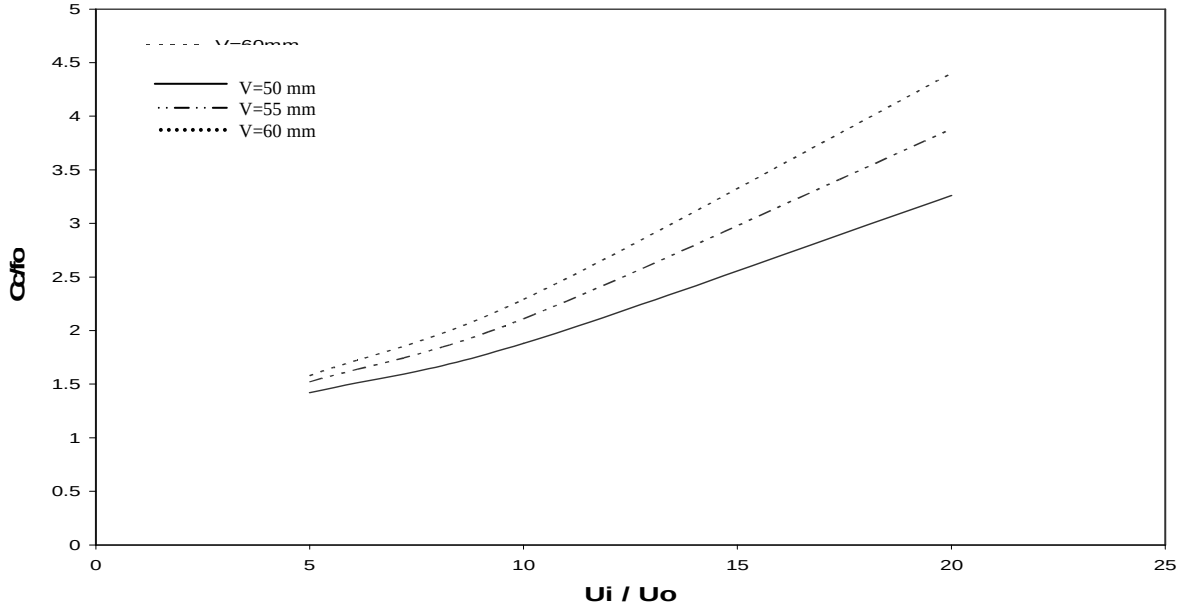

Figure (4-14): The relative chromatic aberration coefficient as a function of Ui / Uo for V = 50, 55 and 60mm.

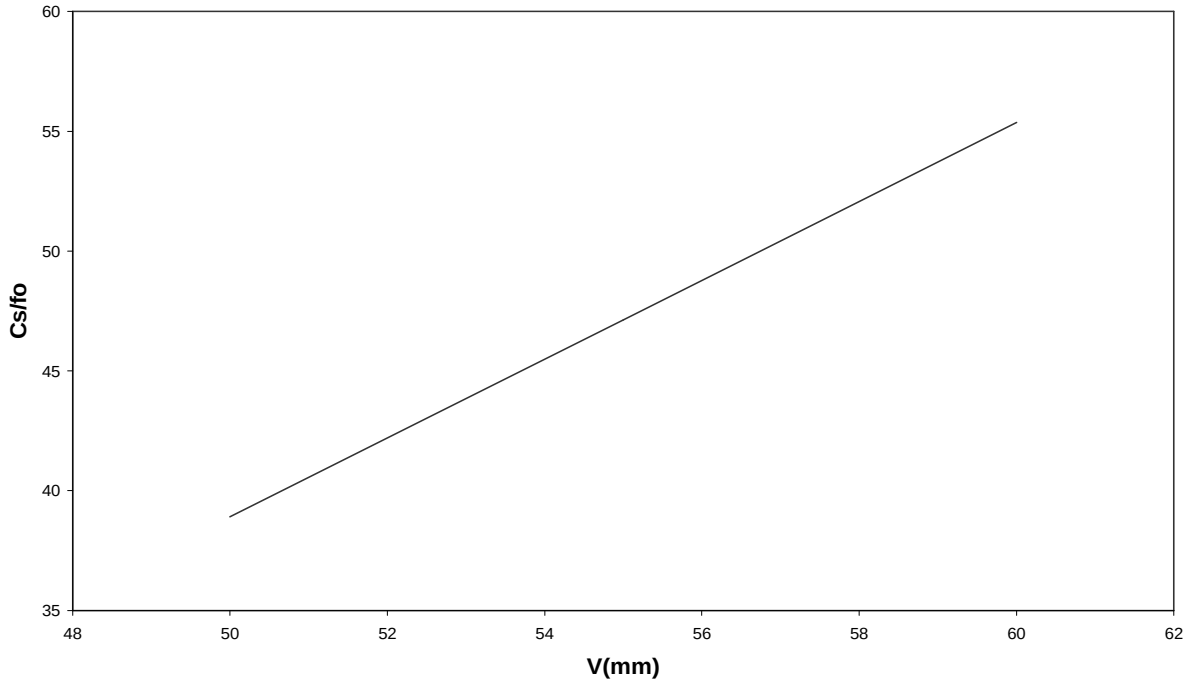

Figure (4-15): The relative spherical aberration coefficient as a function of vertical dimension V.

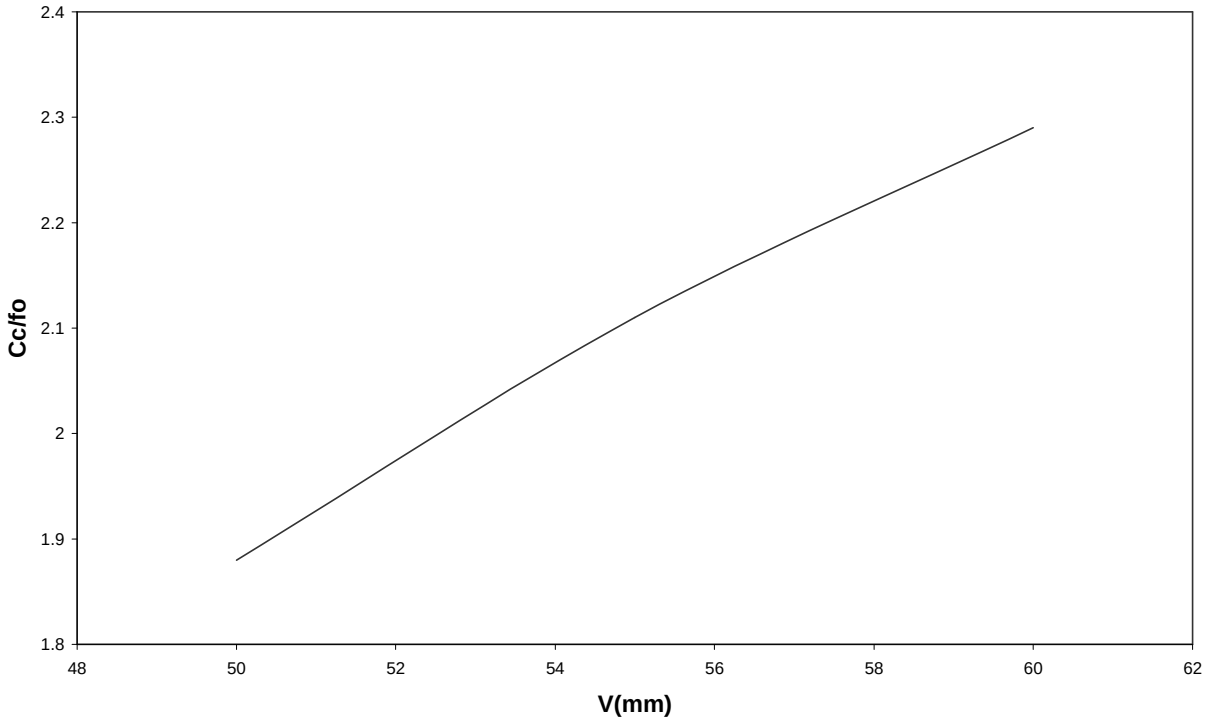

Figure (4-16): The relative chromatic aberration coefficient as a function of vertical dimension V.

4-3-2 Zero magnification condition

The same values of the vertical dimensions, V = 50, 55 and 60mm, are used in the calculations under this operating condition. The results of spherical and chromatic aberrations are shown in figures (4-17) and (4-18). As same as the infinite magnification condition results the vertical dimension V = 50mm give us the lower values for both spherical and chromatic aberration as is shown in these two figures. Also, the relative spherical and chromatic aberrations have the same proportion with the vertical dimension V as shown in figures (4-19) and (4-20).

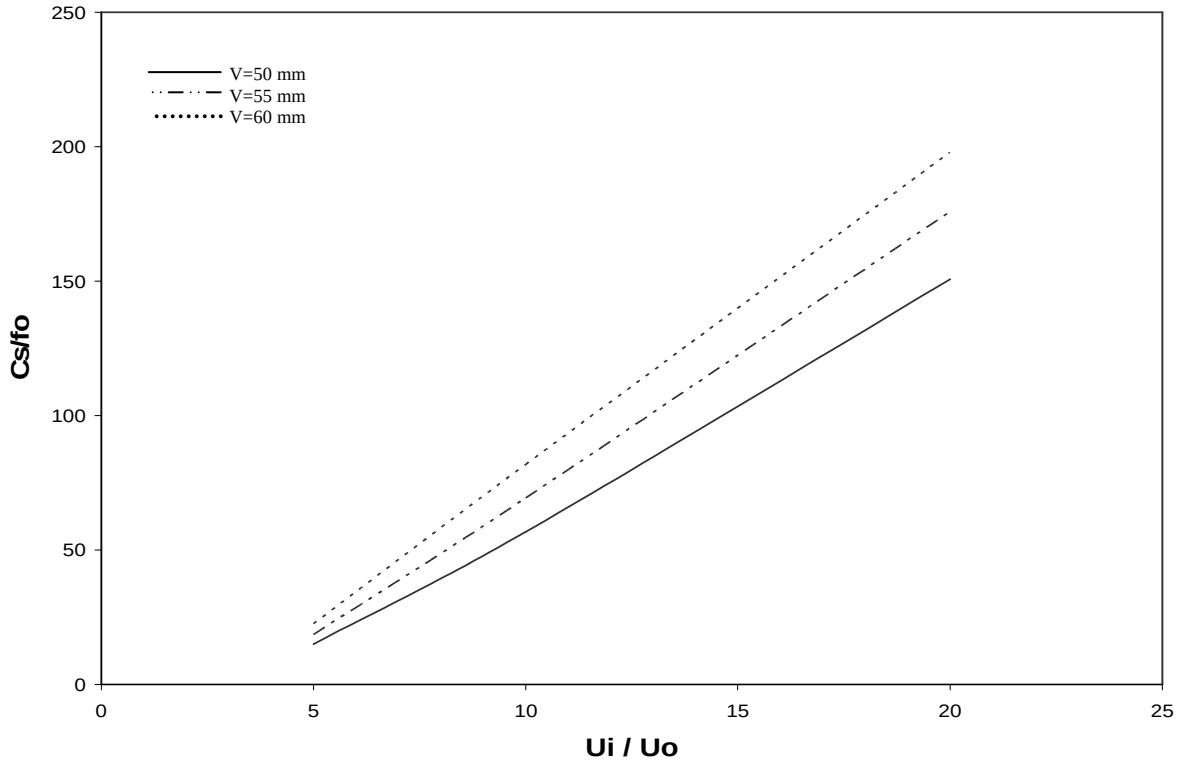

Figure (4-17): The relative spherical aberration coefficient as a function of Ui / Uo for V = 50, 55 and 60mm.

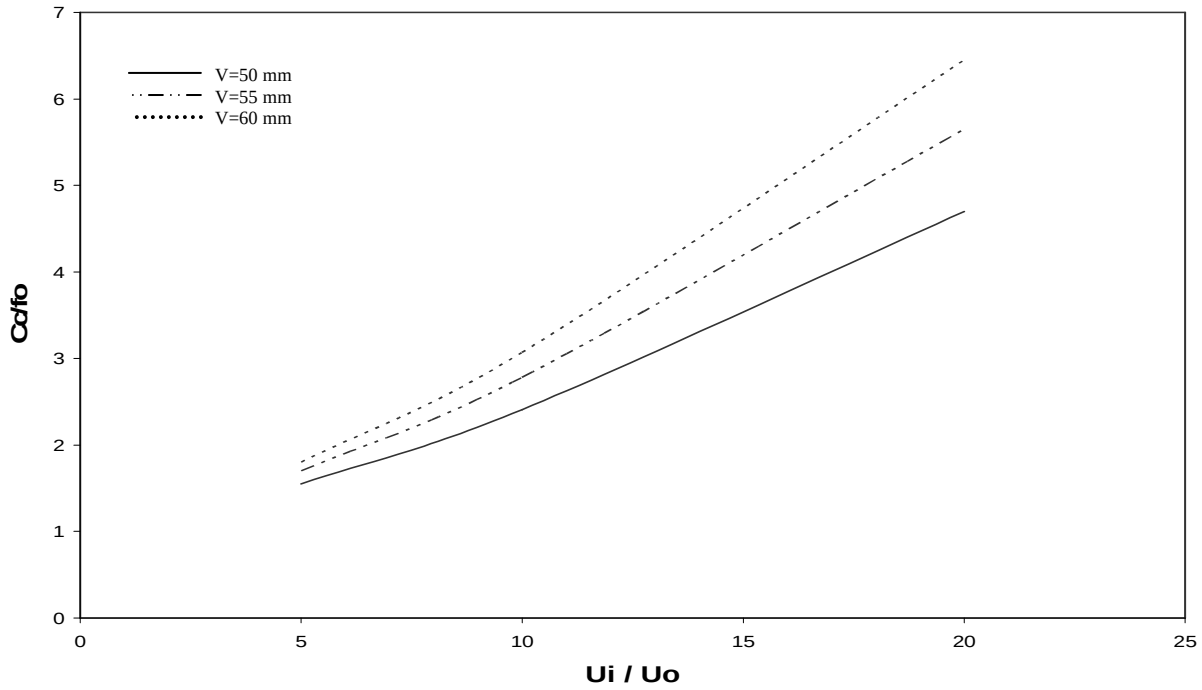

Figure (4-18): The relative chromatic aberration coefficient as a function of Ui / Uo for V = 50, 55 and 60mm.

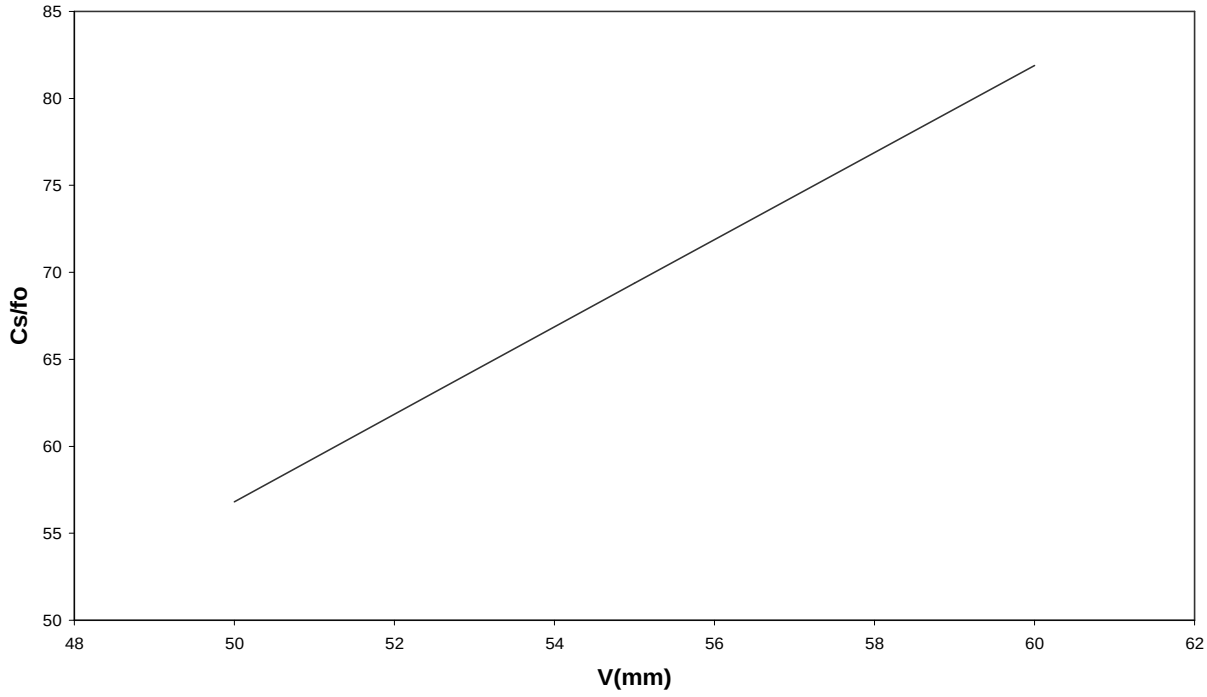

Figure (4-19): The relative spherical aberration coefficient as a function of vertical dimension V.

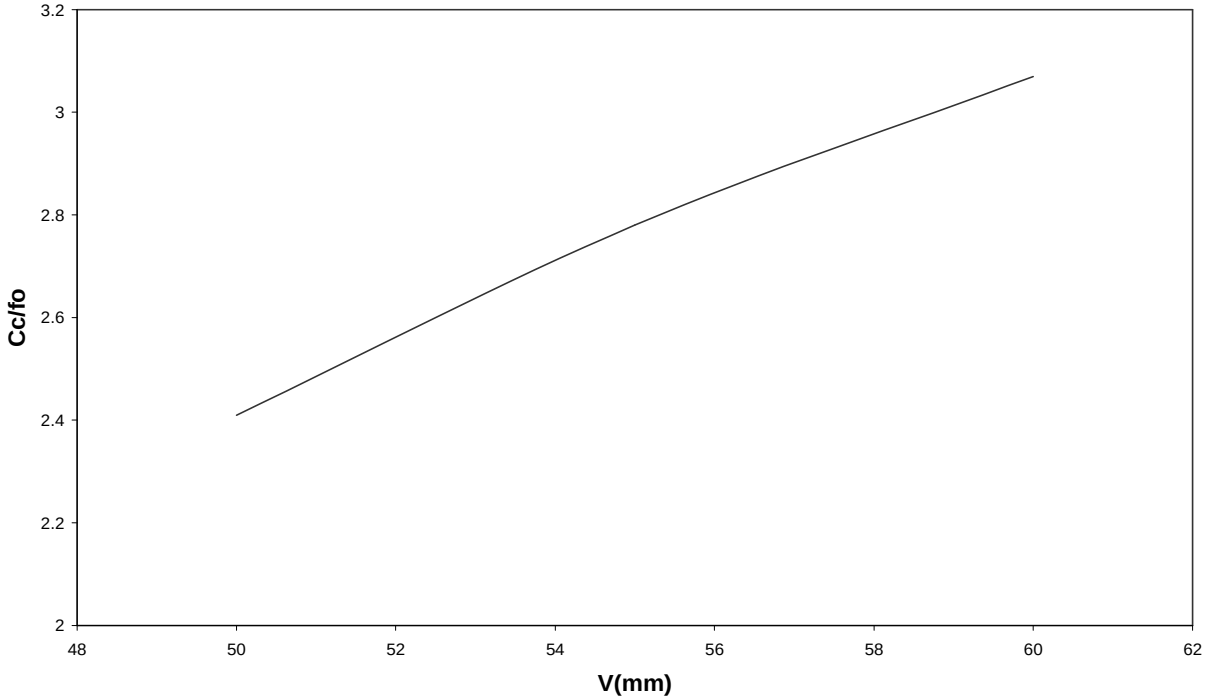

Figure (4-20): The relative chromatic aberration coefficient as a function of vertical dimension V.

4-4 The Suggested Potential Distribution

After using the analysis approach to find a better design of an electrostatic deflector, the synthesis approach has been used to achieve the same aim. Therefore, we suggest the following axial potential distribution for the symmetrical electrostatic deflector:

$$U(z)=U_O\ (1-bZ^2) \qquad (4-1)$$

where U_O is the maximum value of potential and b is constant can be choice depending on the axial potential distribution of the deflector which is calculated from analysis approach where b = 0.004 in this case. The axial potential distribution which is computed by using equation (4-1) is shown in figure (4-21). The comparison with the symmetrical deflector calculations is made in figure (4-22).

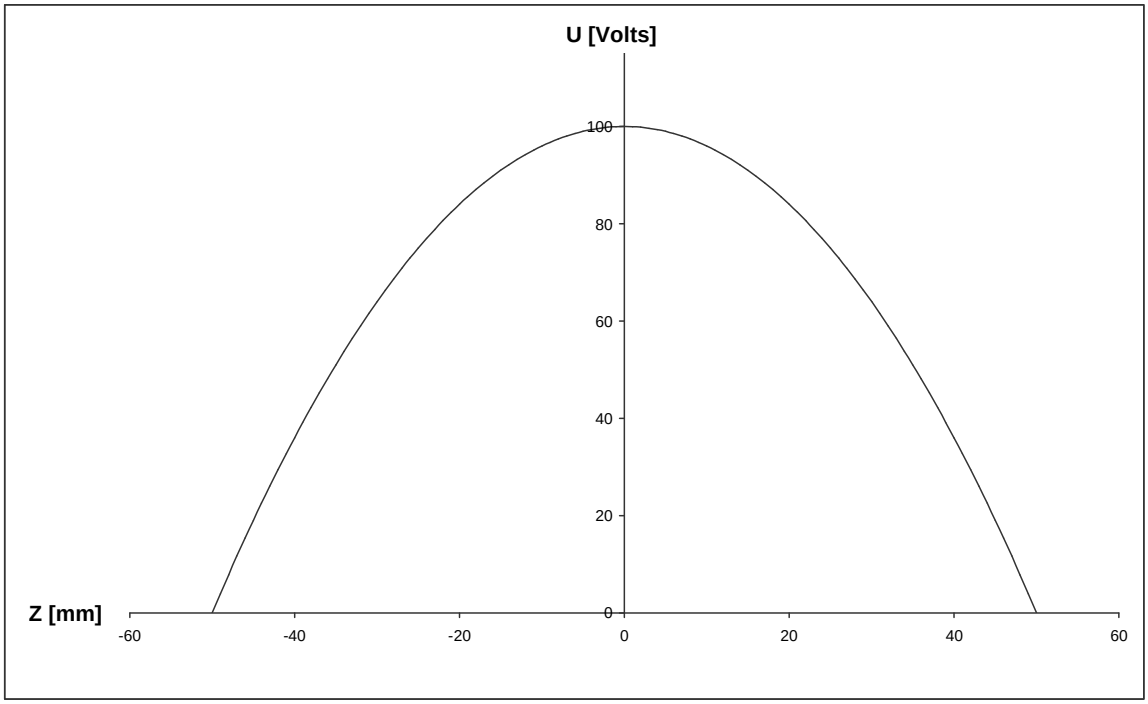

Figure (4-21): The axial potential distribution of electrostatic deflector which is computed using equation (4-1) .

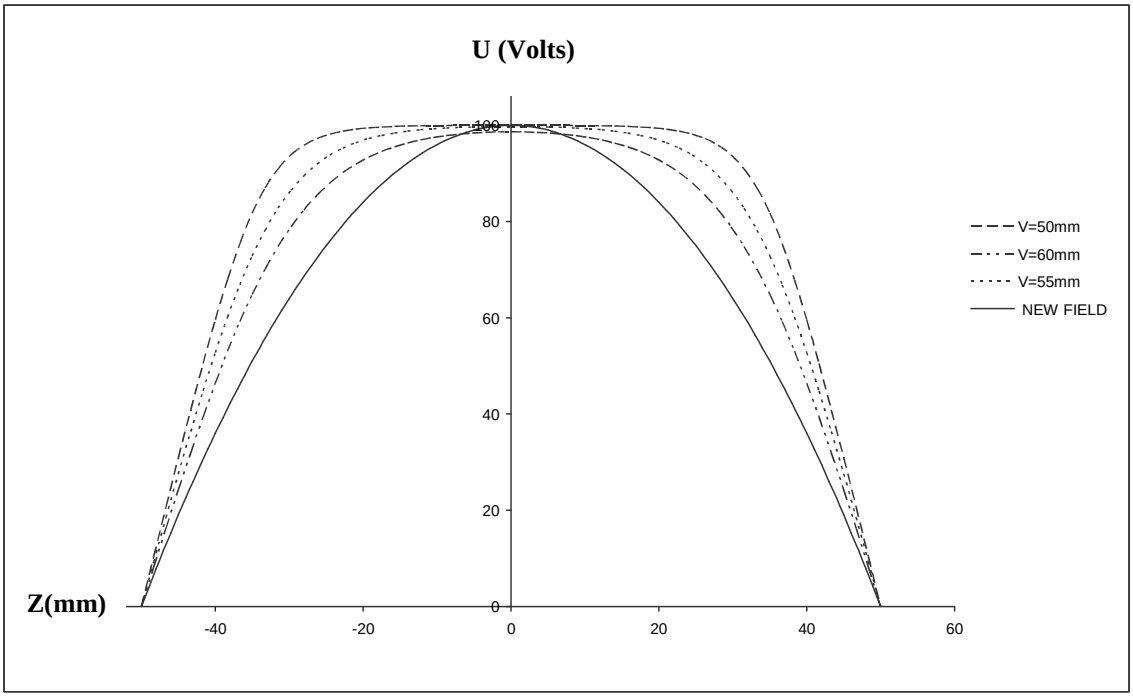

Figure (4-22): A comparison between the potential distribution of electrostatic deflector which is computed using equation (4-1) and the potential distribution of symmetrical electrostatic deflectors which are computed using the analysis approach.

4-4-1 Infinite and zero magnification condition

By using the suggestion potential distribution during the synthesis approach , we find that the results of both infinite and zero magnification condition are the same and they take the exact values of the spherical and chromatic aberrations. Also, the calculations of spherical aberration are able to reduce the relative spherical aberration to at small potential ratio Ui / Uo = 5 as is shown in figure (4-23). The calculations of chromatic aberration give us good results as is shown in figure (4-24) where at Ui / Uo = 6 the values of Cc/fo = 1.07 . From these two figures one can see that the relative spherical and chromatic aberrations increase as Ui / Uo increase.

In comparison with the results of the symmetrical electrostatic deflector calculations when the analysis approach is used, we find that the calculations of the synthesis approach gives us better results than those of both spherical and chromatic aberrations in the analytical approach as is shown in figures (4-25) and (4-26).

The shape of electrostatic deflector is found by using the reconstruction method and the shape of the plate of this deflector is shown in figure (4-27).

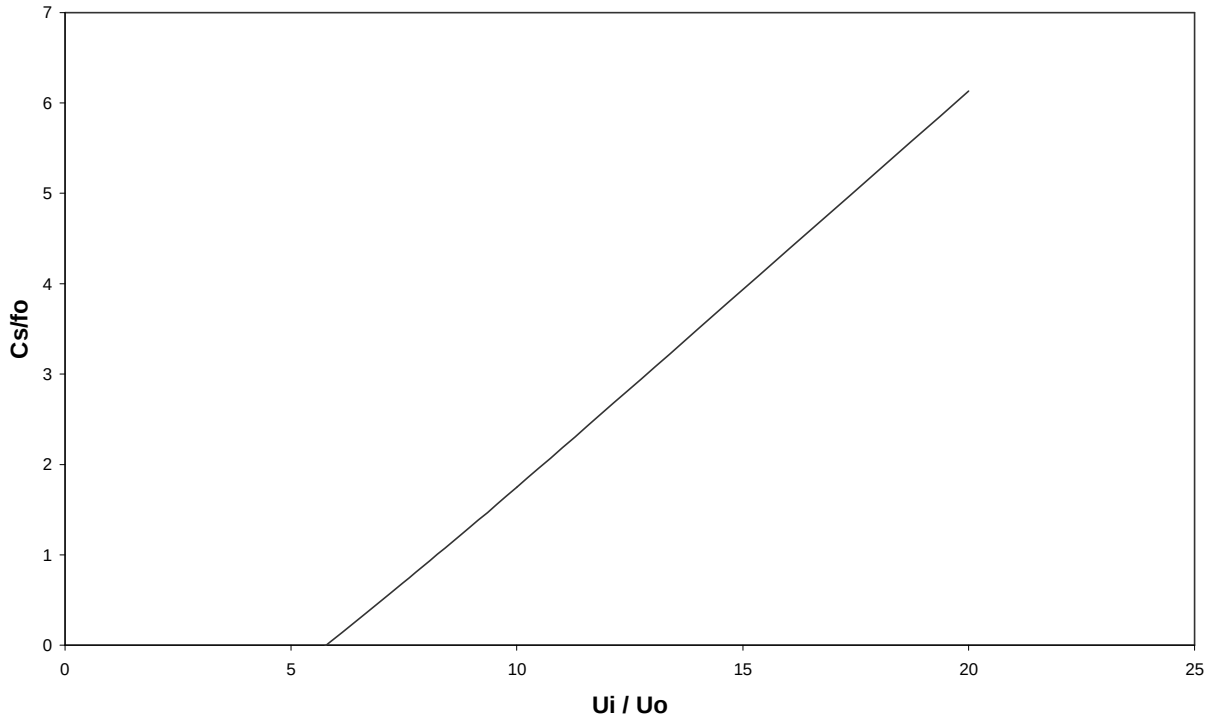

Figure (4-23): The relative spherical aberration coefficient as a function of Ui / Uo .

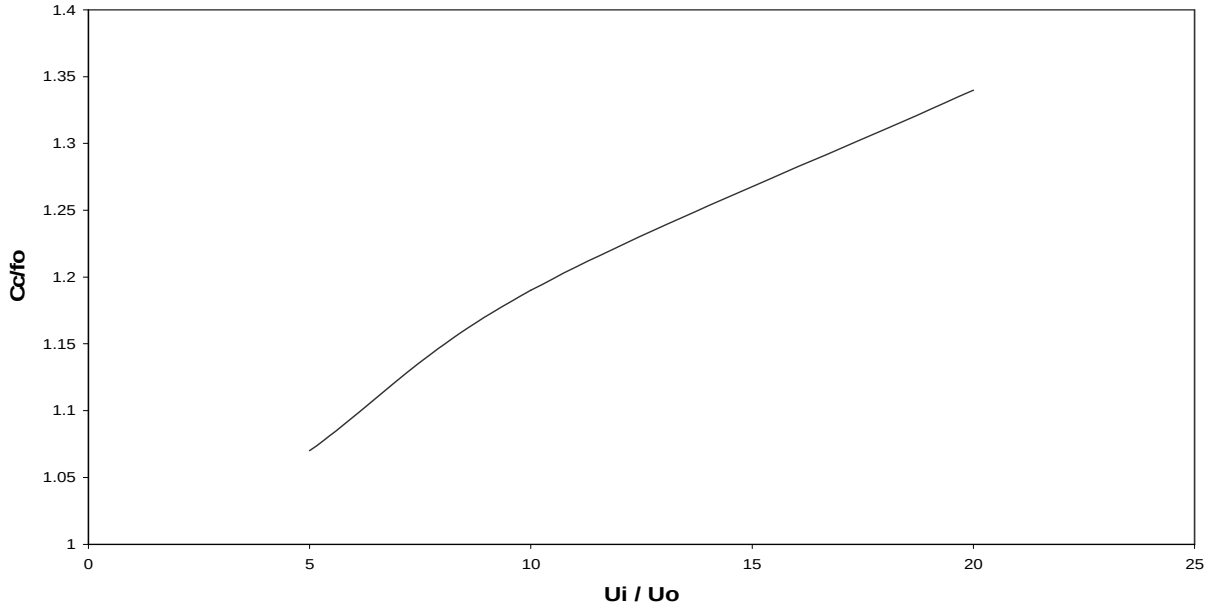

Figure (4-24): The relative chromatic aberration coefficient as a function of Ui / Uo .

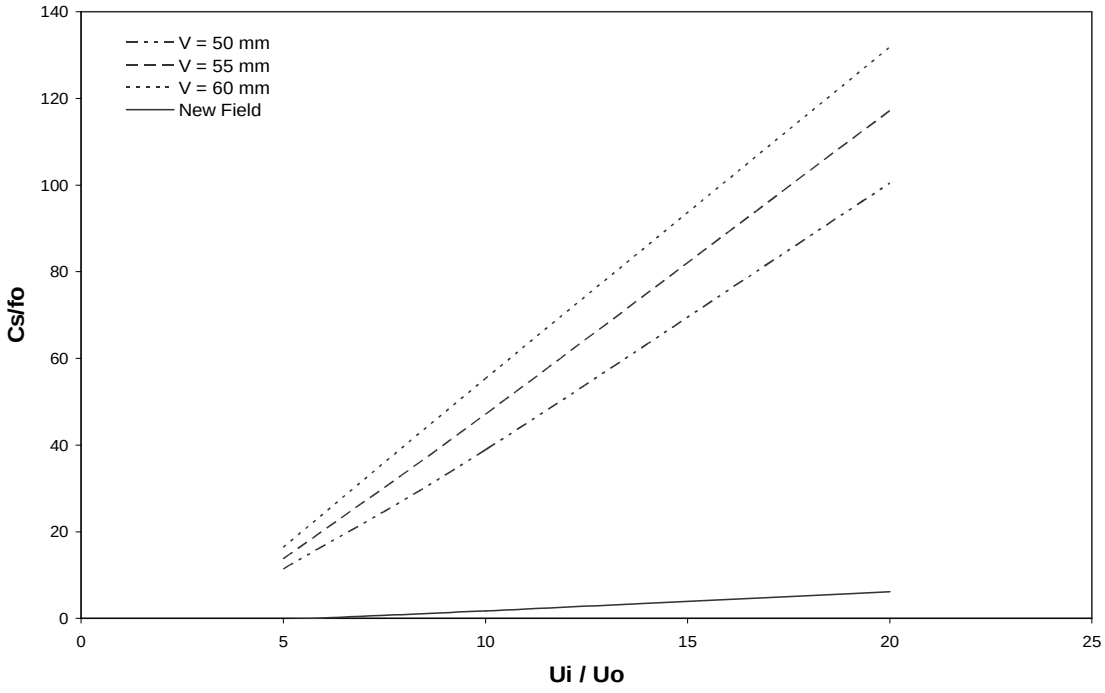

Figure (4-25): A comparison between the calculations of the relative spherical aberration coefficient by using the analysis approach of symmetrical electrostatic deflector and the calculation by using the synthesis approach by using the suggested potential distribution .

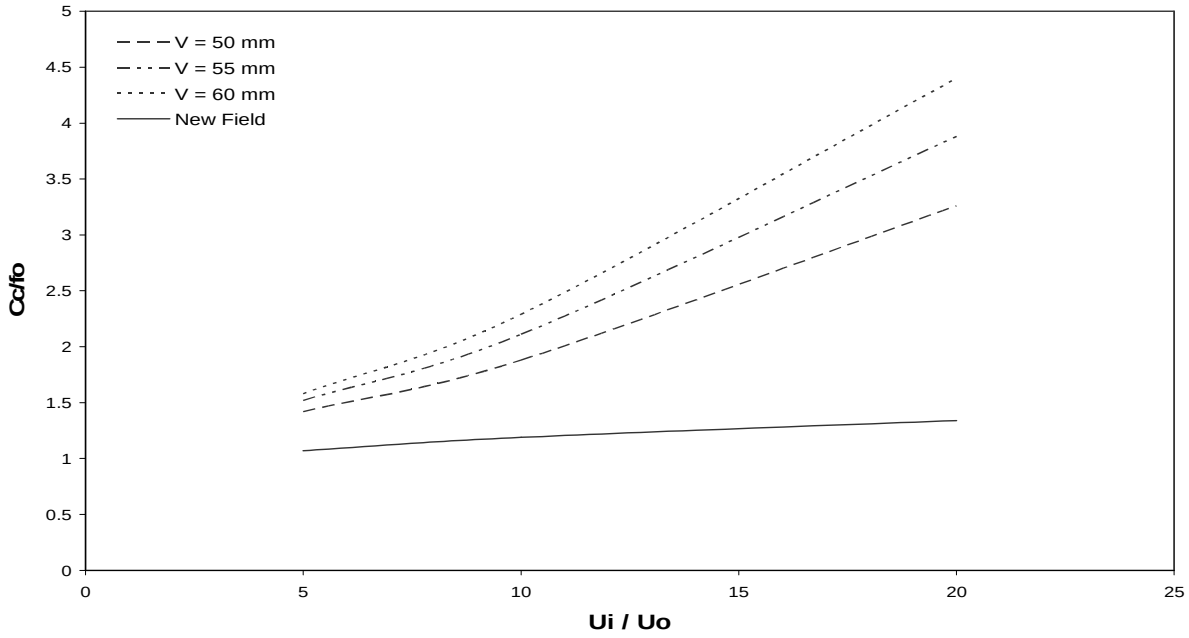

Figure (4-26): A comparison between the calculations of the relative chromatic aberration coefficient by using the analysis approach of the symmetrical electrostatic deflector and the calculation by using the synthesis approach.

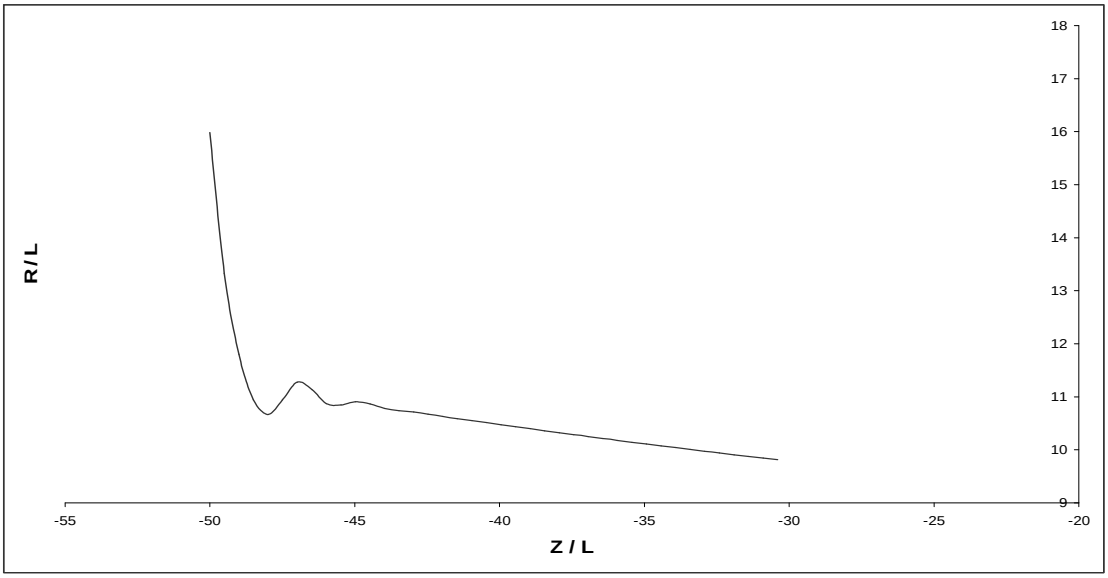

Figure (4-27): The shape of electrostatic deflector which is computed by using the suggested potential distribution .

Chapter Five

5- Electron-Optical Column

5-1 Electron-Optical Column Design

One of the important applications is the ion and electron lithography, which uses the electron-optics as a tool, these devices need the electron-optical column to achieve many purposes. The electron-optical column consists of a series of magnetic and / or electrostatic lenses and / or deflectors. The incoming accelerated electron-beam enters a field of the first optical-element which is operated under zero or infinite magnification condition and then it emerges from the first optical-element to enter the field of the next optical-element which also operates under a limited operating condition and this process is repeated to final stage.

One can use the magnetic and electrostatic deflectors which are studied in our present work to make many types of electron-optical column. The arrangement of the magnetic and electrostatic deflectors gives us the final properties of the electron-optical column, and this arrangement gives us the operating mode of the column.

Figures 5-1, 5-2, 5-3 and 5-4 show the different types of the electron-optical column. For example, the electron-optical column of figure 5-1 consists of six deflectors: the symmetrical electrostatic deflector, the magnetic deflector, the symmetrical electrostatic deflector, the asymmetrical electrostatic deflector, the asymmetrical electrostatic deflector and the magnetic deflector. The accelerated electron-beam enters the first symmetrical electrostatic deflector which has an

infinite operating condition closed to optical-axis then it exits from this deflector with a shifting equal to one unit and the electron-beam enters the magnetic deflector which operates under zero magnetic condition then the electron-beam retrain to the optical-axis and at the next stage the electron-beam enters the symmetrical electrostatic deflector and emerges to enter the asymmetrical electrostatic deflector which has the infinite magnification condition then the fifth and sixth stages consist of asymmetrical electrostatic and magnetic deflectors with zero magnification condition, respectively. The final result of the whole column represents the zero magnification condition and this result is the same as that in figures 5-3 and 5-4, while the column in figure 5-2 represents the infinite magnification condition.

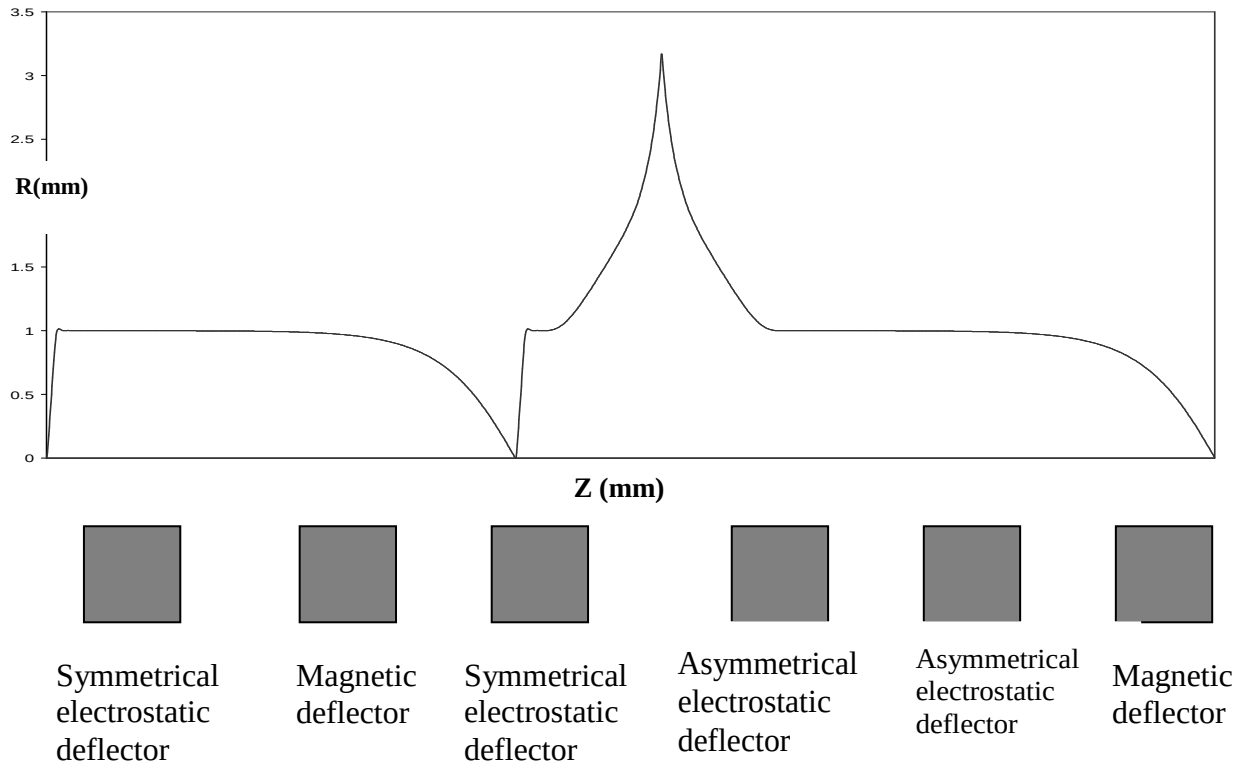

Figure 5-1: The trajectory of the accelerated electron-beam along the optical axis of the electron-optical column.

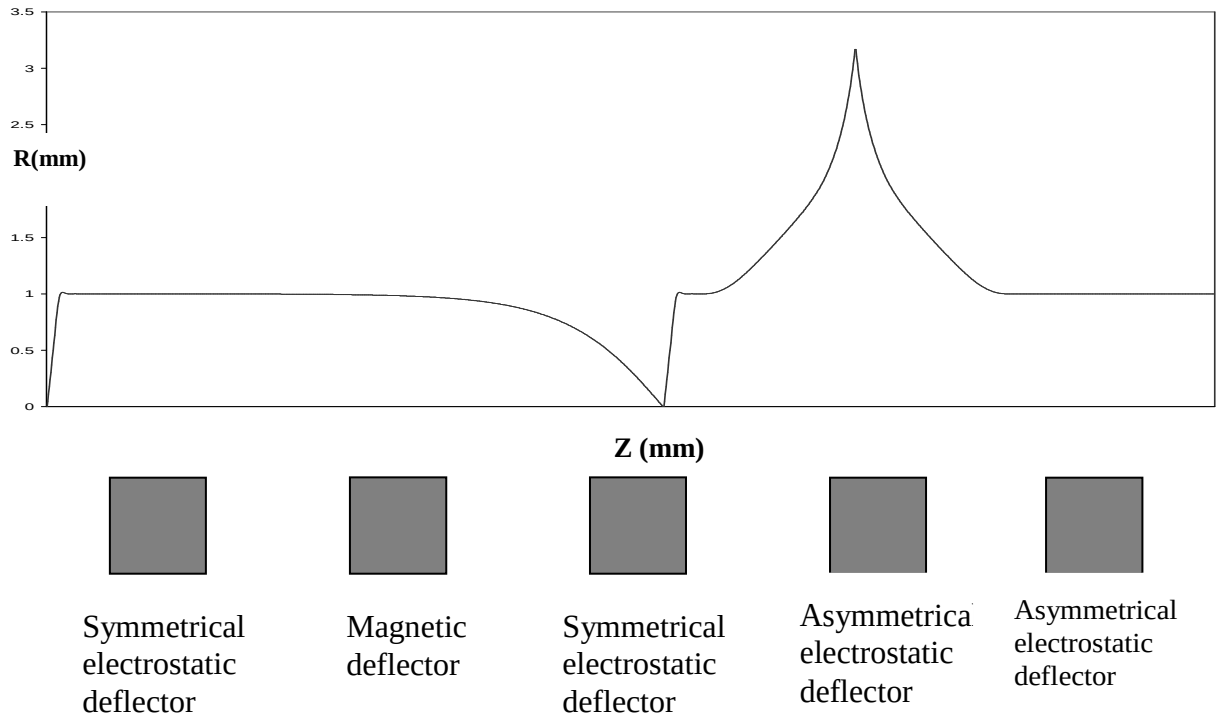

Figure 5-2: The trajectory of the accelerated electron-beam along the optical axis of the electron-optical column.

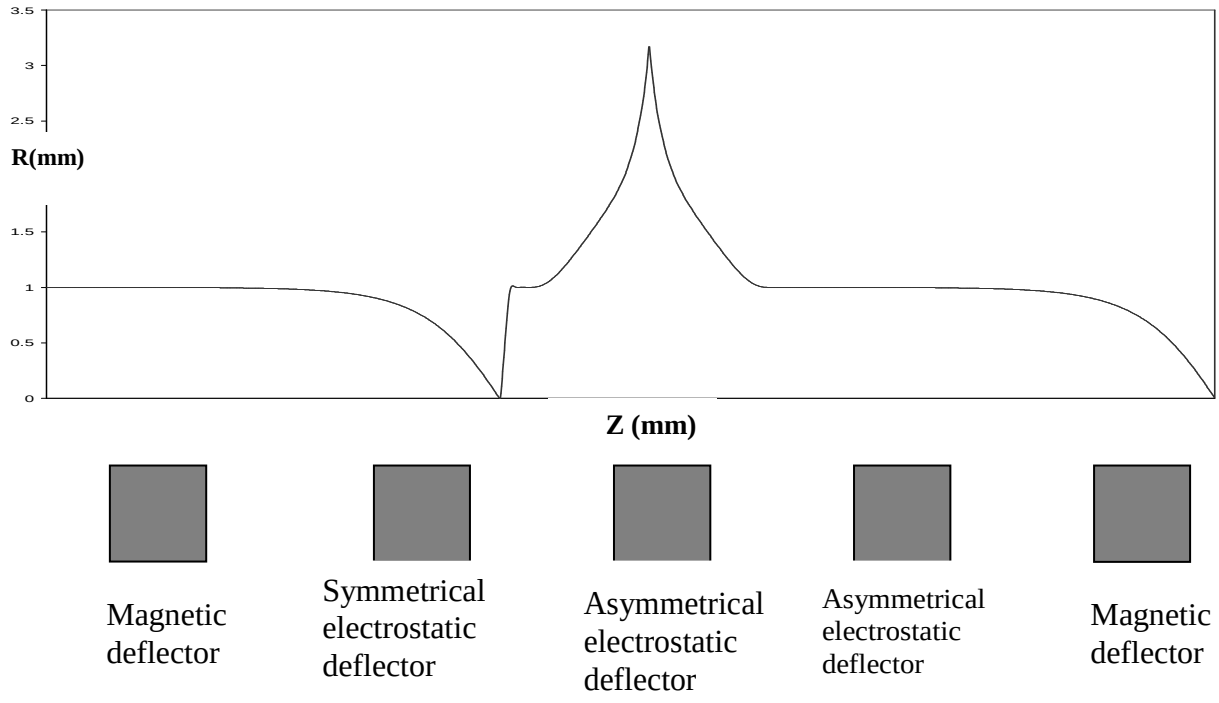

Figure 5-3: The trajectory of the accelerated electron-beam along the optical axis of the electron-optical column.

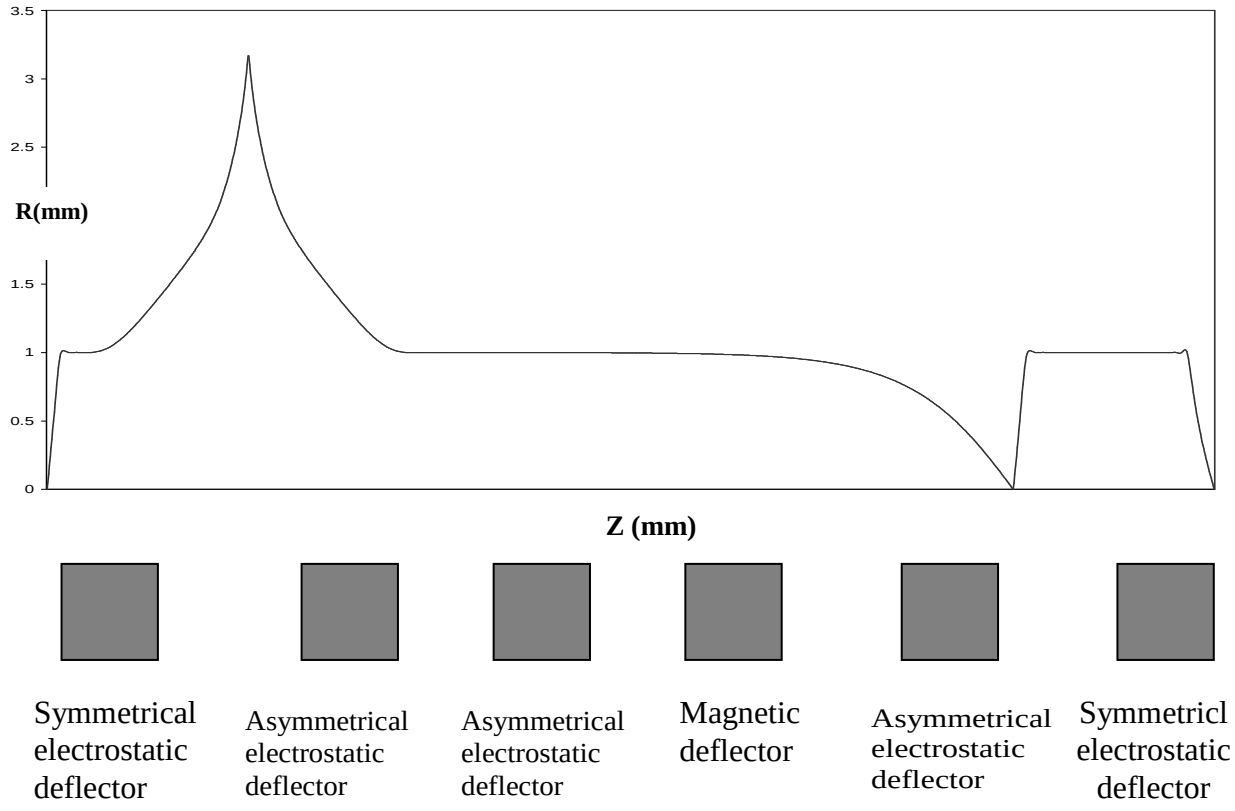

Figure 5-4: The trajectory of the accelerated electron-beam along the optical axis of the electron-optical column.

Chapter Six

6- Conclusion And Suggestions For Future Work

6-1 Conclusion Of Magnetic Deflector Calculations

By using the synthesis approach in magnetic deflector calculations it is found that: the optimization can be made via changing the axial field distribution model and the new axial field distribution model could be suggested. Secondly, the optimization can be achieved by changing the geometrical shape of the coil where the variation of the angle of the coil reduces either the spherical aberration or the chromatic aberration or both. Then the spherical and chromatic aberration can be reduced in another stage by changing the length of the coil. In many cases the optimization calculations succeeds to reduce either the spherical aberration or the chromatic aberration and in some cases both spherical and chromatic aberrations are reduced.

To find the optimum results one can choose the best value of NI / SQRT [Vr] which gives us the minimum values of the relative spherical and chromatic aberrations, where at a limited value of NI / SQRT [Vr] we have the minimum value of relative spherical and chromatic aberrations.

6-2 Conclusion Of Electrostatic Deflector Calculations

By using the analysis approach in the calculations of electrostatic deflectors it is found that the spherical and chromatic aberrations can be reduced by choosing the best geometrical shape and one can find the best geometrical shape by testing some vertical and horizontal dimensions of the parallel-plates. In some cases the

chromatic aberrations can be reduced to a very small values by choosing the special dimensions.

By using the potential distributions of the cases which are computed by the finite element method [FEM] in the analysis approach one can suggest the new potential distribution in the synthesis approach and this potential distribution can give us the best result. Also, we find that the suggested potential distribution succeeds to reduce the spherical aberration to be zero and the result of the suggested potential distribution is better than that of the analysis approach. Finally, in the synthesis approach and with the suggested potential distribution the results of the infinite and zero magnification condition coincide.

Future Work

One can use a different approach to do the optimization, where in the case of magnetic deflectors one can use other types of coils as sources of magnetic deflection field and the geometrical shapes of these coils can be changed to reach an optimum design. Also, one can use another type of axial magnetic deflection models, and also, another new axial magnetic deflection field distribution can be suggested.

In the case of electrostatic deflectors one can use another mathematical method, for example: the FDM, to determine the axial potential distribution in analysis approach calculations. Different types of electrostatic deflectors can be studied and by varying their geometrical dimensions and the distance between plates of deflectors one can find an optimum design.

Chapter One

1- General Introduction

1-1 Introduction

The analogy between electron optics and light optics extends to the domain of deflection systems [Paszkowski 1968]. The systems which deflect electron rays correspond to prisms in ordinary optics; thus, they are often called electron prisms. Electron beams are deflected for many purposes [Szilagyi 1988]. The most common and classical type of deflection is used in cathode ray tubes, lithography machines, scanning electron microscopes, electron accelerators, electron-beam manufacturing technologies and some other analytical instruments. Its purpose is to scan the beam over a surface.

A deflection system is an arrangement of electrodes or coils by means of which it is possible to exert an influence on the path of an electron ray. A fundamentally different type of deflection is needed in cycle particle accelerators, mass and beta spectrometers, and energy analyzers. In this case, deflection is used either for guidance of beams along curved trajectories or separation of particles with different energies and/or masses from each other. In both cases the main trajectory of the beams is a curve.

A deflection system must satisfy a number of conditions. First of all, it should have a high deflection sensitivity which is the ratio of the displacement of the spot on the screen (surface) to the deflection voltage or to the current flowing in the deflection coil. This displacement should be proportional to the factor causing the deflection. Moreover, this system

should not introduce distortion by de-focusing the electron ray at the surface of the luminescent screen.

Electron deflection systems are regions in which there is a two-dimensional electrostatic or magnetic field of plane symmetry. In fixed-beam instrument [Hawkes and Kasper 1989], essentially in conventional transmission electron microscopes, deflection plays a minor role and is provided only to permit nonmechanical alignment of the column. In scanning devices, the role of the optics of the deflection system is to move a focused spot in a raster pattern over a prescribed area of a specimen or a viewing screen, or to sweep a two-dimensional image over a small detector, and its design is at least as important as that of the lenses. The deflection system becomes just one member of the complex sequence of optical components that make up these hybrid instruments.

The deflection system may be either magnetic or electric, or mixed, and each type has practical application. In television tubes, for example, the power consumption is higher for magnetic deflectors, but these are nevertheless preferred, for it is easier to provide the required deflection current than the voltage needed in an electric system; moreover, the distortions are lower. In the range of frequencies used in television systems, induction effects do not yet play a role.

The electrostatic deflectors usually consist of pairs of plates, symmetrical about a plane through the optical axis. They may have a wide variety of shapes, ranging from simple rectangles parallel to each other with tilted or curved surface (see figure 1-1). By choosing the electrode potentials appropriated, not only can deflection at an arbitrary azimuth be achieved but the aberration can also be partially corrected.

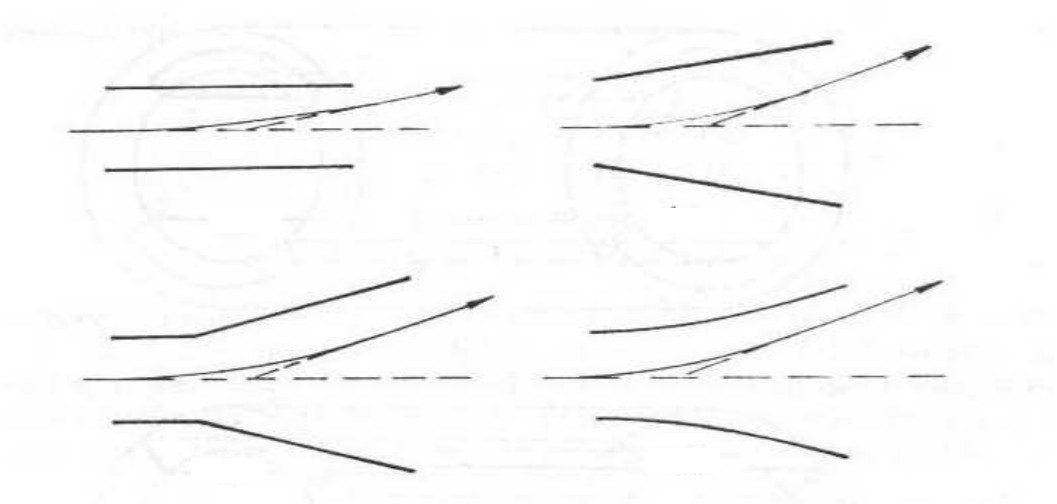

Figure (1-1): Shape of electrostatic deflector [Hawkes and Kasper 1989]

In the magnetic deflectors, two geometries are common: saddle coils and toroidal coils. Saddle coils (see figure 1-2) are usually enclosed in a ferrite sheath, thereby reducing the wastage of flux. The shielding is omitted only in devices design function at high deflection frequencies in order to reduce the inductance. In toroidal structures illustrated in figure 1-3, the turns of the two individual coils are wound meridionally, (lengthwise around a ferrite yoke) which may have a more complicated shape than a simple cylinder or cone.

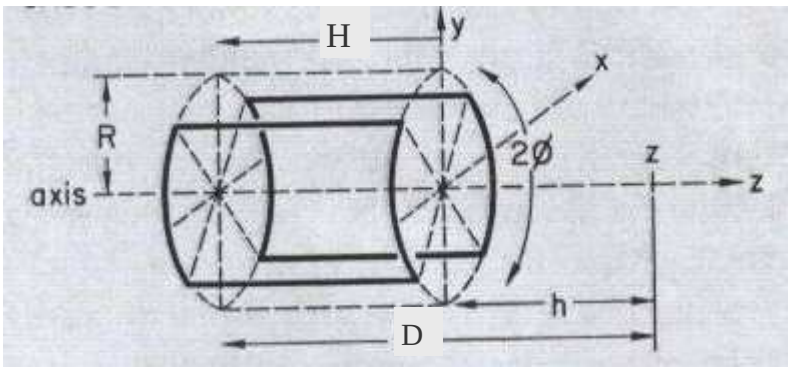

Figure (1-2): Saddle deflection coil [Hawkes and Kasper 1989].

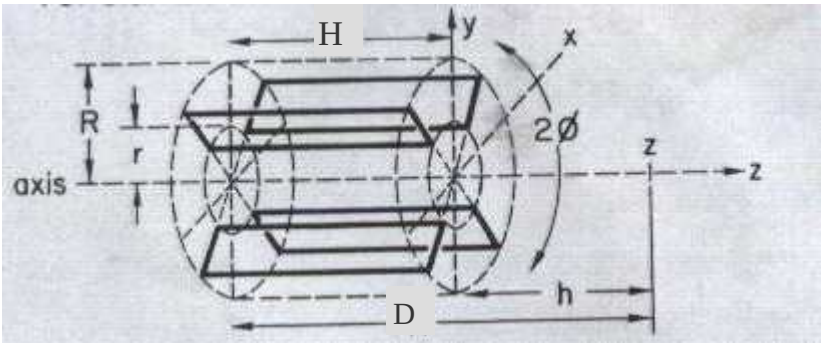

Figure (1-3): Toroidal deflection coil [Hawkes and Kasper 1989].

The study of the deflection systems optics passes essentially through the same stages as those already encountered for round lenses or quadruples; the novel aspects arise from the new symmetry conditions.
The treatment of the deflection system have considered the system a rotationally symmetric similar to the round-lenses case and the line of intersection of the symmetry or antisymmetry planes in quadruple system – to have experienced no transverse force.

1-2 Historical Development

1-2-1 Electrostatic deflector

The calculation of energy distribution was used by Poulin [1978] for optimization of 180^{o} hemispherical electrostatic deflector. Energy distribution has been computed for a large range of possible dimensions by means of least-square fits. Munro and Chu [1981a] used the numerical analysis of electron beam lithography system to describe the numerical computation of the field in electrostatic deflectors by the charge density method and finite element method. The electrostatic deflectors are

assumed to have a fourfold symmetry, with electrodes consisting of cylindrical and/or conical segments.

High performance electrostatic deflectors are required for wide angle and high precision deflection systems. Much work has been performed and reported regarding multipole-type deflectors without asymmetrical errors. Asymmetrical errors may deteriorate wide range deflection properties. Geometrical errors in manufacturing were taken into account by Idesawa et al [1983] in evaluating nonequisectored-type multipole electrostatic deflectors. A contribution factor was introduced to evaluate wide range deflection properties. They demonstrated that the deflection performance of manufactured deflectors could easily be evaluated by the proposed method from their geometrical dimension.

Soma et al [1984] developed an interactive computer aided design and evaluation system sectored-type electrostatic deflectors. The geometrical dimensions of a deflector were measured and a computer model was constructed. By this system, the wide area deflection properties can be estimated from the computer model and displayed graphically.

The concept of asymptotic aberrations of combined focusing-deflection systems were discussed by Tang [1986]. The first order asymptotic chromatic and third-order geometrical aberration coefficients of combined electrostatic focusing-deflection system had been derived. Each of the aberration coefficients was expressed as polynomials in object distance or in reciprocal of magnification.

An optimization method for nonequiradial electrostatic deflection systems was made by Grigorov [1988]. The improvement of the electrostatic deflectors characteristics could be achieved by a nonequiradial arrangement of the deflection electrodes. A graphical method for determining the parameters of nonequiradial deflectors based on the known integral equation method was developed.

The aberration of electrostatic lens and electrostatic deflection systems due to misalignment was analyzed by Kurihara [1990] for the design of micro fabrication system. The potential for lens and deflector having an electrode axis shift was approximated by introducing a shift function that expressed the electrode shift from the optical axis. On the basis of this approximation, mixed aberrations due to misalignment of lens and deflector electrodes could be analyzed, including the effect of a nonuniform electrode axis shift.

Electrostatic deflection systems in which the deflector plates are edgeways to the beam were investigated by Read [1999]. A deflection system that can deflect in both transverse directions was considered and the geometry was optimized to minimize the aberrations, which were found to be 4 to 30 times smaller than the aberrations of conventional deflection system.

1-2-2 Magnetic deflector

Munro [1974] derived the formula for calculating the first- order optical properties, third-order geometrical aberrations, and first-order chromatic aberrations of combined round magnetic lens and two-dimensional deflection systems. His formulae are applicable to the general case in which the lens and deflector field are superimposed on one another. Munro [1975] introduced the methods for computing the optical properties of any combination of magnetic lenses and deflection yokes, including the most general case in which the lens and deflector fields may physically be superimposed.

The design of improved postlens deflection coils for electron-beam microfabrication was described by Amboss [1975]. These coils were made for use in a Cambridge Instrument Co. model S-4 scanning electron microscope column.

The considerations and results of designing air-core scanning systems comprising round lenses and saddle-type deflection coils were presented by Ohiwa [1977]. He found that, if the deflection coils were cosine distributed, the third-order deflection aberrations were similar to those of a round magnetic lens. This round lens type deflection aberration can be eliminated or reduced by using the Moving Objective Lens (MOL) and predeflection.

A method called " dynamic programming" was introduced by Szilagyi [1977a,b , 1978]. In this approach the integration interval between the object and the image is divided into a set of small

subintervals; then starting from the object coordinate, for instance for spherical aberration is minimized under given constrains in each of these subintervals. The result is an analytic axial field distribution, which is then assumed to be the best field.

Goto et al [1978] introduced design calculations of a variable-aperture aberration and scanning exposure system. Aberration formulas were developed for the focus deflection system, which could handle systems consisting of a set of focus and deflection coils arranged in rotated angular positions, taking into account the finiteness of the object.

Lencova [1980] had shown that the aberration coefficients of an electron-beam deflection system with several deflection stages could be expressed for given geometry and different excitations and rotation of individual stages with the help of coefficients of individual stages and a set of auxiliary coefficients. Then the optimum geometry and set-up of an electron-beam scanning system was found.

Kuroda [1980] introduced the method for calculating the deflective aberration for a deflection system with two deflectors and a lens by using the independent aberration of each deflector. The method gives the deflective aberrations without the calculation of deflection fields or paraxial trajectories when the conditions (rotation angle and coil current) of each deflector are changed. This method can be applied successfully whenever the centers of the deflection fields are separated from each other by more than the half value width of the wider deflection field.

The numerical analysis of magnetic deflector in electron-beam lithography system was carried out by Munro and Chu [1981b]. Formulae were derived for calculating the first and third harmonic components of the magnetic deflection field, for both toroidal and saddle yokes, either in free-space regions by using the Biot-Savard law or in the presence of rotationally symmetric ferromagnetic materials by using the finite element method.

A combined system consisting of round lenses and magnetic deflector with superimposed fields had been studied by Jiye [1981]. The general expressions for superimposed fields and trajectories were obtained. The Gaussian optical properties of the system were discussed and the effect of magnetic deflector on the round magnetic and electrostatic lens migth be considered as the linear transformations for Gaussian trajectory parameters. Then the expressions for calculating the aberrations were given in a compact matrix form appropriate for numerical computation.

A method of analytical field calculation was presented by Kasper [1981], which was suitable for solution of Dirichlet problems in rotationally symmetric domains with arbitrary boundary values depending also on the azimuth. This method consisted of the linear superposition of the fields of coaxial rings carrying a harmonic source distribution to be determined from the boundary values. The application of this method was used for toroidal magnetic deflection system.

A novel deflection system had been developed by Pfeiffer [1981], which essentially eliminates off-axis aberrations including the transverse chromatic aberration by employing a variable axis lens (VAL). This lens

shifts the electron optical axis in synchronism with the deflected beam. The system comprises two precision pole piece lenses to achieve telecentricity, two composite predeflection yokes, and two yokes positioned in the pole piece region of the final lens.

A focusing and deflection system with vertical landing and reduced aberrations was developed by Kuroda [1983], for direct electron-beam lithography. The system consisted of two magnetic lenses and a magnetic deflector. The excitations of the lenses were opposite to each other. The deflector, which had saddle coils was set inside the first lens. By using the expression of the field parameters and with the aid of the Orthogonat Design Method, Zhi-xing et al [1986] optimized the design of the saddle deflection yoke with a ferromagnetic shield.

A unified deflection aberration theory had been further developed by Ximen et al [1996a] for magnetic deflection system with curvilinear or rectilinear axis. By using variable method, primary-order deflection aberrations with respect to curvilinear or rectilinear axis could be universally calculated by means of gradient operations on eikonal (the function of optical length). Based on the variational deflection aberration theory, a magnetic deflection system consisting of homogeneous deflection field and a homogeneous sextupole field had been further investigated [Ximen 1996b].

Zhao and Khursheed [1999] introduced the variable axis lens (VAL) system for magnetic round lenses which could be achieved by using electrostatic deflectors (ME-VAL) instead of magnetic deflectors (MM-VAL). The condition for ME-VAL was obtained from the paraxial ray equation rather than from axial focusing field expansions. The study

introduced that the ME-VAL also reduced the off-axis aberrations significantly, though not as much as its MM-VAL counterpart.

The surface charge density method and the Fourier spatial harmonic expansion technique for three-dimensional magnetic field calculations were studied by Wang et al [1999]. Spatial harmonic components of the magnetic field generated by the magnetized ferromagnetic core of deflection yokes were derived by the surface magnetic charge method.

Nakagawa and Nakata [2000] proposed an improved power-series expansion method for the analysis of magnetic deflection yoke in a cathode-ray tube (CRT). The magnetic field was expanded to either of two different power-series formulations, depending on the radial position from the central axis of the deflection yoke. The coefficients of the power series were calculated by symbolically differentiating the magnetic field expressed by the surface magnetic charge method formulation.

1-2-3 Combined electrostatic and magnetic deflector

Chu and Munro [1981a] derived the formula for computing the optical properties of lithograph systems containing any combination of magnetic and electrostatic lenses and deflectors. The general case of a dual-channel deflection system was considered, in which the main-field deflectors and sub-field deflectors could either be magnetic , electrostatic, or mixed. Chu and Munro [1981b] described how the damped least squares method could be applied to the design and optimization of combined focusing and deflection systems for electron beam lithography.

A deflector for electron or ion beam lithography was described by Kuo and Groves [1983]. It combines the functions of focusing and deflection in a single unit. Focusing was accomplished by means of a uniform magnetic field oriented parallel with the optical axis of the system. A uniform electric field oriented perpendicular to the magnetic field provided the deflection capability.

Smith and Munro [1986] presented an aberration theory that could handle any combination of electrostatic round quadrupole and octople lenses, electrostatic and magnetic deflectors, and crossed electrostatic and magnetic quadrupole lenses. Yu [1986] derived the relativistic fifth-order geometrical aberration equation of a combined electric-magnetic focusing-deflection system with superimposed field by using variational principle and taking symbolic derivatives and inner product of complex numbers as a mathematical tools. Lencova [1988] summarized some basic ideas used in the design of combined deflection and focusing systems. The aberration coefficients of post-lens and pre-deflection were discussed. Also the deflection aberrations of pre-deflection followed by lens and the aberration of two-stage pre-deflection were discussed.

1-3 Optimization: Analysis And Synthesis

Any reasonable design of an electron or an ion optical system must take the aberrations into account. There are two fundamental approaches to optimize the parameters of a charged-particle optical system: (i) the analysis and (ii) the synthesis of electron and ion systems [Szilagyi 1985]. The optimization approach looks for such electron and ion optical elements that would provide the required optical properties with minimum aberrations.

The method of synthesis is usually trial and error. The designer starts with given simple sets of electrodes or pole pieces and tries to improve the design by analyzing the optical properties and changing the geometrical dimensions as well as the electric and magnetic parameters of the system. This process must be repeated until it converges to an acceptable solution. Due to the infinite number of possible configurations, the procedure is extremely slow and tedious. It can yield quick and reliable results only if a reasonable guess of the answer is already available from a previous design or from an expert before the work starts. The iterations can be automated by using the damped least squares method [Chu and Munro 1981b].

Optimization by synthesis, which is sometimes called inverse design procedure, has been one of the most ambitious goals of electron and ion optics. This approach is based on the fact that for any imaging field, its optical properties and aberrations are totally determined by the axial distribution of the field. This has been dealt with by many authors [Septier 1966, Moses 1973, Szilagyi 1977a, Chu and Munro 1981c, Szilagyi 1983]. Only the axial distributions and their derivatives appear in those expressions. Then, instead of analyzing a hopelessly vast amount of different electrode and pole piece configurations we can take the criteria defining an optimum system as initial conditions and try to find the imaging field distribution (and hence synthesis the electrodes or pole pieces) that would produce it. i.e. in synthesis approach, one tries to find the best axial field distribution or the best shapes of these axial distributions that would satisfy the given constraints.

1-4 Aim Of The Project

The present work, aims at finding the optimum design of magnetic and electrostatic deflectors which give rise to the minimum spherical and chromatic aberration. Both analysis and synthesis approaches of optimization method are used in this work.

In magnetic deflector calculations, the synthesis approach is used to find the optimum design of the magnetic deflector of the saddle yoke deflection coil, with the moving objective lens concept. Deflection aberrations are minimized by changing the geometrical shape of the deflection coil, where the length and angle are varied.

In electrostatic deflector calculations, both analysis and synthesis approaches are used to find an optimum design, which gives rise to minimum aberrations for electrostatic deflector designs which consist of two parallel-plates, and the optimization is made by changing the geometrical shape of the deflector by varying the dimensions of the parallel-plates. Both symmetric and asymmetric electrostatic deflectors are studied. Secondly, the synthesis approach is used to find minimum values of the aberration by means of the new axial field distribution that has been put forward in the present work for the electrostatic deflectors under investigation. The shape of the deflector is found by using the reconstruction method. Finally, the magnetic and electrostatic deflectors are assembled to give complete columns of deflection systems and plot the trajectories of the beam traversing them.

Chapter Two

2- Electron-Optical Considerations

2-1 Introduction

Electron and ion optics is the theory and practice of production, control, and utlilization of charged-particle beams. Charged-particle beams can only be controlled(acclerated, focused, and deflected) by external electromagnetic fields. Electric fields are produced by a set of electrodes held at a suitably chosen voltage. Coils surrounded by ferromagnetic materials provide magnetic fields. Different symmetries may be utilized for electron and ion optical elements such as lenses, deflectors, etc.

In a typical device, the beam originates with some energy from the electron source and enters the focusing field of an objective lens at a certain acceptance angle, focused to a point image at a reasonable working distance behind the lens. However, due to the geometrical and chromatic aberrations of the lens, a point image can never be achived. There will be a crossover of different trajectories instead. This crossover can be imaged by a projector lens and deflected by a suitable deflector element. The deflector itself is a source of additional aberrations.

2-2 Tarjectory Equations

2-2-1 Paraxial-ray equation in electrostatic field

The trajectory of electrostatic symmetrical electron or ion optical system is given by the following equation (see for example, Szilagi 1988):

$$\frac{d^2r}{dz^2}+\frac{dr}{dz}\frac{U'}{2U}+\frac{U''}{4U}r=0 \qquad (2-1)$$

where *r* is the radial displacement of the beam from the optical axis z, and the primes denote a derivative with respect to *z*. *U=U(z)* is the electrostatic potential distribution along the optical axis *z*. Equation (2-1) is a linear homogeneous second-order differential equation, known as the paraxial-ray equation which describes the paths of charged particles moving through a roationally symmetrical electrostatic field characterized by the potential function *U*. The paraxial-ray equation was first derived by Busch in 1926. Many important deductions can be made from this equation:

a. The quotient of charge-to-mass (q/m) does not appear in the equation. Therefore, the trajectory is the same for any charged particle eneterning the field with the same initial kinetic energy, but arrives to the same focus at different times.

b. The equation is homogeneous in *U*. Therefore, an equal increase (or decrease) in the potential *U* at all the points of field (multiplying the potential by any constant) does not change the trajectory.

c. The equation is homogeneous in *r* and *z* which indicates that any increase in the dimensions of the whole system produces a corresponding increase in the dimensions of the trajectory, since the equipotentials, though of the same form, are enlarged. If the object is doubled in size, the image will be doubled in size too; the ratio between the two remains constant.

2-2-2 Paraxial-ray equation in magnetic field

The motion of an electron in an axially symmetrical field may be derived from many departure points. One can start from the agrangian [Hawkes 1982; Silagyi 1988] or from a more familiar method of elementary mechanics [Pierce 1954, Klemperer and Barnett 1971; Hawkes 1972; El-Kareh and El-Kareh 1970; Grivet 1972]. The paraxial-ray equation of an electron in a magnetic field of axial symmetry is given by:

$$\frac{d^2 r}{dz^2} + \left(\frac{e}{8 m V_r} \right) B_Z^2 \, r = 0 \qquad (2-2)$$

where e and m are the charge and mass of the electron respectively, and V_r is the relativistically corrected accelarating voltage which is given by:

$$V_r = V_a \, (1 + 0.978 \times 10^{-6} V_a) \qquad (2-3)$$

where V_a is the accelerating voltage. It can easily be realized from equation (2-2) that the force driving the electrons towards the axis is directly propotional to the radial distance r. This is the principle of a focusing field. Futhermore, this force is propotional to the square of the magnetic flux density which means that if the direction of the magnetic field is reversed by reversing the current, the direction of the force towards the axis should not change, i.e. there will be no change in the focus.

2-3 Defects Of Electron Optical System

The electron paths, which leave points of the object close to the axis at small inclinations with respect to the axis, intersect the image plane in points forming a geometrically similar patteren. This ideal image is known as the Gaussian image, and the plane in which it is formed as the Gaussian image plane. If an electron leaving an object point a finite distance from the axis with a particular direction and velocity intersects the Gaussian image plane at a point displaced from the Gaussian image points, this displacement is defined as *the aberration* [El-Kareh and El-Kareh 1970].

The quality of an electron optical system depends not only on the wavelength of electrons, but also on the aberrations from which it may suffer. These aberrations can arise from a number of different reasons. If the accelarating potential fluctuate about his mean value, *chromatic aberration* will mar the image. If the properties of the system are investigated, using a more exact approximation to the refractive index than is employed in the Gaussian approximation, one would find that the geometrical aberrations affect both the quality and the fidelity of the Gaussian image. When the properties of the system are analyzed using the nonrelativistic approximation, the disparities between the relativistic and nonrelativistic can conveniently be regarded as *relativistic aberration*. These are the most important types of aberration in electron optical systems, unless there are regions where the electron current density is very high; in such a system, the space-charge aberration produced by the interaction between the electron charges may have to be considered [Hawkes 1967].

2-4 Aberrations Of Axial Symmetrical Optical System

2-4-1 The spherical aberration

The spherical aberration is one of the most important geometrical aberrations; these aberrations are sometimes, called *aperture defect* and they are one of the principal factors that limit the resolution of the optical system. This defect occurs because the power of the optical system (magnetic or electrostatic optical system) is greater for off-axis rays than the paraxial rays, i.e. the beams passing within the optical system area at a considerable distance from the axis are more (or less) refracted than the paraxial beams so that they intersect closed to (or farther from) the image plane [Zhigarev 1975], as is shown in figure (2-1).

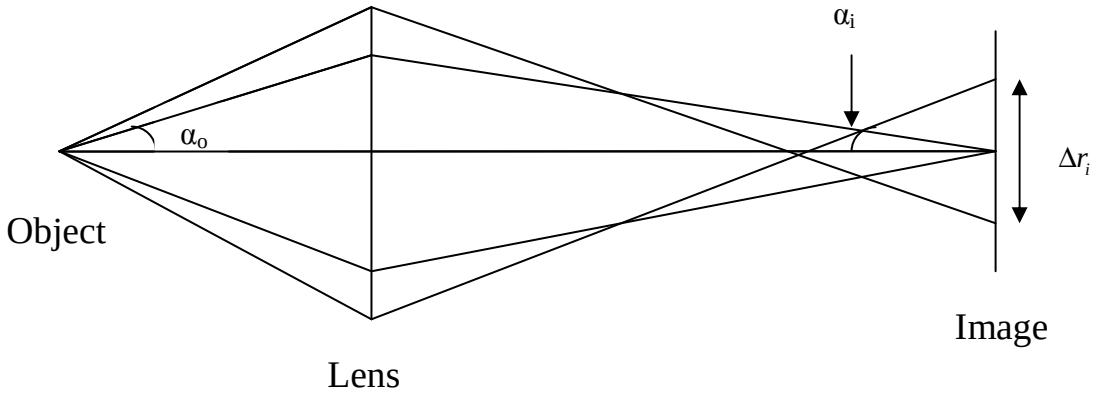

Figure (2-1): Spherical aberration

The rays confined within the aperture angle α_o are spread over a disc of radius Δr_i given by:

$$\Delta r_i = C_{Si}\,\alpha_i^3 \qquad (2-4)$$

where C_{Si} is the spherical aberration coefficient referred to image side.

The spherical aberration coefficient C_{SO}, of axial symmetric magnetic optical element (lens or deflector), referred to the object side is calculated from the following formula [Kato and Tsuno 1990] :

$$C_{SO}=\left(\frac{\eta}{128V_r}\right)\int_{zo}^{zi}\left[\frac{3\eta}{V_r}B_z^4\,r_\alpha^4+8B_z'^2\,r_\alpha^4-8B_z^2\,r_\alpha^2\,r_\alpha'^2\right]dz \qquad (2-5)$$

where η is the charge-to-mass quotient of the electron, V_r is the relativistically corrected accelerating voltage, B_Z is the axial flux density distribution, and r_α is the solution of the paraxial-ray equation with an initial condition depending on the operation mode. Actually, the integration covers the whole interval from object plane (Zo) to image plane (Zi) in spite of the magnetic limits.

The spherical aberration coefficient C_{SO} of an axially symmetric electrostatic optical element referred to the object side is given by [Scheinfeir and Galantai 1986, Szilagyi 1987] :

$$C_{SO}=\frac{U_O^{-1/2}}{16r_o'^4}\int_{zo}^{zi}\left[\frac{5}{4}\left(\frac{U''}{U}\right)^2+\frac{5}{24}\left(\frac{U'}{U}\right)^2+\frac{14}{3}\left(\frac{U'}{U}\right)^3\frac{r'}{r}-\frac{3}{2}\left(\frac{U'}{U}\right)^2\frac{r'^2}{r^2}\right]\sqrt{U}\,r^4\,dz \qquad (2-6)$$

where $U=U(z)$ is the axial potential, the primes denote derivatives with respect to z, and $U_O=U(zo)$ is the potential at the object where $z=zo$.

2-4-2 Chromatic aberration

This type of aberration is a consequence of the fact that fluctuations in the electron-optical element focal length because of a spread in electron energy (due to different initial energy of electrons, the inhomogeneous interaction of electrons with specimen,and fluctuation in the electron-optical element excitation) result in the superposition of the final screen of a number of images of different size with a consequent loss of image definition.

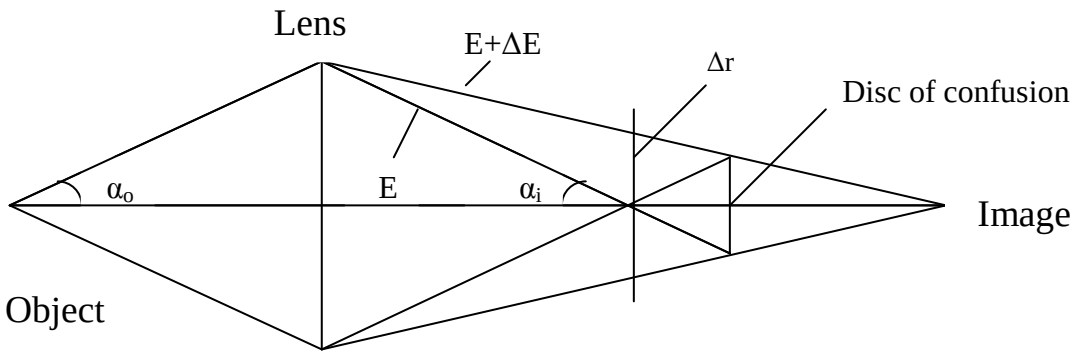

Figure (2- 2): Chromatic aberration

Figure (2-2) represents a simplified diagram defining this defect. A ray of energy $E+\Delta E$ will reach the image plane for energy E at a distance Δr_i from the axis. At a plane about halfway between the points where the two rays intersect the axis in image space, the bundle of rays having energies between E and $E+\Delta E$ are contained within a disc of confiusion of radius about one-half [Hall 1966] where

$$\Delta r_i = C_{Ci}\,\alpha_i\,\frac{\Delta E}{E} \qquad (2-7)$$

C_{Ci} is the chromatic aberration coefficient referred to image plane.

The chromatic aberration coefficient Cc of magnetic optical element , with axial symmetric field condition, is given by [Szilagyi 1985] :

$$C_{CO} = \frac{\eta}{8V_r} \int_{zo}^{zi} B_z^2 \, r_\alpha^2 \, dz \qquad (2-8)$$

where the parameters in this equation are the same as those used in equation (2-5). The chromatic aberration coefficient Cc of electrostatic optical element, with axial symmetric field condition, is given by [Scheinfeir and Galantai 1986, Szilagyi 1987, Kiss 1988] :

$$C_{CO} = \frac{\sqrt{U_O}}{r_O'^2} \int_{zo}^{zi} \left[\frac{1}{2}\left(\frac{U'}{U}\right) r' + \frac{1}{4}\left(\frac{U''}{U}\right) r \right] \frac{r}{\sqrt{U}} \, dz \qquad (2-9)$$

where the parameters in this equation are the same as those used in equation (2-6).

2-5 Magnetic Deflection Field

In magnetic deflector, two geometries are common: saddle coils and toroidal coils [Hawkes and Kasper 1989]. In the present work, only the saddle coils are taken into consideration as the source of the magnetic deflection field. Saddle coils ,figure (1-2), are usually enclosed in a ferrite sheath, thereby reducing the wastage of flux. The shielding is omitted only in devices design to function at high deflection frequencies in order to decrease the inductance.

The method used for calculating the deflection yoke fields depends on whether the deflection coils are near the magnetic materials [Septier 1980]. If the coils are not near any magnetic materials, their fields can be computed using Biot-Savart's formula. The deflection field at the axis of an air-cored saddle yoke, figure (1-2), is obtained by using the formula given by [Munro 1975]:

$$B\ (z)=\frac{N\,I\sin\phi}{\pi}\left[\frac{D(D^2+2R^2)}{R(D^2+R^2)^{3/2}}-\frac{h(h^2+2R^2)}{R(h^2+R^2)^{3/2}}\right] \qquad (2-10)$$

If the deflection yokes are near magnetic materials (for example, if the coils are wound on a magnetic former), then the yoke fields must be computed by a numerical technique such as the finite element method. The finite element method has been adopted in the present work.

2-6 The Moving Objective Lens (MOL) Concept

Ohiwa et al [1971] pointed out that the aberrations of a combined focusing and deflection system can greatly be reduced by using an arrangement of the type shown in figure (2-3). A point source of electrons, emitted from *zo*, is imaged by a lens at *zi*. The beam is deflected by the first deflector so that it enters the lens off axis. A second deflector, placed inside the lens, shifts the electrical center of the lens off axis. This so-called *Moving Objective Lens (MOL)* reduces the effect of the off axis aberrations. The spherical and chromatic aberration of the lens can be kept small by having a short working distance L_2. At the same time, the deflection aberrations can be kept small by having a large distance L_1 from the first deflector to the image plane.

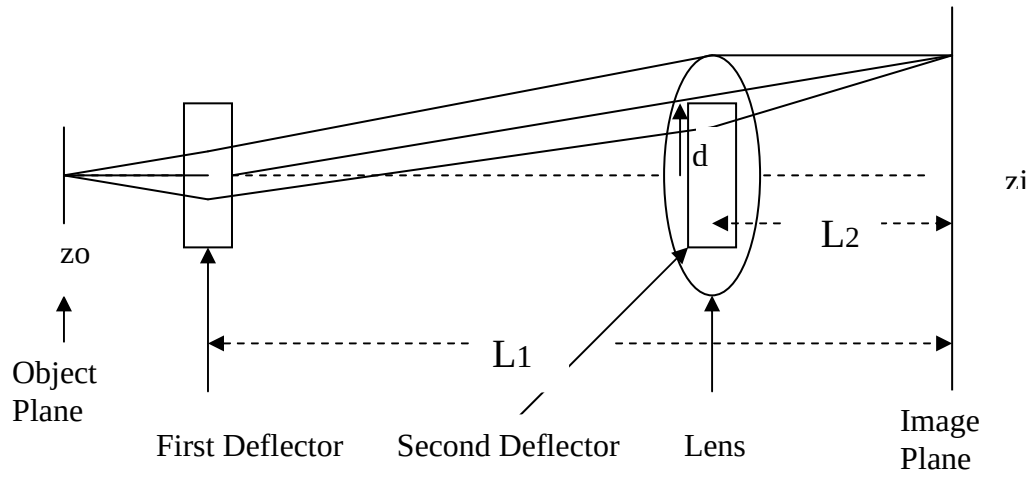

Figure (2-3): MOL arrangement [Ohiwa 1971].

Let *B(z)* be the axial flux-density distribution for the lens and *D(z)* be the deflection flux density required at the axis. Then, the following relation holds [Ohiwa 1977&1978, Kern 1979]:

$$D(z) = \frac{1}{2} d\, B'(z) \qquad (2-11)$$

where d is the displacement by the first deflector (pre-deflection).

2-7 Pole pice Design

The final task optimization of magnetic or electrostatic field is to reconstruct the pole pieces shape or electrodes shape of deflector that would produce such field. This problem has been solved by using two different approaches (i) the analytic approach and (ii) the numerical approach; the standard finite element method has been used.

2-7-1 Analytic approache

One can apply the technique used by Silagyi [1984] for constructing the electrodes of an electrostatic lens to reconstruct the pole piece shape of magnetic deflector and electrode shape of electrostatic deflector. According to this technique the equation of equipotential surfaces (the pole piece in case of magnetic deflector) is

$$R_P(z) = 2\left[(V_z - V_P)/V_z''\right]^{1/2} \qquad (2-12)$$

where R_P is the radial height of the pole piece, V_Z is the axial potential distribution, V_Z'' is the second derivative of V_Z with respect to z and V_P is the value of the potential at any one of the two pole pieces or electrodes.

2-7-2 Numerical approache

In the technique of reconstructing the pole piece or electrode shape, one would need the solution of Laplace's equation. To solve Laplace's equation numerically two different methods have been used, namely, the finite element method (FEM) and the finite difference method (FDM). The finite element method has been used in the present work.

2-7-3 The finite element method (FEM)

It is a numerical application of calculus of variation. FEM was first introduced in electron and ion optics by Munro [1971] who used it for the computation of magnetic field in round lenses. The base of this method comprises the dividing of the region to be analyzed into a large number of small finite elements (meshes), usually of a triangular shape. A potential value is assigned to each mesh-point, and the potential is

assumed to vary linearly across each triangular finite element. The differential equation of the system (Laplace's equation in this case) is replaced by an appropriate *functional*. The minimization of this functional with respect to the changes in the potentials at each mesh-point corresponds to the original differential equation. The functional must have a stationary value with respect to the small change in the potentials at each mesh-point. This condition makes it possible to set up a nodal equation for each mesh-point, relating the potential at that node to the potentials at adjacent nodes. The set of algebraic nodal equations thus obtained is solved by a suitable numerical method, to yield the potential at every nodal point. The functional is a volume integral [Munro 1971]:

$$I = \iiint_{totalvolume} \frac{1}{2} grad\, V . grad\, V \; dv \qquad (2-13)$$

where *v* is the volume.

The integral depends on the type of coordenates, the potential *V*, and its first derivatives with respect to the coordinates. The field is subdivided into triangles, each node represents the common vertex of the adjacent triangles (figure 2-4). Within each triangle the potential is expressed by a lower order polynomial of the coordinales; in most practical cases by a linear function [Kasper 1980]. With this approximation, the potential throughout each element is uniquely determined by the potentials at its vertices. Hence, the contribution from each element to the value of the functional can be expressed in terms of the vertex potential.

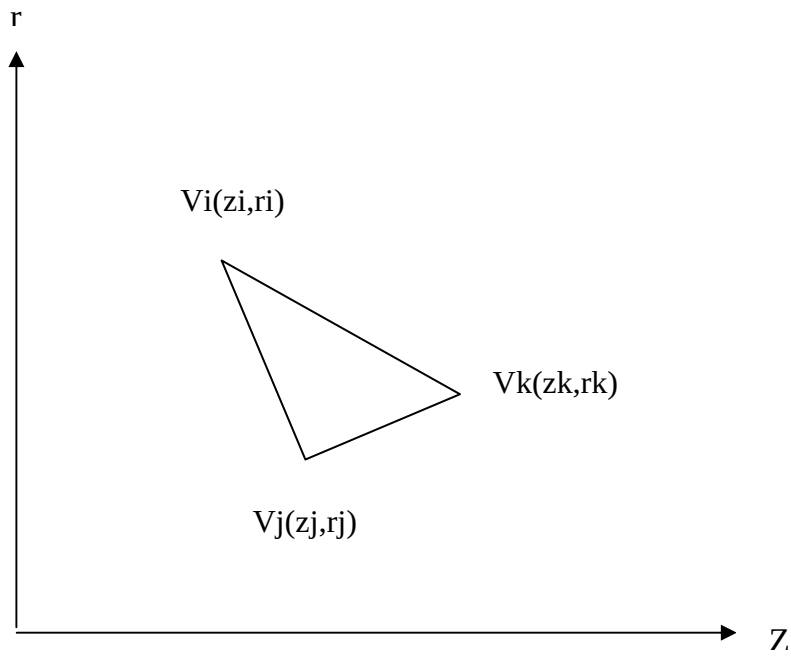

Figure (2-4): Mesh of the finite-element method.

Minimizing the functional yields a set of linear algebraic relations of the type given by the following equation:

$$V_i = \sum_{j=1}^{N} A_{ij}\, V_j + B_i \qquad (2-14)$$

Equation (2-14) relates the potentials at each vertex and its neighbours, where A_{ij} depends on the coordinates of all vertices involved, i.e. on the shape of all adjacent triangles. This set of linear equations is solved to give the potential at each mesh-point, for more specific details one can see Munro [1971, 1973] and Hawkes [1989].

2-8 Definitions And Operating Conditions

Some definitions and operating conditions of charged-particle optical systems are given in this section.

Object side: is the side of lens or deflector at which the charged particles enter.

Image side: is the side of lens or deflecor at which the charged particles leave.

The object plane (Z_O): is the plane at which the physical object is placed, or a real image is formed from a previous lens or deflector, on the object side.

The image plane (Z_i): is the plane at which the real image of the object plane Z_O is formed, on the image side.

Magnification (M): In any optical system the ratio between the transverse dimension of the final image and the corresponding dimension of the original object is called the lateral magnification:

$$M = \frac{image\ height}{object\ height} \qquad (2-15)$$

There are three magnification conditions under which a lens or deflector can operate, namely:

(i) zero magnification condition: In this operational condition $Z_O = -\infty$ as is shown in figure (2-5). For example, the final probe-forming lens in a scanning electron microscope (SEM) is usually operated under this condition.

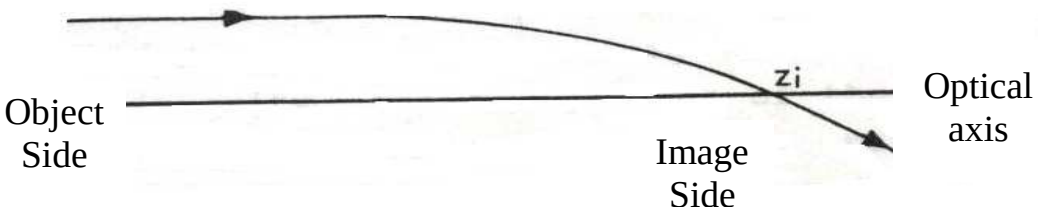

Figure (2-5): Zero magnification condition.

(ii) Infinite magnification condition: In this case $Z_i = +\infty$ as is shown in figure (2-6). For example, the objective lens in a transmission electron microscope (TEM) is usually operated under this condition.

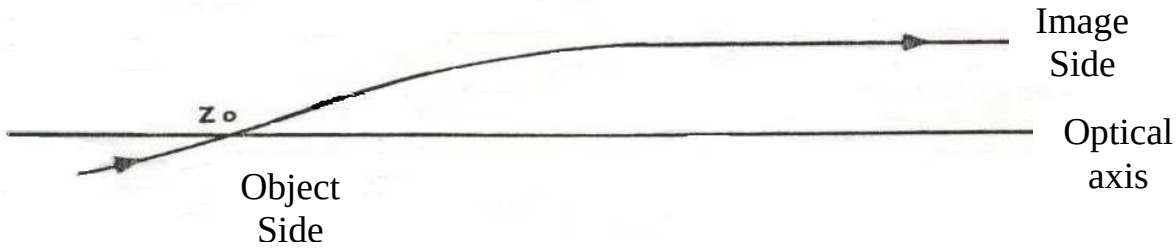

Figure (2-6): Infinite magnification condition.

(iii) Finite magnification condition: Under this operational condition Z_O and Z_i are at finite distances, as is shown in figure (2-7). As an example, the electrostatic lens in field-emission gun is usually operated under this condition [Munro 1975].

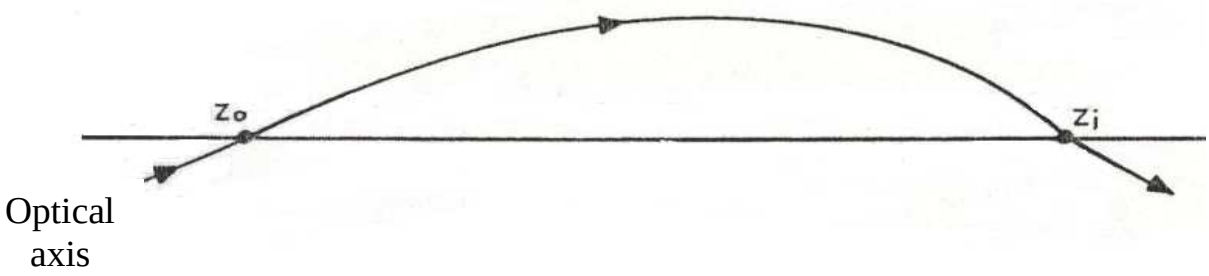

Figure (2-7): Finite magnification condition.

Examination Committee Certificate

We certify that we have read the thesis entitled

"A COMPUTATIONAL OPTIMIZATION OF AN ELECTRON BEAM DEFLECTING SYSTEM"

And as Examining Committee, examined the student

UDAY ALI HUSSAIN Al-OBAIDY

In its contents and what is related to it, and that in our opinion it is adequate as standard of thesis, with *Excellent* Degree of Doctor of Philosophy In *Physics*

Signature:
Name: **Prof. Dr. Inaam S. Al-Nakeshli**
Title: Professor (Chairman)
Date: / /2005

Signature:
Name: **Dr. Hassan H. Muhammad**
Title: Chief Researcher (Member)
Date: / /2005

Signature:
Name: **Dr. Ali H. Abd - Almonaam**
Title: Senior Scientific Researcher (Member)
Date: / /2005

Signature:
Name: **Dr. Samir K. Al-Ani**
Title Assist. Professor (Member)
Date: / /2005

Signature:
Name: **Dr. Abd-A. K. Al - Saadi**
Title: Assist. Professor (Member)
Date: / /2005

Signature:
Name: **Dr. Ahmad K. Ahmad**
Title: Assist. Professor (Supervisor)
Date: / /2005

Approved by the University Committee of Postgraduate Studies

Signature:
Name: **Dr. Laith A. Al-Ani**
Title: Assist. Professor
(Dean of the college of science)
Date: / /2005

LIST OF SYMBOLS

a	The field width at half maximum $B_m / 2$.
B(z)	Magnetic flux density (Tesla).
B_m	Maximum value of axial magnetic flux density distribution (Tesla).
$B_x(z)$	The deflection field at the axis of an air-cored saddle yoke (Tesla).
C_c	Chromatic aberration coefficient (mm) .
C_{ci}	Chromatic aberration coefficient referred to image side (mm).
C_{co}	Chromatic aberration coefficient referred to object side (mm).
C_s	Spherical aberration coefficient (mm).
C_{si}	Spherical aberration coefficient referred to image side (mm).
C_{so}	Spherical aberration coefficient referred to object side (mm).
D(z)	Deflection magnetic flux density (Tesla).
d	Displacement by the first magnetic deflector (mm).
E	Energy of electron beam .
e	Electron charge (1.6×10^{-19} C).
fo	Object focal length (mm).
M	The magnification.
m	Electron mass ($m = 9.1 \times 10^{-31}$ kg).
NI	Magnetic deflector excitation (ampere-turn, A-t).
$NI / (V_r)^{1/2}$	Magnetic deflector excitation parameter (Amp. turns / sqrt(volts)).
$R_p(z)$	Radial height of the pole pieces along the deflector axis (mm).
r	Trajectory radial along the deflector axis.
r_α	Solution of paraxial-ray equation.
V_a	Accelerating voltage (volt).
V_r	Relativistic corrected accelerating voltage (volt).
$V_z = V(z)$	Axial magnetic scalar potential.
V_p	Pole piece potential (volts).
v	Volume (mm^3).
z	Deflector optical axis (mm).
z_i	Image plane position (mm).
z_o	Object plane position (mm).
U	Electrostatic potential distribution along the optical axis z (volts).
U_i	Voltage of the image side (volts).
U_o	Voltage of the object side (volts).
α_i	Trajectory angle with deflector axis in image side.
α_0	Trajectory angle with deflector axis in object side.

ΔE	Fluctuation in the electron beam energy.
Δr_i	Fluctuation in the electron beam focus.
η	Electron charge to mass quotient, e / m.

References

Amboss, K. (1975)
Design of fast deflection coils for an electron-beam microfabrication system
J. Vac. Sci. Technol. 12 1152-1155

Chu, H. C. and Munro, E. (1981a)
Calculation of the optical properties of electron focusing systems and dual-channel deflection systems with combined magnetic and electrostatic field
Optik 61 121-145

Chu, H. C. and Munro, E. (1981b)
Computerized optimization of the electron optical performance of electron beam lithography systems using the damped least squares method
Optik 61 213-233

Chu, H. C. and Munro, E. (1981c)
Computerized optimization of electron-beam lithography system
J. Vac. Sci. Technol. 19 1053-1057

El-Kareh, A. B. and El-Kareh, J. C. J, (1970)
Electron Beams, Lenses, and Optics
(Academic Press)

Goto, E., Soma, T., and Idesawa, M. (1978)
Design of a variable-aperture projection and scanning system for electron beam
J. Vac. Sci. Technol. 15 883-886

Goto, M., Wada, H., Nakasuji, and Yoshikawa, Y. (1984)
Automatic column control for high speed electron delineator
J. Vac. Sci. Technol. B3 181

Grigorov, G. N. (1988)
An optimization method for nonequiredial electrostatic deflection systems
Vacuum 38 1025-1028

Grivet, P. (1972)
Electron Optics
2 nd. ed. (Pergamon Press)

Hall, C. E. (1966)
Introduction to Electron Microscopy
2 nd. ed. (Mc Graw-Hill)

Hawkes, P.W. (1967)
Lens aberrations focusing of charged particles
ed. Septer, A., pp 411-468
(Academic Press, New York)

Hawkes, P.W. (1972)
Electron optics and Electron Microscopy
(Taylor and Francis: London) pp 27-82

Hawkes, P.W. (1982)
Magnetic Electron Lenses
(Springer-Verlag)

Hawkes, P.W. (1987)
Computer simulation of electron optical systems
Nucl. Instr. Meth. Phys. Reas. A258 466-479

Hawkes, P.W. and Kasper, E. (1989)
Principles of Electron Optics vol. 1
(Academic Press: London)

Idesawa, M., Soma, E. and Saski, T. (1983)
Numerical considerations on multipole-type electrostatic deflectors
J. Vac. Sci. Technol. B1 1322-1326

Jiye, X. (1981)
On the linear transformations for Gaussian trajectory parameters in the combined electron optical systems
Optik 59 237-249

Kasper, E. and Scherle, W. (1981)
On the analytical calculation of fields in electron devices
Optic 60 339-352

Kato, M. and Tsuno, K. (1990)
Optimization of Electron Lens Shape Giving Minimum Spherical aberration Coefficient
IEEE Transaction on Magnetic 26 1023-1025

Kiss, L. (1988)
Computerized investigation of electrostatic lens potential distribution
12 th IMACS World congress, ed. Vicherestsky, R.
Paris (1988)

Kern, D. (1979)
Optimization of electron probe forming systems with respect to aberrations and vertical beam landing
J. Vac. Sci. Technol. 16 1686-1691

Klemprer, O. and Barnett, M. E. (1971)
Electron Optics
3 rd. ed. (Cambridge)

Kuo, H. P. and Groves, T. R. (1983)
A large area deflection system with very low aberration
J. Vac. Sci. Technol. B1 1316-1321

Kurihara, K. (1990)
Aberration due to misalignment in the electrostatic lens and deflection systems
J. Vac. Sci. Technol. B8 452-455

Kuroda, K. (1980)
Simplified method for calculating deflective aberration of electron optical system with two deflectors and lens
Optic 57 251-258

Kuroda, K. , Ozasa, S. and Komoda, K. (1983)
A simplified focusing and deflection system with vertical beam landing
J. Vac. Sci. Technol. B1 1303-1306

Lencova, B. (1980)
Deflection aberrations of multi-stage deflection systems
Optik 58 25-35

Lencova, B. (1988)
On the design of electron beam deflection systems
Optik 79 1-12

Moses, R. w. (1973)
Lens optimization by direct application of the calculations of variations
Image processing and Computer-aid Design in Electron Optics ed. P. W. Hawkes
(Academic Press: London and New York) pp. 250-272

Munro, E. (1971)
Computer-aided – design methods in electron optics
Ph.D. Thesis University of Cambridge, UK

Munro, E. (1973)
Computer-aided design of electron lenses by the finite element method
Image Processing and Computer-aided Design in Electron Optics
ed. Hawakes, P. W.
(Academic Press: London and New York) pp. 284-323

Munro, E. (1974)
Calculation of the optical properties of combined magnetic lenses and deflection systems with superimposed field
Optik 39 450-466

Munro, E. (1975)
Design and optimization of magnetic lenses and deflection systems for electron beams
J. Vac. Sci. Technol. 12 1146-1151

Munro, E. and H. C. Chu (1981a)
Computation of fields in electrostatic deflector
Optik 61 1-16

Munro, E. and H. C. Chu (1981b)
Computation of fields in magnetic deflectors
Optik 60 371-390

Nakagawa, T. and Nakata, S. (2000)
Improved Power-Series Expansion Method for the Analysis of Magnetic Deflection Yokes
IEEE Transactions on Magnetics 36 581-585

Ohiwa, H. (1977)
J. phys. D 10 1437-1449

Ohiwa, H. (1978)
Design of electron-beam scanning systems using the moving objective lens
J. Vac. Sci. Technol. 15 849-851

Ohiwa, H., Goto, E. and Ono, A. (1971)
Electron. Commun. Jpn. 54B 44-51

Paszkowski, B. (1968)
Electron optics
(Iliffe Book: London)

Pierce, J. R. (1954)
Theory and Design of Electron Beams 2 nd ed.
(D. Van Nostrand: Princet and London)

Pfeiffer, H. C. and Langner, G. O. (1981)
Advanced deflection concept for large area, high resolution e-beam lithography
J. Vac. Sci. Technol. 19 1058-1063

Poulin, A. and Roy, D. (1978)
Optimization of the 180 degree hemispherical electrostatic deflector
J. Phys. E: Sci. Instrum. 11 35-42

Read, F. H. (1999)
Edgesways electrostatic deflectors with reduced aberrations
Nucl. Instr. Meth. Phys. Reas. A427 177-181

Scheinfein, M. and , Galantai, A. (1986)
Multiobjective optimization techniques for design of electrostatic charged particle lens
Optik 74 154-164

Septier, A. (1966)
The struggle to overcome spherical aberration in electron optics
Adv. Optic. Electron Microscopy vol.1
ed. R. Barer and V. E. Cosslett
(Academic press: London and New York) pp. 204-274

Septier, A. (1980)
Applied Charged Partical Optics – Part B PP. 102
(Academic Press)

Smith, M. R. and Munro, E. (1986)
A unified aberration theory for electrostatic round lenses, multipole lenses and deflectors
Optic 74 7-16

Soma, T., Idesawa, M., Goto, E., and Saski, T. (1984)
Computer-aided evaluation system for sectored-type multipole electrostatic deflectors
J. Vac. Sci. Technol. B3 177-180

Szilagyi, M. (1977a)
A new approach to electron optical optimization
Optik 48 215-224

Szilagyi, M. (1977b)
A dynamic programming search for magnetic field distributions with minimum spherical aberration
Optic 49 223-246

Szilagyi, M. (1978)
A dynamic programming search for electrostatic immersion lenses with minimum spherical aberration
Optik 50 35-57

Szilagyi, M. (1983)
Improvement of electrostatic lenses for ion beam lithography
J. Vac. Sci. Technol. B1 1137-1140

Szilagyi, M. (1984)
Reconstruction of electron and pole pieces from optimized axial field distribution of electron and ion optical systems
Appl. Phys. Lett. 45 499-501

Szilagyi, M. (1985)
Electron optical synthesis and optimization
Proc. IEEE 73 412-418

Szilagyi, M. (1987)
Electrostatic spline lenses
J. Vac. Sci. Technol. A5 273-278

Szilagyi, M. (1988)
Electron and Ion Optics
(Plenum Press: New York)

Tang, T. (1986)
Asymptotic aberrations of combined electrostatic focusing-deflection systems
Optic 74 43-47

Ximen, J., Tong. L. and Liu, Z. (1996a)
A Unified Aberration Theory for Magnetic Deflection System with Rectilinear or Curvilinear Axes
IEEE Transaction on Electron Devices 43 1297-1303

Ximen, J., Tong. L., Liu, Z. and Tu, Y. (1996b)
Electron Optical Aberration Calculations in a Homogeneous Magnetic deflection System with Curved Axis at Extra-Large Deflection angles
IEEE Transactions on Electron Devices 43 501-508

Yu, L. (1986)
On the relativistic fifth order geometrical aberration equation of a combined focusing-deflection system
Optik 74 65-70

Wang, L., Tang, T. and Lu, Q. (1999)
Surface Magnetic Charge Method Combined with Spatial Harmonic Expansion for Magnetic Field Analysis of Deflection Yokes
IEEE Transactions on Magnetics 35 4166-4170

Zhao, Y. and Khursheed, A. (1999)
Comparative study on magnetic variable axis lenses using electrostatic and magnetic in-lens deflectors
Proceedings of SPIE—Volume 3777
Charged Particle Optics IV, PP. 107-114

Zhigarev, A. (1975)
Electron Optics and Electron Beam Devices

Zhi-xing, X. , Da-quan, H. and Qing-gai, S. (1986)
Optimization of the magnetic deflection system by the method of orthogonal design
J. Vac. Sci. Technol. B5 153-155

الإهداء

إلى من قدموا أرواحهم كي نعيش بعز وكرامة ورفعة

الى تلك الأرواح الطاهرة .. عرفاناً بالجميل

أهدي جهدي المتواضع هذا

الخلاصة

تم استخدام التقريبين التحليلي والتركيبي لطريقة الامثلية في الدراسة الحالية لايجاد التصميم الامثل للحارفات المغناطيسية والكهروسكونية التي تعطي اقل زيغ كروي ولوني. استخدم التقريب التركيبي في حسابات الحارفة المغناطيسية وتم استخدام ملف الانحراف ذو النير الراكب (saddle yoke deflection coil) مصدرا للمجال المغناطيسي، عدة نماذج لتوزيع المجال المحوري استخدمت في الحسابات وكذلك تم استخدام أنموذج جديد تم اقتراحه في الدراسة الحالية. فكرة العدسة الشيئية المتحركة أعتمدت في حسابات مجال الانحراف، زيوغ الانحراف خفظت لكل أنموذج لتوزيع المجال بتغيير شكل ملف الانحراف، حيث غير الطول والزاوية. باستخدام أمثل توزيع للمجال المحوري لكل حالة تم ايجاد تصميم قطع القطب التي تعطي توزيعات المجال هذه باستخدام طريقة اعادة البناء.

في حسابات الحارفة الكهروسكونية، كل من التقريبين التحليلي والتركيبي استخدما لايجاد التصميم الامثل الذي يعطي اقل زيغ. تم اولاً، استخدام التقريب التحليلي لدراسة بعض تصاميم الحارفات الكهروسكونية والتي تتكون من صفيحتين متوازيتين؛ الوصول للامثلية تم بتغيير الشكل الهندسي للحارفة عن طريق تغيير ابعاد الصفائح المتوازية.

ثانياً، التقريب التركيبي استخدم لايجاد اقل قيم للزيغ باستخدام توزيع جديد اقترح في الدراسة الحالية للحارفات الكهروسكونية تحت البحث. شكل الحارفة تم ايجاده باستخدام طريقة اعادة البناء.

أخيرا، الحارفات المغناطيسية والكهروسكونية جمعت وركبت لتعطي عامود كامل لانظمة الانحراف ورسمت مقاطع مستعرضة لمسارات الحزم.

A COMPUTATIONAL OPTIMIZATION OF AN ELECTRON BEAM DEFLECTING SYSTEM

A THESIS
SUBMITTED TO THE COLLEGE OF SCIENCE OF Al-NAHRAIN UNIVERSITY IN PARTIAL FULFILLMENT OF THE REQUIREMENTS FOR THE DEGREE OF DOCTOR OF PHILOSOPHY
IN
PHYSICS

BY

UDAY ALI HUSSAIN Al-OBAIDY

(B.Sc. 1998)
(M.Sc. 2001)

Jumada I ***1426 A. H.***
June ***2005 A. D.***

حسابات الأمثليه

لمنظومة حرف الحزمة الالكترونية

رسالة

مقدمة إلى كلية العلوم في جامعة النهرين

وهي جزء من متطلبات نيل درجة

دكتوراه فلسفة

في

الفيزياء

إعداد

عدي علي حسين العبيدي

(بكالوريوس ١٩٩٨)

(ماجستير ٢٠٠١)

جمادي الاولى ١٤٢٦هـ

حزيران ٢٠٠٥ م

Contents ***Page***

I certify that this thesis was prepared by Uday Ali Hussain Under my supervision at Al-Nahrain University, College of Science. In partial fulfillment of the requirements for the degree of Ph.D. in physics.

Signature:

Name: Dr. Ahmad K. Ahmad
(Assist. Prof.)
Department of physics
College of Science
Al-Nahrain University
Date: 26 / 3 / 2005

In view of the available recommendations, I forward this thesis for debate by the examining committee

Signature:

Name: Dr. Ahmad K. Ahmad
(Head of department)

Date: 26 / 3 / 2005

Abstract

Both analysis and synthesis approaches of optimization method are used in the present work to finding the optimum design of magnetic and electrostatic deflectors which give rise to the minimum spherical and chromatic aberration. In magnetic deflector calculations, the synthesis approach is used; the saddle yoke deflection coil is used as the source of magnetic field, then some axial field distribution models are to be used and new field distribution model to be suggested. The moving objective lens concept is included in the computation of deflection field. Deflection aberrations are minimized for each field distribution model by changing the shape of the deflection coil, where the length and angle are varied. By using the optimum axial field distribution for each case, the pole pieces design which give rise to these field distributions is to be found by using reconstruction method.

In electrostatic deflector calculations, both analysis and synthesis approaches are used to find optimum design, which give rise to minimum aberrations. Firstly, the analysis approach is used to study some electrostatic deflector designs which consists of two parallel-plates, and the optimization is made by changing the geometrical shape of the deflector by varying the dimensions of the parallel-plates. Secondly, the synthesis approach is used to find minimum values for the aberration by means of the new axial field distribution that has been put forward in the present work for the electrostatic deflectors under investigation. The shape of the deflector is found by using the reconstruction method. Finally, the magnetic and electrostatic deflectors are to be assembled to give complete columns of deflection systems and plot the trajectories of the beam traversing them.

Contents ***Page***

LIST OF SYMBOLS

a	The field width at half maximum $B_m / 2$.
B(z)	Magnetic flux density (Tesla T).
B_m	Maximum value of axial magnetic flux density distribution (T).
$B_x(z)$	The deflection field at the axis of an air-cored saddle yoke.
C_c	Chromatic aberration coefficient .
C_{ci}	Chromatic aberration coefficient referred to image side.
C_{co}	Chromatic aberration coefficient referred to object side.
C_s	Spherical aberration coefficient .
C_{si}	Spherical aberration coefficient referred to image side.
C_{so}	Spherical aberration coefficient referred to object side.
D(z)	Deflection magnetic flux density.
d	Displacement by the first magnetic deflector.
E	Energy of electron beam.
e	Electron charge (1.6×10^{-19} C).
fo	Object focal length.
M	The magnification.
m	Electron mass ($m = 9.1 \times 10^{-31}$ kg).
NI	Magnetic deflector excitation (ampere-turn, A-t).
$NI / (V_r)^{1/2}$	Magnetic deflector excitation parameter.
$R_p(z)$	Radial height of the pole pieces along the deflector axis.
r	Trajectory radial along the deflector axis.
r_α	Solution of paraxial-ray equation.
V_a	Accelerating voltage (volt).
V_r	Relativistic corrected accelerating voltage (volt).
V_z =V(z)	Axial magnetic scalar potential.
V_p	Pole piece potential.
v	Volume.
z	Deflector optical axis.
z_i	Image plane position.
z_o	Object plane position.
U	Electrostatic potential distribution along the optical axis z.
U_i	Voltage of the image side
U_o	Voltage of the object side.
α_i	Trajectory angle with deflector axis in image side.

α_0	Trajectory angle with deflector axis in object side.
ΔE	Fluctuation in the electron beam energy.
Δr_i	Fluctuation in the electron beam focus.
η	Electron charge to mass quotient, e / m.

بسم الله الرحمن الرحيم

اقرأ باسم ربك الذي خلق ☼ خلق الانسان من

علق ☼ اقرأ وربك الأكرم☼ الذي علم بالقلم

☼ علم الانسان ما لم يعلم ☼

صدق الله العظيم

(سورة العلق ١ - ٥)